

OPTIMIZATION OF MATERIAL DAMPING AND STIFFNESS OF  
LAMINATED FIBER-REINFORCED  
COMPOSITE STRUCTURAL ELEMENTS

BY

JIING-KAE WU

A DISSERTATION PRESENTED TO THE GRADUATE SCHOOL OF  
THE UNIVERSITY OF FLORIDA IN PARTIAL  
FULFILLMENT OF THE REQUIREMENT FOR THE DEGREE OF  
DOCTOR OF PHILOSOPHY

UNIVERSITY OF FLORIDA

1985

## ACKNOWLEDGEMENTS

The author wishes to express his deep appreciation to his major professor, Dr. Chang-Tsan Sun, whose valuable advice brings a nice end to this study.

The author is also indebted to Professor Malvern for his invaluable comments and constructive criticisms. Profound appreciation is also due to Professors Kurzweg, Taylor, and Verma, other committee members, for their worthy comments and for the time they spent in reviewing this dissertation.

Much thanks are given to Jenny Sun for her contribution in typing this dissertation. And the author gratefully acknowledges support of this research work from the U.S. Air Force Office of Scientific Research under Grant No. AFOSR-83-0154 and AFOSR-83-0156 monitored by Dr. D. R. Ulrich.

Finally, the author expresses his greatest appreciation to his parents and his wife, Mong-Shya Rau Wu, for encouraging him to study in the U.S.A. and for providing warm family support during the past four years.

## TABLE OF CONTENTS

	<u>Page</u>
ACKNOWLEDGEMENTS . . . . .	ii
LIST OF TABLES . . . . .	vi
LIST OF FIGURES . . . . .	vii
ABSTRACT . . . . .	xiv
 CHAPTERS	
1 INTRODUCTION . . . . .	1
1.1 Literature Survey . . . . .	2
1.2 Scope of This Study . . . . .	4
1.3 Material Constants and Ranges of Design Parameters . . . . .	5
2 DAMPING . . . . .	8
2.1 Definition of Damping . . . . .	8
2.2 Damping Mechanism . . . . .	9
2.2.1 Viscous Damping . . . . .	9
2.2.2 Dry or Coulomb Damping. . . . .	10
2.2.3 Material Damping . . . . .	11
2.3 Types of Damping Representation . . . . .	15
2.3.1 Damping Ratio . . . . .	16
2.3.2 Logarithmic Decrement . . . . .	17
2.3.3 Loss Tangent . . . . .	18
2.3.4 Specific Damping Capacity for Cyclic Loading . . . . .	20
3 DAMPING OF UNIDIRECTIONAL SHORT-FIBER COMPOSITES . . . . .	23
3.1 Introduction . . . . .	23
3.2 Damping Analysis of Unidirectional Fiber Composites . . . . .	24
3.2.1 Short-Fiber Composite Model . . . . .	24

CHAPTER		Page
	3.2.2 Damping Analysis of Aligned Fiber Composites . . . . .	30
4	DAMPING OF RANDOMLY ORIENTED SHORT-FIBER COMPOSITES . . . . .	40
	4.1 Introduction . . . . .	40
	4.2 Damping Analysis of In-Plane Randomly Oriented Short-Fiber Composites . . . . .	41
5	DAMPING OF LAMINATED FIBER COMPOSITES-- LAMINATED PLATE THEORY APPROACH . . . . .	45
	5.1 Introduction . . . . .	45
	5.2 Damping Analysis of Laminated Fiber Composite Through Laminated Plate Theory Approach . . . . .	45
6	DAMPING OF LAMINATED FIBER COMPOSITES-- ENERGY APPROACH . . . . .	54
	6.1 Introduction . . . . .	54
	6.2 Damping Analysis of Laminated Fiber Composites Through Energy Approach . . . . .	55
7	EXPERIMENTAL MEASUREMENT OF DAMPING . . . . .	61
	7.1 Introduction . . . . .	61
	7.2 Apparatus . . . . .	62
8	OPTIMIZATION OF DAMPING AND SPECIFIC STIFFNESS FOR FIBER COMPOSITES . . . . .	69
	8.1 Introduction . . . . .	69
	8.2 Brief Introduction to Sequential Simplex Method . . . . .	70
	8.3 Mathematical Formulation of Design Problems . . . . .	74
9	RESULTS AND CONCLUSIONS . . . . .	85
	9.1 Preliminary Remarks . . . . .	85
	9.2 Damping and Stiffness of Uni- directional Fiber Composites . . . . .	86
	9.3 Damping and Stiffness of Randomly Oriented Short- Fiber Composites . . . . .	89

9.4	Damping and Stiffness of Laminated Fiber Composites-- Laminated Plate Theory Approach . . . . .	90
9.5	Damping and Stiffness of Laminated Fiber Composites-- Energy Approach . . . . .	93
9.6	Experiemntal Results of Damping and Stiffness . . . . .	95
9.7	Optimization of Damping and Specific Stiffness of Fiber Composites . . . . .	96
9.8	Conclusions . . . . .	98

## APPENDICES

A	HYSTERESIS LOOP OF VISCOELASTIC MATERIALS . . . . .	147
B	EXPRESSIONS OF $\beta$ 'S . . . . .	151
C	AN ALTERNATIVE WAY OF DETERMINING $\tilde{E}_r$ and $\tilde{G}_r$ . . . . .	154
D	INVERSION OF A SYMMETRIC COMPLEX MATRIX . . . . .	157
E	ENERGY EXPRESSION OF DAMPING FOR LAMINATED COMPOSITES . . . . .	160
F	FORMULATION OF FINITE ELEMENT METHOD . . . . .	163
	F.1 Stiffness Matrix . . . . .	163
	F.2 Formulation of Finite Element Method . . . . .	166
	REFERENCES . . . . .	170
	BIOGRAPHICAL SKETCH . . . . .	176

## LIST OF TABLES

<u>Table</u>	<u>Page</u>
1.1      Material Properties Data of the Matrix and the Fibers . . . . .	7
3.1      Influence of $V_f^i$ and $s/d$ on $\tanh (\beta s/2) (\beta s/2)$ . . . . .	28
9.1      Experimental Results of $0_5/90_5/0_5$ Glass Epoxy Composite Plates . . . . .	.145
9.2      Influence of Weighting Constants on Optimum Design for Case One . . . . .	.145
9.3      Optimum Design of Cross Ply Composite Plates for Case One. . . . .	.146
9.4      Optimum Design of Cross Ply Composite Plates for Case Two. . . . .	.146

## LIST OF FIGURES

<u>Figure</u>		<u>Page</u>
2.1	Sketch of Hysteresis Loop . . . . .	14
2.2	Sketch of Viscous Damping Model . . . . .	16
2.3	Sketch of Logarithmic Decrement . . . . .	18
2.4	Rotating-Vector Representation of Harmonic Motion . . . . .	19
2.5	Hysteresis Loop of an Inelastic Body . . .	21
3.1	Short-Fiber Composite Model . . . . .	24
3.2	Representative Volume Element of Off-Axis Short-Fiber Composites . . . . .	30
5.1	Sketch of Laminated Fiber Composite Plate . . . . .	46
7.1	Schematic Drawing of the Experimental Set-up . . . . .	66
7.2	Typical Display of Real and Imaginary Parts of Frequency Response Function for a Graphite Epoxy Composite Beam . . . . .	67
7.3	Enlarged Schematic Drawing of Real Part of Frequency Response Function . . . . .	68

<u>Figure</u>		<u>Page</u>
8.1	Rule 1 of Sequential Simplex Method . . . .	73
8.2	Rule 2 of Sequential Simplex Method . . . .	73
8.3	Rule 3 of Sequential Simplex Method . . . .	74
9.1	Plots of $E'_x/E'_m$ vs $s/d$ using $\theta$ as a Parameter for Graphite Epoxy Composites .	101
9.2	Plots of $E''_x/E''_m$ vs $s/d$ using $\theta$ as a Parameter for Graphite Epoxy Composites .	102
9.3	Plots of $\eta_x/\eta_m$ vs $s/d$ using $\theta$ as a Parameter for Graphite Epoxy Composites .	103
9.4	Plots of $E'_x/E'_m$ vs $\theta$ using $s/d$ as a Parameter for Graphite Epoxy Composites .	104
9.5	Plots of $E''_x/E''_m$ vs $\theta$ using $s/d$ as a Parameter for Graphite Epoxy Composites .	105
9.6	Plots of $\eta_x/\eta_m$ vs $\theta$ using $s/d$ as a Parameter for Graphite Epoxy Composites .	106
9.7	Plots of $E'_x/E'_m$ vs $s/d$ using $\theta$ as a Parameter for Kevlar Epoxy Composites . .	107
9.8	Plots of $E''_x/E''_m$ vs $s/d$ using $\theta$ as a Parameter for Kevlar Epoxy Composites . .	108
9.9	Plots of $\eta_x/\eta_x$ vs $s/d$ using $\theta$ as a Parameter for Kevlar Epoxy Composites . .	109
9.10	Plots of $\eta_x/r_m$ , $E'_x/E'_m$ and $E''_x/E''_m$ vs $\theta$ keeping $s/d=100$ for Kevlar Epoxy Composites . . . . .	110



<u>Figure</u>		<u>Page</u>
9.11	Plots of $\eta_x/\eta_m$ and $E'_x/E'_m$ vs $\theta$ keeping s/d=100 for Graphite Epoxy Composites and Kevlar Epoxy Composites . . . . .	111
9.12	Plots of $E'_x/E'_m$ vs $\theta$ using $V_f$ as a Parameter for Graphite Epoxy Composites . . . . .	112
9.13	Plots of $\eta_x/\eta_m$ vs $\theta$ using $V_f$ as a Parameter for Graphite Epoxy Composites . . . . .	113
9.14	Three-Dimensional Plots of $E'_x/E'_m$ vs $\theta$ and s/d for Kevlar Epoxy Composites . . .	114
9.15	Three-Dimensional Plots of $\eta_x/\eta_m$ vs $\theta$ and s/d for Kevlar Epoxy Composites . . .	115
9.16	Contour curves of $E'_x/E'_m$ vs $\theta$ and s/d for Kevlar Epoxy Composites . . . . .	116
9.17	Contour curves of $\eta_x/\eta_m$ vs $\theta$ and s/d for Kevlar Epoxy Composites . . . . .	117
9.18	Plots of $\eta_x/\eta_m$ , $E'_r/E'_m$ and $E''_r/E''_m$ vs s/d for Randomly Oriented Glass Epoxy Composites . . . . .	118
9.19	Plots of $\eta_x/\eta_m$ , $E'_r/E'_m$ and $E''_r/E''_m$ vs s/d for Randomly Oriented Graphite Epoxy Composites . . . . .	119
9.20	Plots of $\eta_x/\eta_m$ , $E'_r/E'_m$ and $E''_r/E''_m$ vs s/d for Randomly Oriented Kevlar Epoxy Composites . . . . .	120

9.21	Plots of $\eta_{Gr}/\eta_{Gm}$ , $G'_r/G'_m$ and $G''_r/G''_m$ vs $s/d$ for Randomly Oriented Glass Epoxy Composites . . . . .	121
9.22	Plots of $\eta_{Gr}/\eta_{Gm}$ , $G'_r/G'_m$ and $G''_r/G''_m$ vs $s/d$ for Randomly Oriented Graphite Epoxy Composites . . . . .	122
9.23	Plots of $\eta_{Gr}/\eta_{Gm}$ , $G'_r/G'_m$ and $G''_r/G''_m$ vs $s/d$ for Randomly Oriented Kevlar Epoxy Composites . . . . .	123
9.24	Plots of $\eta_r/\eta_m$ vs $V_f$ using $s/d$ as a Parameter for Randomly Oriented Glass Epoxy Composite . . . . .	124
9.25	Three-Dimensional Plots of $E'_r/E'_m$ vs $s/d$ and $E'_f$ for Randomly Oriented Fiber Composites . . . . .	125
9.26	Three-Dimensional Plots of $\eta_r/\eta_m$ vs $s/d$ and $E'_f$ for Randomly Oriented Fiber Composites . . . . .	126
9.27	Contour Curves of $E'_r/E'_m$ vs $s/d$ and $E'_f$ for Randomly Oriented Fiber Composites . .	127
9.28	Contour Curves of $\eta_r/\eta_m$ vs $s/d$ and $E'_f$ for Randomly Oriented Fiber Composites . .	128
9.29	Plots of $D'_{11}/D'_m$ and $F\eta_{11}/\eta_m$ vs $s/d$ for Quasi-Isotropic Graphite Epoxy Composites . . . . .	129

9.30	Plots of $D'_{66}/D'_{Gm}$ and $F\eta_{66}/\eta_{Gm}$ vs $s/d$ for Quasi-Isotropic Graphite Epoxy Composites . . . . .	130
9.31	Plots of $E'_{11}/E'_m$ vs $\theta$ using $s/d$ as a Parameter for Angle Ply Graphite Epoxy Composites . . . . .	131
9.32	Plots of $I\eta_{11}/\eta_m$ vs $\theta$ using $s/d$ as a Parameter for Angle Ply Graphite Epoxy Composites . . . . .	132
9.33	Plots of $E'_{66}/E'_m$ vs $\theta$ using $s/d$ as a Parameter for Angle Ply Graphite Epoxy Composites . . . . .	133
9.34	Plots of $I\eta_{66}/\eta_m$ vs $\theta$ using $s/d$ as a Parameter for Angle Ply Graphite Epoxy Composites . . . . .	134
9.35	Comparisons of $D'_{11}/D'_m$ vs $s/d$ for Four Kinds of Laminated Graphite Epoxy Composites . . . . .	135
9.36	Comparisons of $F\eta_{11}/\eta_m$ vs $s/d$ for Four Kinds of Laminated Graphite Epoxy Composites. . . . .	136
9.37	Comparisons of $D'_{66}/D'_{Gm}$ vs $s/d$ for Four Kinds of Laminated Graphite Epoxy Composites . . . . .	137

<u>Figure</u>		<u>Page</u>
9.38	Comparisons of $F_{\eta_{66}}/\eta_{Gm}$ vs $s/d$ for Four Kinds of Laminated Graphite Epoxy Composites and Hybrid Fiber Composites . .	138
9.39	Influence of $s/p$ on the In-Plane Longitudinal Damping Through Energy Approach . . . . .	139
9.40	Influence of $a/h$ on the In-Plane Longitudinal Damping of Laminated Graphite Epoxy Composites Through Energy Approach . . . . .	140
9.41	Influence of $a/h$ on the Flexural Normal Damping of Laminated Graphite Epoxy Composites Through Enery Approach . . . . .	141
9.42	Comparison Between Analytical Results and Experimental Results for Unidirectional Discontineous Graphite Reinforced Epoxy Composite Beams . . . . .	142
9.43	Comparison Between Analytical Results and Experimental Results for Off- Axis Unidirectional Continuous Graphite Reinforced Epoxy Composites Beams . . . .	143
9.44	Contour Curves of Objective Function for Case One vs $s/d$ and $s/p$ for Graphite Epoxy Composite Plate . . . . .	144

<u>Figure</u>		<u>Page</u>
A.1	Hysteresis Loop of a Viscoelastic Material . . . . .	149
F.1	Principal Coordinates of a Fiber Composite Material . . . . .	165

Abstract of Dissertation Presented to the Graduate School  
of the University of Florida in Partial Fulfillment of the  
Requirements for the Degree of Doctor of Philosophy

OPTIMIZATION OF MATERIAL DAMPING AND STIFFNESS  
OF LAMINATED FIBER-REINFORCED  
COMPOSITE STRUCTURAL ELEMENTS

By

Jiing-Kae Wu

December 1985

Chairman: C. T. Sun  
Major Department: Engineering Sciences

Analysis of material damping and optimization of both material damping and specific stiffness of laminated, continuous or discontinuous fiber reinforced polymer matrix is the major objective of this study.

Two different approaches, laminated plate theory approach and energy approach, are used in conjunction with elastic-viscoelastic correspondence principle for the analysis of the material damping for fiber reinforced composites. Damping values obtained through these two approaches are close to each other under certain situations. A discontinuous fiber composites model is developed to determine the longitudinal modulus of discontinuous fiber reinforced composites. Aligned or off-axis unidirectional fiber composites, in-plane randomly

oriented fiber composites, and several kinds of laminated fiber composites are considered in damping and stiffness analysis. Experimental results on damping and stiffness by the impulse hammer technique agree with the analytical results for unidirectional fiber composites and for certain cross ply fiber composites. In the energy approach, a three-dimensional finite element method based on three-dimensional elasticity is applied to determine the strain field of an elastic body. Dissipated energy can be determined through this strain field and loss moduli. Damping through energy approach depends on the boundary conditions, the loading conditions, and the geometry (especially the dimension in thickness direction) of the body.

Sequential Simplex method, laminated plate theory, and an elastic-viscoelastic correspondence principle are used to optimize both material damping and specific stiffness of composites. Minimum flexure deformation design of orthotropic laminated fiber composite plates is obtainable through this optimization procedure.

## CHAPTER 1 INTRODUCTION

Due to the high strength-to-weight and stiffness-to-weight ratios, composite materials are ideal for weight-sensitive structures such as aircraft, spacecraft, and automotive vehicles. In recent years, with the advent of jet propulsion, particularly with the current increased interest in short take-off and landing aircraft, it has become necessary to pay increasing attention to the higher frequency motions of such structures. These motions depend strongly on the structure's damping or capability for dissipation of vibratory energy [1]. In addition, a new type of excitation has become more prevalent, random excitation either of mechanical or acoustical origin [2]. For example, jet engine exhaust generally contains a noise spectrum wide enough to excite most of the natural frequencies encountered in aircraft structures [3]. The natural resonance phenomena, so produced, can be very destructive. Since near resonant conditions can no longer be avoided in many types of structures, the maximization of damping within a structural system provides a most useful concept in controlling resonance [4]. Unfortunately, as will be shown in later chapters, high damping is mostly coupled with low stiffness, and high



stiffness is mostly coupled with low damping. Therefore, the optimization of damping and of the stiffness-to-weight ratio is a practical idea in designing a proper composite material to be used in aircraft and space vehicles.

### 1.1 Literature Survey

Most results from a series of researches on damping beginning in the 1920's [5] indicated that damping is a material property.

Kimball and Lovell [5] experimentally showed that for stress cycles of frequency of from two to three a minute, up to fifty a second the frictional loss (a kind of energy loss) is independent of the frequency but is dependent on the amplitude of strain of the cycles for eighteen different solids, including several metals, glass, celluloid, rubber and maple wood, when strain was below the elastic limit. Crandall [6] pointed out that the values for material damping which will be introduced in Section 2.3.3 encountered in practice ranged from about 0.00001 to 0.2; however, Lazan [4] pointed out the material damping ranged from 0.001 to 0.1. And the material damping depends on both the amplitude and frequency of the oscillation. If, however, the system is completely linear, then damping is independent of amplitude [6].

Recently, the composite materials got more attention in industrial application. Lazan [4] gave a detailed review on material damping of materials and material

composites. Kume, Hashimoto and Maeda [7] used the damping-stress function, derived by Lazan [8], to calculate the material damping of cantilever beams. They found that low order modes of a cantilever beam with equal maximum stress amplitude gave almost the same material damping, theoretically, and experimental results have the same order of magnitude as the theoretical results when the maximum stress amplitude is less than a certain value. Schultz and Tsai [9] indicated that unidirectional glass fiber reinforced composites exhibit anisotropic, linear viscoelastic behavior when those undergoing small oscillation and that damping increases in magnitude with change in fiber orientation angle with respect to loading direction in the order  $0^\circ$ ,  $22.5^\circ$ ,  $90^\circ$ ,  $45^\circ$ . Ni, Lin, and Adams [10, 11] used the laminated plate theory and two-dimensional energy approach to predict the flexural damping of laminated composites. In their work, damping coefficient was determined by free-free flexural modes of vibration [12]. Siu and Bert [13] discussed the vibration of composite plates having material damping. Suarez, Gibson, and Deobald [14] observed the dependence of damping on frequency of fiber reinforced epoxy or polyester. Gibson and Plunkett [15] found that for small strain, damping and stiffness are independent of amplitude of strains, but, once the threshold strain is exceeded (i.e., failure starts), the resulting increase in damping is much more significant than the corresponding reduction in stiffness. Similar

results were also observed by Tauchert and Hsu [16]. Bert and Clary [17, 18] gave a complete review on measurement and analysis of damping and dynamic stiffness for composites. The first paper to optimize the damping of the structure was perhaps that of Plunkett and Lee [19]. The damping of a beam is improved by introducing thin constrained visco-elastic layers on the top and bottom of the structure. These viscoelastic layers are then stiffened by properly designed constraining layers.

Cox [20] discussed the stress distribution in fibrous materials. Cox's shear lag stress analysis was later on used to analyze the stress distribution of short-fiber composites, as in studies [21, 22]. Photoelasticity [23, 24] and finite element methods [25, 26] were used to investigate the stress concentration in the matrix around fiber tips of short-fiber composites. Strength of short-fiber composites was analyzed in several studies [27, 28]. Analysis of complex moduli for such kind of material was presented in studies [29, 30, 31]. High damping of short-fiber composites was analytically and experimentally observed in references [31, 32]. Material damping of randomly oriented and unidirectional laminar short-fiber composites has been discussed by Sun, Wu, Chaturvedi, and Gibson [33, 34].

### 1.2 Scope of This Study

The objectives of this study are to analyze the material damping and to optimize the specific stiffness (the

ratio of the stiffness to the density) and material damping of continuous and/or discontinuous fibers reinforced laminated composite structure elements. The work involved in this research is briefly introduced as follows:

- A. To develop a short-fiber composite model to determine the moduli of short-fiber composites.
- B. To analyze the stiffness and material damping of unidirectional laminar fiber composites, randomly-oriented fiber composites, and certain kinds of laminated fiber composites through classical laminated plate theory approach.
- C. To analyze the material damping of laminated fiber composites by an energy approach, where a three-dimensional displacement finite element method is used.
- D. To optimize material damping and the specific stiffness of laminated composite plates.

### 1.3 Material Constants and Ranges of Design Parameters

In this study, four different kinds of widely-used fiber composites (i.e., glass epoxy, Kevlar epoxy, graphite epoxy, and boron epoxy) are involved; and much interest is concentrated on graphite epoxy and Kevlar epoxy, because, generally speaking, the former has higher stiffness, while the latter has higher damping.

In order to compare with the experimental results of Suarez, etc. [35, 36], the material constants used in this study are the same as those of the experimental specimens. Some material constants, which are not given in those experimental data, are obtained from reference [37]. Unless specially specified, the material constants used in this study are given in Table 1.1.

The length of fiber is one of the characteristic parameters of short-fiber composites. Due to the existence of a critical fiber length,  $s_c$  (i.e. the minimum fiber length in which the ultimate strength  $\sigma_{fu}$  can be achieved [38]), there is a minimum value for fiber length,

$$\frac{s}{d} \geq \frac{s_c}{d} = \frac{\sigma_{fu}}{2\tau_y} \quad 1.1$$

where  $\tau_y$  is the matrix yield stress in shear, and  $d$  is the fiber diameter. The lowest  $\sigma_{fu}$  of those four fiber composites is 2750 MPa, as given in reference [37], for graphite T-300. And the matrix yield shear stress is, according to the manufacturer's test results, 97 MPa of AS4/3501 graphite-epoxy tape. Therefore, the fiber aspect ratio, the ratio of fiber length to its diameter, should be

$$s/d \geq 14.2 \quad 1.2$$

In this study, the fiber aspect ratio is chosen to be between 25 and 10000; while the fiber volume fraction  $V_f$  is chosen to be 0.65 for the most cases or 0.5 for randomly oriented fiber composites.

Table 1.1: Material Properties Data of the Matrix and the Fibers

Constants	Matrix	Fibers			
	Epoxy	Glass	Kevlar	Graphite	Boron
$E_1$ (Gpa)	3.94	72.4	99.8	175.8	381.9
$E_2$ (Gpa)	3.94	13.8	6.9	13.8	35.0
$G_{12}$ (Gpa)	1.465	27.6	13.8	27.6	70.0
$\nu_{12}$	0.345	0.22	0.376	0.16	0.21
$k$ (Gpa)	4.236	—	—	—	—
$\eta_1$	0.015	0.0015	0.011	0.0015	0.0019
$\rho$ (kg/m <sup>3</sup> )	1220.	2539.	1479.	1760.	2481.
$\xi_1$	—	2	2	2	2
$\xi_2$	—	1	1	1	1

where  $\xi_1$  and  $\xi_2$  are constants used in Halpin-Tsai Equation,  $\eta_1$  is the longitudinal damping,  $k$  is the bulk modulus, and  $\rho$  is the density.

## CHAPTER 2 DAMPING

### 2.1 Definition of Damping

The process by which vibration steadily diminishes in amplitude is called damping. In many ways, the assumption that systems possess no damping is a mathematical convenience, rather than a reflection of physical evidence. In fact, if a system is set in motion and allowed to vibrate freely, the vibration will eventually die out; the rate of decay depends on the amount of damping. This reduction in vibrating amplitude occurs because the energy of the vibrating system is dissipated as friction or heat or is transmitted as sound [39]. And this is why damping is also interpreted as any phenomenon within the body of the material where energy is dissipated [40].

The concept of an undamped system serves not only a useful purpose in analysis, but can also be justified in certain circumstances. For example, if the damping is small and one is interested in the free vibration of a system over a short interval time, there may not be sufficient time for the effect of damping to become noticeable. Similarly, for small damping one may not be able to notice the effect of damping in the case of a system with harmonic excitation, provided the driving



frequency is not in the neighborhood of any of the natural frequencies of the system [41]. On the other hand, damping of a given system should be considered if this system is subjected to vibration near its resonant frequencies because damping has a large influence on the amplitude in the frequency region near resonance [42].

## 2.2 Damping Mechanism

There are many mathematical models representing damping. The mechanism of damping can take any of these forms and often more than one form may be present at a time. Therefore, in order to analyze or predict the damping of a given system, one ideally should take into account all possible damping mechanisms; fortunately, in most practical cases, one or two mechanisms predominate so that one may neglect the effect of all others. Three widely used mathematical models for damping are introduced below:

### 2.2.1 Viscous Damping

The viscous damping force is defined as

$$F_d = -C\dot{x} \quad 2.1$$

where the constant  $C$  (of dimension force per unit velocity) is called the coefficient of viscous damping. This type of damping occurs in lubricated sliding surfaces, dash-pots, hydrolic shock-absorbers [43]. The minus sign indicates



that this damping force is always opposite to the direction of the motion. The work done by damping force, namely, dissipated energy during one cycle of harmonic motion,  $x = A_0 \sin \omega t$ , will be

$$(U_D)_{\text{cyc}} = \int F_d \, dx = \int_0^{2\pi} C \left( \frac{dx}{dt} \right)^2 dt = \pi C A_0^2 \omega \quad 2.2$$

where  $\omega$  is the circular frequency in radians per unit time. Apparently, dissipated energy due to viscous damping in a cyclic motion is proportional to the frequency and to the square of the amplitude of motion.

### 2.2.2 Dry or Coulomb Damping

This type of damping occurs in the sliding of dry surfaces. The damping force during motion is constant and is given, according to Coulomb's law, by

$$F_d = -fN \quad 2.3$$

where  $N$  is the normal component of the force upon the surface of contact, and  $f$  is the coefficient of dry friction. Damping induced by the joints is mainly because of dry damping. And it is known that damping of built-up structures (i.e. structure made by joining together skins, strings, frames, etc.) could further be caused by the effect of the joint [1].

### 2.2.3 Material Damping

This kind of damping is also referred to as internal, hysteresis or structural damping. It is caused by the internal friction, the viscoelastic behavior of the material, and the interfacial slip in the material itself.

It is well known that an elastic body which is repeatedly stressed becomes hot. If an elastic body is subjected to forced oscillation, a positive work of the exciting force must be spent to keep the amplitude of the oscillations constant in time. The reason for the heating of the body and the expenditure of external work is the internal friction of the material. Although this explanation can be easily accepted in a qualitative way, it is more difficult to translate the problem into mathematical terms.

Three principal hypotheses have been proposed to explain the phenomenon of internal friction, i.e., the viscous theory, the hereditary theory, and the hysteresis loop.

Viscous theory. The viscous theory assumes that in solid bodies, there exist some viscous actions which can be compared to the viscosity of fluids. These viscosity effects are assumed to be proportional to the first time derivative of strain. The coefficient of the proportionality (constant for each material at constant temperature) is called the coefficient of viscosity. Based on this assumption, many mathematical models (such as Maxwell model, Kelvin-Voigt model, and three-parameter

models [44, 45]) have been introduced to represent different materials. For the case of Kelvin-Voigt model under normal deformation, the relationship between stress  $\sigma$  and strain  $\epsilon$  is expressed by

$$\sigma = E\epsilon + \xi \frac{d\epsilon}{dt} \quad 2.4$$

where  $E$  is Young's modulus and  $\xi$  is the coefficient of viscosity of the material.

Hereditary theory. The hereditary theory attributes the dissipation of energy due to material damping to the elastic delay by which the deformation lags behind the applied force [43]. According to this theory, the deformation at a given instant, instead of depending only on the actual applied stress at that time as it would if the materials followed Hooke's law, depends on all the stresses previously applied to the elastic body. The stress-strain relationship is given by

$$\sigma = E\epsilon + \int_{-\infty}^t \phi(t, \tau) \epsilon(\tau) d\tau \quad 2.5$$

where  $t$  is the actual time and  $\tau$  is an instant of time between  $t = -\infty$  and  $t = t$ . The function  $\phi(t, \tau)$  is called the hereditary kernel or memory function.

Hysteresis loop. For a material under a cyclic loading, the stress-strain curve is a closed curve which is called the hysteresis loop. The physical meaning of

this hysteresis loop is given in Section 2.3. The area within the hysteresis loop is proportional to the dissipated energy. This area, being a material property, may or may not depend on the frequency. A mathematical model can be used to explain the energy dissipation, when this energy dissipation is independent of frequency in a material loaded by a cyclic force. In this mathematical model, the damping force is assumed to be proportional to velocity and inversely proportional to frequency, i.e.

$$F_d = \frac{h}{\omega} \dot{x} \quad 2.6$$

If an external force  $F_e$  is applied just enough to balance the damping force and to maintain a simple harmonic motion,  $x = A_0 \sin \omega t$ , then

$$F_e = Kx + \frac{h}{\omega} \dot{x} \quad 2.7$$

where  $Kx$  represents the elastic force of the system; for example, a single spring,  $\omega$  is the circular frequency,  $A_0$  is the amplitude, and  $h$  is the hysteretic damping constant. The relationship between  $F_e$  and  $x$  is given in Equation 2.7, and the plot of external force  $F_e$  as a function of displacement is a skewed ellipse, as in Figure 2.1.

$$\left(\frac{x}{A_0}\right)^2 + \left(\frac{F_e - Kx}{hA_0}\right)^2 = 1 \quad 2.8$$

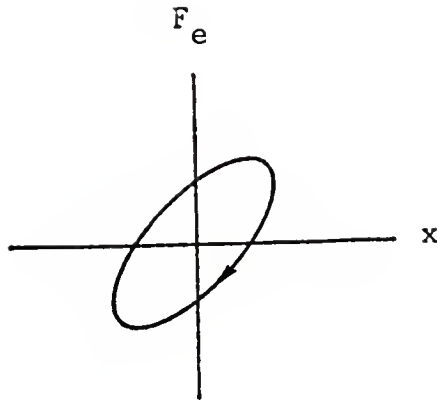


Figure 2.1: Sketch of Hysteresis Loop

The work done by damping force (dissipated energy) in one cycle  $(U_D)_{cyc}$  is

$$(U_D)_{cyc} = \int F_d dx = \int_0^{\frac{2\pi}{\omega}} \frac{h}{\omega} (\dot{x})^2 dt = \pi h A_0^2$$

2.9

Thus, the energy dissipated in one cycle is proportional only to the square of the amplitude. This expression agrees with the results of experiments of Kimball and Lovell [5] which indicate that for a large variety of materials such as metals, glass, rubber and maple wood, subject to cyclic stress such that the strains remain below the elastic limit, the internal friction is entirely

dependent on the rate of strain. Equation 2.9 also agrees with Lazan's notes [46] on dissipated energy. For example, at low amplitudes of stress, the dissipated energy is proportional to the square of the stress amplitude, and the hysteretic loop is elliptical in form.

Unlike homogeneous materials, fiber reinforced materials have interfaces between matrix and fiber. When a fiber reinforced composite is subject to a tensile strain cycle, the high shear stress may cause the fiber matrix interface to fail so that energy is dissipated by friction as the matrix slides over the fibers [47]. Damping is then increased due to interfacial slips between matrix and fiber. In this study, perfect bonding between matrix and fiber is assumed; consequently, interfacial slip is not considered.

### 2.3 Types of Damping Representations

Many different disciplines have been concerned with damping measurements, and this has further complicated nomenclature. Confusion has been caused not only by the large variety of damping units used, but also by the lack of unique definition for many well-accepted units. It is, therefore, desirable to review the various damping units currently used and to indicate relationships between them.

### 2.3.1 Damping Ratio ( $\zeta$ )

Figure 2.2 shows a single degree of freedom system with viscous damping, excited by force  $F(t)$ .

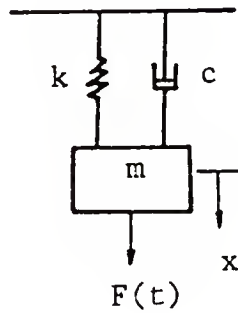


Figure 2.2: Sketch of Viscous Damping Model

Its differential equation of motion is found to be

$$M\ddot{x} + C\dot{x} + Kx = F(t) \quad 2.10$$

If  $F(t)=0$ , one has the homogeneous differential equation whose solution corresponds physically to that of free-damped vibration. The general solution to this homogeneous equation is

$$x = e^{-(c/2m)t} (c_1 e^{bt} + c_2 e^{-bt}) \quad 2.11$$

where

$$b = [(c/2m)^2 - k/m]^{1/2} \quad 2.12$$

$c_1$  and  $c_2$  are constants to be determined by initial conditions. In order to have oscillation, one will expect to have

$$(c/2m)^2 < k/m \quad 2.13$$

Apparently, there exists a critical value  $c_c$  for  $c$ , when  $(c/2m)^2$  equals  $k/m$ . Damping ratio [38],  $\zeta$ , is defined as

$$\zeta = \frac{c}{c_c} \quad 2.14$$

where

$$c_c = (4mk)^{\frac{1}{2}} \quad 2.15$$

### 2.3.2 Logarithmic Decrement ( $\delta$ )

A convenient way to determine the amount of damping present in a system is to measure the rate of decay of free oscillations. Logarithmic decrement [38] is defined as the natural logarithm of the ratio of any two successive amplitudes, as in Figure 2.3, of a free vibration.



$$\delta = \ln \frac{x_i}{x_{i+1}}$$

2.16

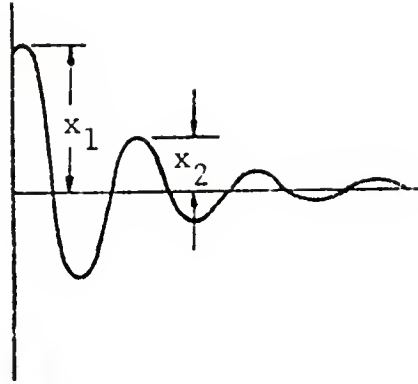


Figure 2.3: Sketch of Logarithmic Decrement

### 2.3.3 Loss Tangent ( $\tan \phi$ )

It is well known that polymer behaves as viscoelastic material, i.e., combining two material properties, one of which is perfectly elastic, while the second is viscous fluid [43]. Let such a viscoelastic material be subject to a sinusoidal stress experiment at frequency  $\omega$  such that the period  $2\pi/\omega$  of oscillation is sufficiently large as compared to the transit time of elastic waves through the specimen that stress and strain can be considered uniform throughout the test section. Under these conditions, the response to a steady-state sinusoidal stress  $\sigma$  is a steady-state sinusoidal strain  $\epsilon$  at the same frequency [44], out of phase by the angle  $\phi$ , e.g.

$$\sigma = \sigma_0 \sin \omega t$$

2.17

$$\epsilon = \epsilon_0 \sin(\omega t - \phi) \quad 2.18$$

Both the response amplitude and the phase-shift (or phase angle)  $\phi$  are frequency-dependent, but in the linear range  $\epsilon_0$  is proportional to  $\sigma_0$ . The phase relationships are conveniently shown in the rotating-vector representation of simple harmonic motion, as in Figure 2.4.

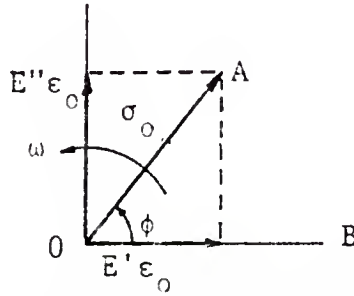


Figure 2.4: Rotating-Vector Representation of Harmonic Motion

The rotating vector OB of magnitude  $E'\epsilon_0$  lags behind the stress OA by  $\phi$  radians. Stress OA may be resolved into two components,  $E'\epsilon_0$  in phase with strain and  $E''\epsilon_0$ ,  $\pi/2$  radians out of phase with strain, as in Figure 2.4. Here  $E'$  is the storage modulus and  $E''$  is the loss modulus. The loss tangent  $\tan \phi$  is defined as

$$\tan \phi = E''/E' \quad 2.19$$

Some authors call  $\tan \phi$  the loss coefficient. The ratio  $E''/E'$  is a measure of the ratio energy loss to energy stored, as will be shown in Appendix A. For viscoelastic material, the moduli are often expressed in terms of a

complex number, called the complex modulus. In this study, the superscript \* is used to indicate the complex modulus, for example:

$$E^* = E' + iE'' \quad 2.20$$

where  $i$  is  $\sqrt{-1}$ .

#### 2.3.4 Specific Damping Capacity for Cyclic Loading ( $\psi_c$ )

The physical meaning of the hysteresis loop of Section 2.2.3 is considered here. Since materials do not behave in a perfectly elastic manner even at very low stress [46], inelasticity is always present under all types of loading, although in many cases extremely precise measurements are necessary to detect it. Under a cyclic loading condition, inelastic behaviors lead to energy dissipation. This means that the stress-strain (or load-deformation) curve is not a single-valued function but forms a hysteresis loop. Energy is absorbed by the material system under cyclic load, and the energy absorbed is proportional to the area within the hysteresis loop [46], as in Figure 2.5.

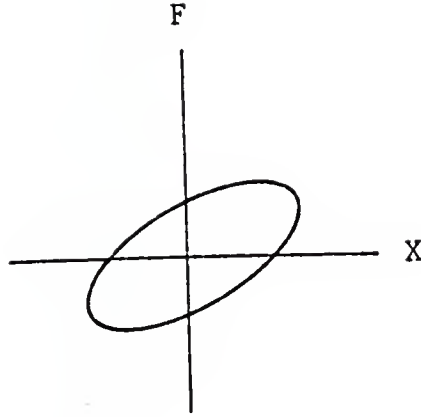


Figure 2.5: Hysteresis Loop of An Inelastic Body

Consequently, another measurement of damping called specific damping capacity [46] can be obtained by comparing the energy dissipated (or absorbed)  $(U_D)_{cyc}$  of the system in a cycle with the maximum strain energy stored  $(U_S)_{max}$  in the system during that cycle.

$$\psi_c = (U_D)_{cyc} / (U_S)_{max} \quad 2.21$$

In Appendix A, viscoelastic material is shown to have such a hysteresis loop under cyclic loading, and the same expression for specific damping capacity is obtained. The difference is that specific damping of viscoelastic material is also a function of frequency, as reported in studies [48, 49]. This is because the storage and loss moduli are functions of frequency.

For small damping, the relationships between those representations of damping are given in references [50, 51].

$$\tan\phi = \frac{\delta}{\pi} = \frac{2\zeta}{(1 - \zeta^2)^{\frac{1}{2}}} = \frac{(U_D)_{\text{cyc}}}{2\pi (U_S)_{\text{max}}} \quad 2.22$$

## CHAPTER 3 DAMPING OF UNIDIRECTIONAL FIBER COMPOSITES

### 3.1 Introduction

The objective of this chapter is to determine theoretically the damping of unidirectional fiber reinforced polymer matrix composites. The major damping mechanism of such composites is the viscoelastic behavior of the polymer and fibers. The analysis is carried out by first applying the concepts of balance of force and equal strain energy on short-fiber composite model to determine the longitudinal modulus of short-fiber composite. Then the elementary mechanics approach is used to find the modulus  $E_x$  along the loading direction as a function of the mechanical properties of the fiber and matrix materials. This is followed by applying the viscoelastic-elastic correspondence principle [45, 52] to express the mechanical properties of the composite, fiber, and matrix; then after the real and imaginary parts of complex modulus are separated, the damping of the composite can be obtained.

## 3.2 Damping Analysis of Unidirectional Fiber Composites

### 3.2.1 Short-Fiber Composite Model

The short-fiber composite model is composed of a finite-length fiber and the polymer matrix, as in Figure 3.1(a).

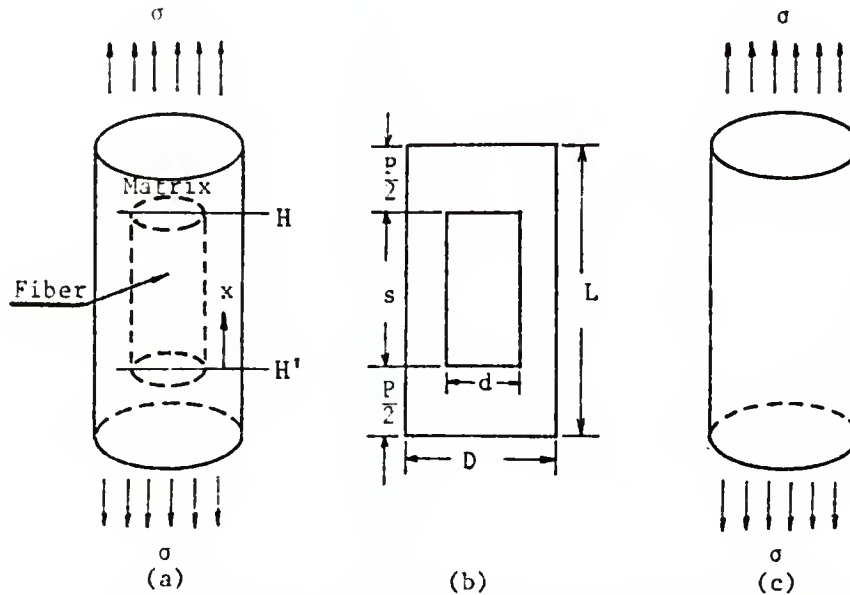


Figure 3.1: Short-Fiber Composite Model

Figure 3.1(c) is the homogeneous material equivalent to the composite of Figure 3.1(a). Figure 3.1(b) is the front middle longitudinal section view of Figure 3.1(a), where  $d$  and  $s$  are the diameter and the length of fiber, respectively;  $D$  and  $L$  are the diameter and the length of the composite model, respectively; and  $P$  is interpreted as the distance between fiber tips along fiber direction. The ratio of  $P$  to  $s$  is defined as  $R$  and is interpreted as the degree of discontinuity. During the derivation of Young's modulus along the fiber direction, the short-fiber composite model is treated as if it is composed of two

materials connected in series along the fiber direction. One material which is between sections H and H' is the mixture of fiber and matrix having length s, while the other material is just the pure matrix having length P.

As in some other analytical work [23, 31, 32] on short-fiber composites, the results of Cox's shear lag stress analysis [20] are used in this study. The expression for elastic stiffness of the discontinuous fiber composite is derived from the average of fiber stress based on Cox's fiber stress distribution (in which the longitudinal fiber stress is a function of position).

$$\sigma_f = \epsilon_f E_f \left\{ 1 - \frac{\cosh[\beta(s/2-x)]}{\cosh(\beta s/2)} \right\} \quad 3.1$$

where x,  $\beta$ , and  $\beta s/2$  are defined in Appendix B, and  $\epsilon_f$  is the strain of the fiber. In this study, the square packing array of fiber composites is considered; therefore,  $\beta s/2$  can be written, according to reference [31], as

$$\frac{\beta s}{2} = 2 \frac{s}{d} \left( \frac{G_m}{E_f \ln \frac{\pi}{4v_f}} \right)^{1/2} \quad 3.2$$

The average fiber stress is

$$\bar{\sigma}_f = \frac{1}{s/2} \int_0^{s/2} \sigma_f \, dx \quad 3.3$$



Substitute Equation 3.1 into Equation 3.3

$$\bar{\sigma}_f = \epsilon_f E_f \left[ 1 - \frac{\tanh(\beta s/2)}{\beta s/2} \right] \quad 3.4$$

For the composite between sections H and H' in Figure 3.1(a), in order to have static equilibrium, the total longitudinal force q applied to this composite must be

$$q = \bar{\sigma}_c A_c = \bar{\sigma}_f A_f + \bar{\sigma}_m A_m \quad 3.5$$

Therefore,

$$\bar{\sigma}_c = E_c \epsilon_c = \bar{\sigma}_f V_f' + \bar{\sigma}_m V_m' \quad 3.6$$

where  $V_f'$  and  $V_m'$  are the fiber volume fraction and matrix volume fraction within sections H and H' separately.

It is assumed that the composite, fiber, and matrix (all between sections H and H') have the same extensional strain  $\epsilon$ . The longitudinal modulus of material between sections H and H' can be obtained from Equation 3.6.

$$E_c = E_f V_f' \left[ 1 - \frac{\tanh(\beta s/2)}{\beta s/2} \right] + E_m V_m' \quad 3.7$$

If  $V_f'$  and  $V_m'$  are expressed in terms of  $V_f$ ,  $V_m$ , and  $R$ , Equation 3.7 can be rewritten as

$$E_c = E_f(V_f + V_f R) \left[1 - \frac{\tanh(\beta s/2)}{\beta s/2}\right] + E_m(V_m - V_f R) \quad 3.8$$

Alternatively, if the same assumption is used as in continuous fiber composites is considered, the fiber stress along longitudinal direction is assumed to be uniform everywhere in fiber, and the longitudinal modulus of material between sections H and H' can be obtained by using rule of mixtures.

$$E_c = E_f(V_f + V_f R) + E_m(V_m - V_f R) \quad 3.9$$

Equations 3.8 and 3.9 show that for continuous fiber composites, the longitudinal Young's modulus obtained by the rule of mixtures is higher than that obtained by Cox's analysis. This is because in the rule of mixture approach, uniform longitudinal fiber stress is assumed, while in the Cox's approach, uniform longitudinal fiber stress exists only at the locations far away from the fiber tips, and this longitudinal fiber stress reduces to zero at fiber tips. Finite element stress analyses [25, 26] show that the reduction of longitudinal fiber stress around fiber tips does exist; and the magnitude of this stress is not zero but finite. So it is hard to say which approach (rule of mixtures or Cox's analysis) is more

nearly correct. However, Table 3.1 shows the values of  $\tanh(\beta s/2)/(\beta s/2)$  of graphite epoxy and Kevlar epoxy with  $V_f'$  being 0.7 or 0.4. This table indicates that the modification term  $\tanh(\beta s/2)/(\beta s/2)$  becomes important when fiber volume fraction and fiber aspect ratio are both small. On the other hand, when the fiber volume fraction is greater than 0.4 and the fiber aspect ratio is greater than 100, the effect of  $\tanh(\beta s/2)/(\beta s/2)$  could be neglected.

Table 3.1: Influence of  $V_f'$  and  $s/d$  on  $\tanh(\beta s/2)/(\beta s/2)$

Composite	$V_f'$	$s/d$	$\tanh(\beta s/2)/(\beta s/2)$
Graphite-epoxy	0.4	5.	0.725
Graphite-epoxy	0.7	5.	0.369
Kevlar-epoxy	0.4	5.	0.610
Graphite-epoxy	0.4	25.	0.180
Graphite-epoxy	0.7	25.	0.074
Kevlar-epoxy	0.4	25.	0.135
Graphite-epoxy	0.4	100.	0.045

When the same external stress  $\sigma$  is applied to short-fiber composite model and to its equivalent homogeneous materials, the same strain energy density  $U$  is presumed for those two materials (Figure 3.1(a) and Figure 3.1(c))

$$U_a = U_c$$

and

$$U_a = \frac{1}{2} \frac{\sigma^2}{E_m} \frac{P}{L} + \frac{1}{2} \frac{\sigma^2}{E_c} \frac{s}{L} \quad 3.11$$

$$U_c = \frac{1}{2} \frac{\sigma^2}{E_L} \quad 3.12$$

where  $E_L$  is the longitudinal Young's modulus of the homogeneous material equivalent to short-fiber composite model. After Equations 3.11 and 3.12 are substituted in Equation 3.10,  $E_L$  can be expressed as

$$E_L = \frac{E_c E_m}{E_c \frac{R}{1+R} + E_m \frac{1}{1+R}} \quad 3.13$$

where  $E_c$  can be obtained by Equation 3.8 or Equation 3.9, and  $R$  is the ratio of  $P$  to  $s$ . When  $R$  equals zero,  $E_L$  equals  $E_c$ . On the other hand, if  $R$  is a very large number,  $E_L$  will be very close to  $E_m$ . Since the fiber aspect ratio considered in this study is between 25 and 10,000, unless specially mentioned, the modified Cox's analysis (i.e., Equations 3.8 and 3.13) is used to analyze the longitudinal Young's modulus of short-fiber composite model.

It should be noted that the continuous fiber composite can be induced either by letting the fiber aspect ratio be a very large number in the modified Cox's analysis or by letting  $R$  be zero in the modified rule of mixture.

### 3.2.2. Damping of Aligned Short-Fiber Composites

A typical representative volume element of off-axis, short-fiber composite is shown in Figure 3.2

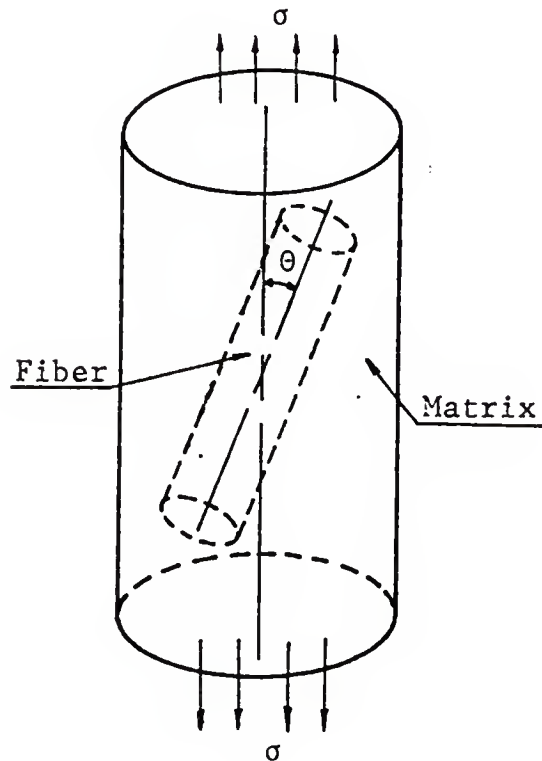


Figure 3.2: Representative Volume Element of Off-Axis Short-Fiber Composites

For a continuous aligned composite, the off-axis modulus  $E_x$  along the loading direction is given in reference [38]

$$\frac{1}{E_x} = \frac{\cos^4 \theta}{E_L} + \frac{\sin^4 \theta}{E_T} + \left( \frac{1}{G_{LT}} - 2 \frac{\nu_{LT}}{E_L} \right) \sin^2 \theta \cos^2 \theta \quad 3.14$$

where  $E_L$  and  $E_T$  represent the moduli along and transverse to the fiber direction respectively,  $G_{LT}$  is the in-plane shear modulus, and  $\nu_{LT}$  is the major Poisson's ratio. Equation 3.14 can be easily derived from the elementary mechanics approach for off-axis continuous fiber composites. For off-axis aligned short-fiber composites, one can derive a similar expression for  $E_x$  from Equation 3.14 by replacing  $E_L$ ,  $E_T$ ,  $G_{LT}$ , and  $\nu_{LT}$  by the corresponding formula for aligned short-fiber composites. The longitudinal modulus can be obtained from Equations 3.8 and 3.13. The transverse modulus  $E_T$ , in-plane shear modulus  $G_{LT}$  and the major Poisson's ratio, those material constants are assumed to be independent of length of fiber, can be obtained by using the Halpin-Tsai Equation [53] and the rule of mixtures, i.e.

$$E_T = E_m \frac{1 + 2n_1 V_f}{1 - n_1 V_f} \quad 3.15$$

$$G_{LT} = G_m \frac{1 + n_2 V_f}{1 - n_2 V_f} \quad 3.16$$

$$\nu_{LT} = \nu_{fLT} V_f + \nu_m V_m \quad 3.17$$

where

$$n_1 = \frac{(E_{fT}/E_m) - 1}{(E_{fT}/E_m) + 2} \quad 3.18$$

$$n_2 = \frac{(G_{fLT}/G_m) - 1}{(G_{fLT}/G_m) + 1} \quad 3.19$$

Up to now, all equations presented in this chapter are derived for elastic material. When a viscoelastic material is considered, the elastic-viscoelastic correspondence principle [52] can be used to obtain the corresponding relationships of viscoelastic material. For viscoelastic material the basic material properties are redefined as

$$E_{fL}^* = E'_{fL} + i E''_{fL}$$

$$E_{fT}^* = E'_{fT} + i E''_{fL}$$

$$G_{fLT}^* = G'_{fLT} + i G''_{fLT}$$

$$E_m^* = E'_m + i E''_m \quad 3.20$$

$$G_m^* = G'_m + i G''_m$$

$$\nu_m^* = \nu'_m + i \nu''_m$$

$$\nu_{fLT}^* = \nu'_{fLT}$$

$$E_x^* = E'_x + i E''_x \quad 3.21$$

Where the prime quantities indicate the storage moduli or storage Poisson's, the double prime quantities indicate the loss moduli or loss Poisson's ratio, and the  $i$  is defined as  $\sqrt{-1}$ . In this research, bulk modulus of epoxy matrix  $K_m$  is assumed to be real and independent of frequency [15]. For isotropic epoxy matrix,

$$K_m = \frac{E_m}{3(1 - 2\nu_m)} \quad 3.22$$



While the viscoelastic behavior of epoxy is considered,

$$K_m = \frac{E'_m + E''_m}{3(1 - 2\nu'_m - i 2\nu''_m)} \quad 3.23$$

The complex form of  $\nu_m$  can be obtained by Equation 3.23

$$\nu'_m + i \nu''_m = \frac{1}{2} \left( 1 - \frac{E'_m + i E''_m}{3K_m} \right) \quad 3.24$$

After separation of the real and imaginary parts of right-hand side of Equation 3.24, one will have

$$\nu'_m + i \nu''_m = \nu'_m + i \left[ \frac{E''_m}{E'_m} \left( \nu'_m - \frac{1}{2} \right) \right] \quad 3.25$$

Similarly, the complex form of shear modulus,  $G'_m + G''_m$  of viscoelastic matrix can be expressed as functions of  $E'_m$ ,  $\nu'_m$ , and  $E''_m$ , i.e.,

$$G'_m + i G''_m = \frac{E'_m}{2(1+\nu'_m)} + i \frac{E'_m}{2(1+\nu'_m)} \frac{9K_m}{9K_m - E'_m} \frac{E''_m}{E'_m} \quad 3.26$$

The complex form of  $\beta s/2$  of Equation 3.3, as shown in Appendix B, is

$$\frac{\beta' s}{2} + i \frac{\beta'' s}{2} = \frac{\beta s}{2} + i \frac{\beta s}{4} \left( \frac{G''_m}{G'_m} - \frac{E'_{fL}}{E'_{fL}} \right) \quad 3.27$$

The reason that the imaginary part of fiber Poisson's ratio is set as zero in the last equation of Equation 3.20 is because first, most fibers are known to be anisotropic materials; therefore, Equation 3.22 is not true for most fibers. Secondly, the corresponding term of  $E''_m/E'_m$  for most fibers (i.e.,  $E''_f/E'_f$ ), except Kevlar fiber, is much less than  $E''_m/E'_m$ . Due to the lack of the available data of transverse damping and shear damping, those two dampings are assumed to be equal to  $E''_{fL}/E'_{fL}$ .

It should be noted that  $\eta_m$  and  $\eta_f$  are treated as material properties, and they are defined as

$$\eta_m = \frac{E''_m}{E'_m} \quad 3.28$$

$$\eta_f = \frac{E''_{fL}}{E'_{fL}} \quad 3.29$$

By using Equations 3.25 and 3.28-3.29, the right-hand side of Equations 3.20, 3.21, and 3.27 can be rewritten as

$$E'_{fL} + i E''_{fL} = E'_{fL} (1 + i \eta_f) = E^*_{fL}$$

$$E'_{fT} + i E''_{fT} = E'_{fT} (1 + i \eta_f) = E^*_{fT}$$

$$G'_{fLT} + i G''_{fLT} = G'_{fLT} (1 + i \eta_f) = G^*_{fLT}$$

3.30

$$E'_m + i E''_m = E'_m (1 + i \eta_m) = E^*_m$$

$$G'_m + i G''_m = G'_m (1 + i \eta_{Gm}) = G^*_m$$

$$v'_m + i v''_m = v'_m + i \eta_m (v'_m - \frac{1}{2}) = v^*_m$$

$$v'_{fLT} = v_{fLT} = v^*_{fLT}$$

$$E'_x + i E''_x = E^*_x$$

$$\frac{\beta's}{2} + i \frac{\beta''s}{2} = \frac{\beta s}{2} [1 + i \frac{1}{2} (\eta_{Gm} - \eta_f)] = \frac{\beta^*s}{2}$$

where  $\eta_{Gm}$  is defined as

$$\eta_{Gm} = \frac{9K_m}{9K_m - E_m} \quad \eta_m = \frac{G''_m}{G'_m} \quad 3.31$$

From Equation 3.31, it is observed that  $\eta_{Gm}$  is higher than  $\eta_m$ . After using Equations 3.20, 3.27, and 3.30, one can rewrite Equations 3.13 and 3.15-3.17 for viscoelastic material, as follows

$$E_L^* = \frac{(E_C' + i E_C'') (E_m' + i E_m'')}{(E_C' + i E_C'') \frac{R}{1+R} + (E_m' + i E_m'') \frac{1}{1+R}} \quad 3.32$$

$$E_T^* = (E_m' + i E_m'') \frac{1 + 2n_1^* V_f}{1 - n_1^* V_f} \quad 3.33$$

$$G_{LT}^* = (G_m' + i G_m'') \frac{1 + n_2^* V_f}{1 - n_2^* V_f} \quad 3.34$$

$$V_{LT}^* = (v_{fLT}' V_f + v_m' V_m) + i \eta_m (v_m' - \frac{1}{2}) V_m \quad 3.35$$

where

$$E_C' + i E_C'' = (E_{fL}' + i E_{fL}'') (V_f + V_f R)$$

$$[1 - \frac{\tanh(\beta^* s/2)}{\beta^* s/2}] + (E_m' + i E_m'') (V_m - V_f R) \quad 3.36$$

$$\tanh(\beta^* s/2) = \tanh(\beta s/2)$$

$$+ i \frac{\beta s}{2} \frac{\eta_{Gm} - \eta_f}{2} \frac{1}{\cosh^2(\beta s/2)} \quad 3.37$$

$$n_1^* = \frac{(E'_{fT} + i E''_{fT}) / (E'_m + i E''_m) - 1}{(E'_{fT} + i E''_{fT}) / (E'_m + i E''_m) + 2} \quad 3.38$$

$$n_2^* = \frac{(G'_{fLT} + i G''_{fLT}) / (G'_m + G''_m) - 1}{(G'_{fLT} + i G''_{fLT}) / (G'_m + G''_m) + 1} \quad 3.39$$

After substitute  $E_L^*$ ,  $E_T^*$ ,  $G_{LT}^*$ , and  $v_{LT}^*$  from Equations 3.32-3.35 for  $E_L$ ,  $E_T$ ,  $G_T$ , and  $v_{LT}$ , respectively, and  $E_x + iE_x$  for  $E_x$  into Equation 3.14, one obtains

$$\frac{1}{E'_x + iE''_x} = \frac{\cos^4 \theta}{E_L^*} + \frac{\sin^4 \theta}{E_T^*} + \left( \frac{1}{G_{LT}^*} - 2 \frac{v_{LT}^*}{E_L^*} \right) \cos^2 \theta \sin^2 \theta \quad 3.40$$

Damping of the aligned short-fiber composite along  $x$  direction,  $\eta_x$ , is then determined by

$$\eta_x = \frac{E''_x}{E'_x} \quad 3.41$$

Equations 3.40 and 3.41 show that material damping and stiffness of aligned short-fiber composite are functions of material properties of fiber (i.e.,  $E'_{fL}$ ,  $E'_{fT}$ ,  $G'_{fLT}$ ,  $v_{fLT}$ , and  $\eta_f$ ) and matrix (i.e.,  $E'_m$ ,  $v'_m$ , and  $\eta_m$ ), fiber aspect ratio ( $s/d$ ), fiber volume fraction ( $V_f$ ), degree of

discontinuity ( $R$ ), loading direction ( $\theta$ ), and packing geometry of fiber. If the four different kinds of pre-packed tapes (glass-epoxy, Kevlar-epoxy, graphite-epoxy, and boron-epoxy) are used to make the fiber composite, the design variables utilized to analyze the stiffness and material damping are  $s/d$ ,  $\theta$ ,  $R$ ,  $V_f$ ,  $\underline{E}_f$  ( $\{E'_{fL}, E'_{fT}, G'_{fLT}, \nu_{fLT}, \nu_f^I, \eta_m\}$ ), and  $\underline{E}_m$  ( $\{E'_m, \nu_m^I, \eta\}$ ), i.e.

$$E'_x = f_1 (\underline{E}_f, \underline{E}_m, s/d, \theta, R, V_f) \quad 3.42$$

$$\eta_x = f_2 (\underline{E}_f, \underline{E}_m, s/d, \theta, R, V_f) \quad 3.43$$

A similar approach can be applied to determine damping along  $y$  direction,  $\eta_y$ , and stiffness along  $y$  direction,  $E'_y$ .

## CHAPTER 4 DAMPING OF RANDOMLY ORIENTED SHORT-FIBER COMPOSITES

### 4.1 Introduction

The objective of this chapter is to determine analytically the material damping of in-plane randomly oriented short-fiber composites. The analysis is carried out by using the extension of the short-fiber composite model and part of the results obtained in Chapter 3. An averaging procedure is first applied to the six off-axis reduced stiffnesses  $Q_{ij}$  ( $i, j = 1, 2, 6$ ) with respect to the angle  $\theta$  between the fiber orientation and the applied load. The results of integration show that in-plane randomly oriented fiber composites behave like a planar isotropic material. By using the properties of isotropic materials, Young's and shear moduli can be obtained as functions of the reduced stiffnesses  $Q_{ij}$  ( $i, j = 1, 2, 6$ ). After the application of the elastic-viscoelastic correspondence principle and separation of the real and imaginary parts of the complex Young's and shear moduli, material damping is obtained.

## 4.2 Damping Analysis of In-Plane Randomly Oriented Short-Fiber Composites

For in-plane randomly oriented short-fiber composites, no difference caused by different direction parallel to the planes on which fibers are laid. The averaging procedure is one of the approaches which will lead to the isotrop. Therefore, an averaging by integrating the six moduli of off-axis short-fiber composites with respect to  $\theta$  from  $\theta=0$  to  $\theta=\pi$  should be used. However, from Equation 3.14 for  $E_x$  and similar Equations for  $E_y$ ,  $G_{xy}$ ,  $\nu_{xy}$ ,  $m_x$  and  $m_y$  [38], one finds that it is not convenient to integrate and obtain the average  $\tilde{E}_x$  in closed form in terms of  $E_L$ ,  $E_T$ ,  $G_{LT}$ , and  $\nu_{LT}$ . Instead of integrating the six engineering moduli, one can integrate the six components of the off-axis reduced stiffness of the plane stress case  $\bar{Q}_{ij}$  ( $i, j = 1, 2, 6$ ) and obtain the average  $\tilde{Q}_{ij}$ , i.e.

$$\tilde{Q}_{ij} = \frac{1}{\pi} \int_0^{\pi} \bar{Q}_{ij} d\theta \quad i, j = 1, 2, 6 \quad 4.1$$

The expression for  $\bar{Q}_{ij}$  ( $i, j = 1, 2, 6$ ) as a function of  $\theta$  can be found in reference [38]. After integrating with respect to  $\theta$  from  $\theta=0$  to  $\theta=\pi$  and then dividing each of the result by  $\pi$ , one obtains



$$\tilde{Q}_{11} = \tilde{Q}_{22} = \frac{3}{8} (Q_{11} + Q_{22}) + \frac{1}{4} (2Q_{66} + Q_{12}) \quad 4.2$$

$$\tilde{Q}_{66} = \frac{1}{8} (Q_{11} + Q_{22}) - \frac{1}{4} Q_{12} + \frac{1}{2} Q_{66} \quad 4.3$$

$$\tilde{Q}_{12} = \frac{1}{8} (Q_{11} + Q_{22}) + \frac{3}{4} Q_{12} - \frac{1}{2} Q_{66} \quad 4.4$$

$$\tilde{Q}_{16} = \tilde{Q}_{66} = 0 \quad 4.5$$

It is easy to show from Equations 4.2-4.4 that the following relation exists

$$\tilde{Q}_{12} + 2\tilde{Q}_{66} = \tilde{Q}_{11} \quad 4.6$$

Therefore, after integration, there are only two independent material constants, namely,  $\tilde{Q}_r$  and  $\tilde{G}_r$ .

$$\tilde{Q}_r = \tilde{Q}_{11} \quad 4.7$$

$$\tilde{G}_r = \tilde{Q}_{66} \quad 4.8$$

This implies, as expected, that in-plane randomly oriented short-fiber composites behave as planar isotropic materials with two independent material constants. The subscript r represents randomly oriented short-fiber composites.

For isotropic materials, the following relations exist

$$\tilde{Q}_r = \frac{\tilde{E}_r}{1 - \tilde{\nu}^2} \quad 4.9$$

$$\tilde{G}_r = \frac{\tilde{E}_r}{2(1 + \tilde{\nu})} \quad 4.10$$

where  $\tilde{\nu}$  is defined by  $\tilde{Q}_{12}/\tilde{Q}_{11}$ . Elimination of  $\tilde{\nu}$  from Equations 4.9 and 4.10 yields the expression for  $\tilde{E}_r$ , the Young's modulus of a randomly oriented short-fiber composite as a function of  $\tilde{G}_r$  and  $\tilde{Q}_r$ .

$$\tilde{E}_r = 4 \tilde{G}_r \left(1 - \frac{\tilde{G}_r}{\tilde{Q}_r}\right) \quad 4.11$$

Substitution of Equations 4.2, 4.3, 4.7, and 4.8 in Equation 4.11 yields  $\tilde{E}_r$  as a function of the four reduced stiffness  $Q_{11}$ ,  $Q_{22}$ ,  $Q_{12}$ , and  $Q_{66}$ .

$$\tilde{E}_r = \left[ \frac{1}{2} (Q_{11} + Q_{22}) - Q_{12} + 2Q_{66} \right] \left[ 1 - \frac{Q_{11} + Q_{22} - 2Q_{12} + 4Q_{66}}{3(Q_{11} + Q_{22}) + 2(Q_{12} + 2Q_{66})} \right] \quad 4.12$$

Similarly,

$$\tilde{G}_r = \frac{1}{8} (Q_{11} + Q_{22}) - \frac{1}{4}Q_{12} + \frac{1}{2}Q_{66} \quad 4.13$$

Since  $Q_{11}$ ,  $Q_{22}$ ,  $Q_{12}$ , and  $Q_{66}$  are directly related to the four basic engineering constants  $E_L$ ,  $E_T$ ,  $G_{LT}$ , and  $\nu_{LT}$  (defined in Equations 3.13, 3.15, 3.16, and 3.17), according to Equations 4.12 and 4.13,  $\tilde{E}_r$  and  $\tilde{G}_r$  can be expressed as functions of  $E_L$ ,  $E_T$ ,  $G_{LT}$ , and  $\nu_{LT}$ .

Next, as in Section 3.2.2 for aligned short-fiber composites, according to the elastic-viscoelastic correspondence principle, one may replace  $\tilde{E}_r$  by  $\tilde{E}_r^* = \tilde{E}_r' + i \tilde{E}_r''$ ,  $\tilde{G}_r$  by  $\tilde{G}_r^* = \tilde{G}_r' + i \tilde{G}_r''$ ,  $E_L$  by  $E_L^*$ ,  $E_T$  by  $E_T^*$ ,  $G_{LT}$  by  $G_{LT}^*$ ,  $\nu_{LT}$  by  $\nu_{LT}^*$  where  $E_L^*$ ,  $E_T^*$ ,  $G_{LT}^*$ , and  $\nu_{LT}^*$ , are defined in Equations 3.32-3.35. After separation of the real and imaginary parts, the material damping constants  $\eta_r$  and  $\eta_{Gr}$  of in-plane randomly oriented short-fiber composites can be obtained.

$$\eta_r = \frac{\tilde{E}_r''}{\tilde{E}_r'} \quad 4.14$$

$$\eta_{Gr} = \frac{\tilde{G}_r''}{\tilde{G}_r'} \quad 4.15$$

An alternative way of determining  $\tilde{E}_r$  and  $\tilde{G}_r$  is given in Appendix C.

CHAPTER 5  
DAMPING OF LAMINATED FIBER COMPOSITES--  
LAMINATED PLATE THEORY APPROACH

5.1 Introduction

In this study, laminated plate theory and an energy approach are used to analyze the material damping and stiffness of symmetrically laminated fiber composites. In this chapter, we will discuss all analytical work of laminated plate theory approach, while in Chapter 6 the energy approach will be presented.

According to laminated plate theory, the constitutive equations (Equation 5.1) have already been given in references [38, 50], in terms of  $[A]$ ,  $[B]$ , and  $[D]$  (i.e.  $[A]^*$ ,  $[B]^*$ , and  $[D]^*$ ) matrices. Material damping of laminated composites can then be derived from the expression of  $[A]$ ,  $[B]$ , and  $[D]$ .

5.2 Damping Analysis of Laminated Fiber Composites  
Through Laminated Plate Theory Approach

For a laminated fiber composite plate, as in Figure 5.1, the constitutive equations are given in references [38, 50] as shown in Equation 5.1.

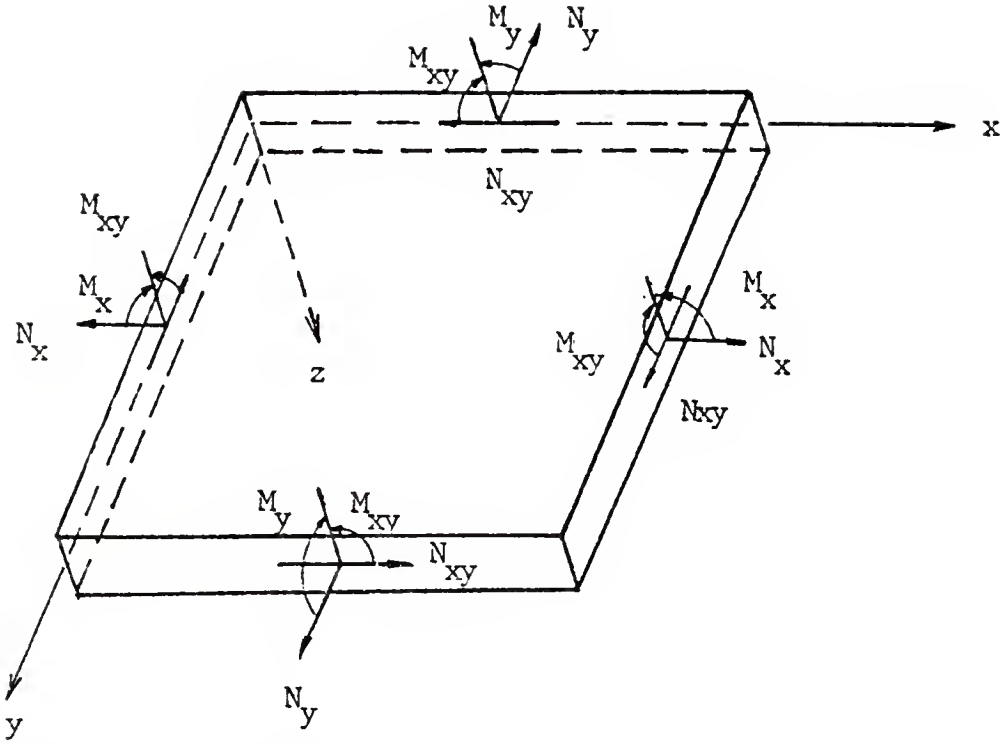


Figure 5.1: Sketch of Laminated Fiber Composite Plate

$$\begin{Bmatrix} N_x \\ N_y \\ N_{xy} \\ M_x \\ M_y \\ M_{xy} \end{Bmatrix} = \begin{bmatrix} A_{11} & A_{12} & A_{16} & B_{11} & B_{12} & B_{16} \\ & A_{22} & A_{26} & B_{12} & B_{22} & B_{26} \\ & & A_{66} & B_{16} & B_{26} & B_{66} \\ & & & D_{11} & D_{12} & D_{16} \\ \text{Symm} & & & & D_{22} & D_{26} \\ & & & & & D_{66} \end{bmatrix} \begin{Bmatrix} \epsilon_x^\circ \\ \epsilon_y^\circ \\ \gamma_{xy}^\circ \\ k_x \\ k_y \\ k_{xy} \end{Bmatrix}$$

In Equation 5.1,  $\epsilon_x^\circ$ ,  $\epsilon_y^\circ$ , and  $\gamma_{xy}^\circ$  are middle plane strains,  $k_x$ ,  $k_y$  and  $k_{xy}$  are plate curvatures defined in [38, 50], and  $A_{ij}$ ,  $B_{ij}$ , and  $D_{ij}$  ( $i, j = 1, 2, 6$ ) are the equivalent reduced in-plane stiffness, coupling stiffness and reduced flexure stiffness, respectively. They are expressed in terms of  $\bar{Q}_{ij}$  and total thickness of the plate,  $h$ , as follows:

$$A_{ij} = \int_{-h/2}^{h/2} \bar{Q}_{ij} dz = \sum_{k=1}^n (\bar{Q}_{ij})_k (h_k - h_{k-1}) \quad 5.2a$$

$$B_{ij} = \int_{-h/2}^{h/2} z \bar{Q}_{ij} dz = \sum_{k=1}^n \frac{1}{2} (\bar{Q}_{ij})_k (h_k^2 - h_{k-1}^2) \quad 5.2b$$

$$D_{ij} = \int_{-h/2}^{h/2} z^2 \bar{Q}_{ij} dz = \sum_{k=1}^n \frac{1}{3} (\bar{Q}_{ij})_k (h_k^3 - h_{k-1}^3) \quad 5.2c$$

where  $\bar{Q}_{ij}$  can be expressed in vector form [50]

$$\left\{ \begin{array}{c} \bar{Q}_{11} \\ \bar{Q}_{22} \\ \bar{Q}_{12} \\ \bar{Q}_{66} \\ \bar{Q}_{16} \\ \bar{Q}_{26} \end{array} \right\} = \left[ \begin{array}{ccc} U_1 & U_2 & U_3 \\ U_1 & -U_2 & U_3 \\ U_4 & 0 & -U_3 \\ U_5 & 0 & -U_3 \\ 0 & \frac{1}{2}U_2 & U_3 \\ 0 & \frac{1}{2}U_2 & -U_3 \end{array} \right] \left\{ \begin{array}{c} 1 \\ \cos 2 \theta \\ \cos 4 \theta \end{array} \right\} \quad 5.3$$

and

$U_i$  ( $i = 1, 2 \dots 5$ ) are defined in [50] as

$$U_1 = \frac{1}{8} (3Q_{11} + 3Q_{22} + 2Q_{12} + 4Q_{66})$$

$$U_2 = \frac{1}{8} (4Q_{11} - 4Q_{22})$$

$$U_3 = \frac{1}{8} (Q_{11} + Q_{22} - 2Q_{12} - 4Q_{66}) \quad 5.4$$

$$U_4 = \frac{1}{8} (Q_{11} + Q_{22} + 6Q_{12} - 4Q_{66})$$

$$U_5 = \frac{1}{8} (Q_{11} + Q_{22} - 2Q_{12} + 4Q_{66})$$

$Q_{ij}$  ( $i, j = 1, 2, 6$ ) are known to be, by references [38, 50],

$$\begin{aligned} Q_{11} &= \frac{E_L}{1 - \nu_{LT} \nu_{TL}} \\ Q_{22} &= \frac{E_T}{1 - \nu_{LT} \nu_{TL}} \\ Q_{12} &= \frac{\nu_{LT} E_T}{1 - \nu_{LT} \nu_{TL}} \\ Q_{66} &= G_{LT} \end{aligned} \tag{5.5}$$

and

$$\nu_{TL} = \frac{\nu_{LT} E_T}{E_L} \tag{5.6}$$

where  $E_L$ ,  $E_T$ ,  $G_{LT}$ , and  $\nu_{LT}$  are defined in Equations 3.13, 3.15-3.17. Interesting relations should be noted that  $\bar{Q}_{ij}$  ( $i, j = 1, 2, 6$ ) of Equation 5.3 will be equal to  $\tilde{Q}_{ij}$  of Equations 4.2-4.5, providing  $U_2$  and  $U_3$  are set as zero.

Equation 5.1 can be rewritten in matrix form as

$$\begin{Bmatrix} N \\ M \end{Bmatrix} = \begin{bmatrix} A & B \\ B & D \end{bmatrix} \begin{Bmatrix} \epsilon^o \\ k \end{Bmatrix} \tag{5.7}$$



For symmetric laminates, the coupling stiffness matrix B is a zero matrix, and Equations 5.1 and 5.7 can be uncoupled as

$$\begin{Bmatrix} N_x \\ N_y \\ N_{xy} \end{Bmatrix} = \begin{bmatrix} A_{11} & A_{12} & A_{16} \\ A_{12} & A_{22} & A_{26} \\ A_{16} & A_{26} & A_{66} \end{bmatrix} \begin{Bmatrix} \epsilon_x^\circ \\ \epsilon_y^\circ \\ \gamma_{xy}^\circ \end{Bmatrix} \quad 5.8a$$

or

$$\{N\} = [A] \{\epsilon^\circ\} \quad 5.8b$$

and

$$\begin{Bmatrix} M_x \\ M_y \\ M_{xy} \end{Bmatrix} = \begin{bmatrix} D_{11} & D_{12} & D_{16} \\ D_{12} & D_{22} & D_{26} \\ D_{16} & D_{26} & D_{66} \end{bmatrix} \begin{Bmatrix} k_x \\ k_y \\ k_{xy} \end{Bmatrix} \quad 5.9a$$

or

$$\{M\} = [D] \{k\} \quad 5.9b$$

From Equation 5.8a and the definition of  $A_{ij}$ , one can express in-plane moduli  $E_{ij}$  ( $i, j = 1, 2, 6$ ) as

$$E_{ij} = \frac{1}{\frac{-1}{A_{ij}}} \frac{1}{h} \quad 5.10$$

where  $h$  is the total thickness of laminated composite and  $A_{ij}^{-1}$  are the elements of the inverse of matrix  $[A_{ij}]$ , and  $A_{ij}^{-1}$  are determined by the following system of equations.

$$\begin{bmatrix} A_{11}^{-1} & A_{12}^{-1} & A_{16}^{-1} \\ A_{12}^{-1} & A_{22}^{-1} & A_{26}^{-1} \\ A_{16}^{-1} & A_{26}^{-1} & A_{66}^{-1} \end{bmatrix} \begin{bmatrix} A_{11} & A_{12} & A_{16} \\ A_{12} & A_{22} & A_{26} \\ A_{16} & A_{26} & A_{66} \end{bmatrix} = \begin{bmatrix} 1 & 0 & 0 \\ 0 & 1 & 0 \\ 0 & 0 & 1 \end{bmatrix} \quad 5.11$$

According to elastic-viscoelastic correspondence principle, when the viscoelastic behaviors of fiber composites are considered the elastic material constants  $E_L$ ,  $E_T$ ,  $G_{LT}$ , and  $\nu_{LT}$  (defined in Equations 3.13, 3.15-3.17) should be replaced by the corresponding complex moduli, respectively. Consequently, the complex form of Equations 5.8 and 5.9 can be written as

$$\begin{Bmatrix} N_x^* \\ N_y^* \\ N_{xy}^* \end{Bmatrix} = \begin{bmatrix} A_{11}^* & A_{12}^* & A_{16}^* \\ A_{12}^* & A_{22}^* & A_{26}^* \\ A_{16}^* & A_{26}^* & A_{66}^* \end{bmatrix} \begin{Bmatrix} \epsilon_x^* \\ \epsilon_y^* \\ \gamma_{xy}^* \end{Bmatrix} \quad 5.12a$$

or

$$\{N^*\} = [A^*] \{\epsilon^o\} \quad 5.12b$$

$$\begin{Bmatrix} M_x^* \\ M_y^* \\ M_{xy}^* \end{Bmatrix} = \begin{bmatrix} D_{11}^* & D_{12}^* & D_{16}^* \\ D_{12}^* & D_{22}^* & D_{26}^* \\ D_{16}^* & D_{26}^* & D_{66}^* \end{bmatrix} \begin{Bmatrix} k_x \\ k_y \\ k_{xy} \end{Bmatrix} \quad 5.13a$$

or

$$\{M^*\} = [D^*] \{k\} \quad 5.13b$$

The corresponding complex form of in-plane complex moduli  $E_{ij}^*$  can be expressed as

$$E_{ij}^* = \frac{1}{(A_{ij}^*)^{-1}} = E'_{ij} + iE''_{ij} \quad 5.14$$

where  $(A_{ij}^*)^{-1}$  is the element in the  $i$ th row and  $j$ th column of the inverse of matrix  $[A_{ij}^*]$ . Appendix D shows the detail of the derivation of  $(A_{ij}^*)^{-1}$ .

The in-plane material damping  $I\eta_{ij}$  and flexure material damping  $F\eta_{ij}$  are defined as follows:

$$I\eta_{ij} = \frac{E''_{ij}}{E'_{ij}} \quad i, j = 1, 2, 6 \quad 5.15$$

$$F_{ij}^{\eta} = \frac{D_{ij}^{\eta}}{D_{ij}'} \quad i, j = 1, 2, 6 \quad 5.16$$

For the same kind of fiber composite, the result obtained by Equation 5.15 for sixteen plies of unidirectional laminated composite is same as that obtained by Equation 3.41 for laminar composite with the same off-axis angle  $\theta$ . This indicates that the approach presented in this chapter is correct, although it may not be convenient because the inverse of a complex matrix is involved.

## CHAPTER 6

### DAMPING OF LAMINATED FIBER COMPOSITES--ENERGY APPROACH

#### 6.1 Introduction

The drawback of damping analysis using laminated plate theory approach is that it does not include the effect of interlaminar stresses (the stresses at the interfaces of laminated composites). It has been shown in study [54] that even when an in-plane uniform tension load is applied to the laminated composites, there do exist appreciable interlaminar stresses around the free edges.

In this chapter, an energy approach in conjunction with a three-dimensional finite-element method [55, 56] is used to analyze the material damping under certain loading and boundary conditions. It is believed that this model represents a more realistic approach by including the energy dissipated at the interfaces. By using this approach, we improve the approach from a two-dimensional, classical, laminated plate theory to a three-dimensional elasticity theory.

## 6.2 Damping Analysis of Laminated Fiber Composites Through Energy Approach

The damping of laminated materials in the first mode vibration is determined as

$$\eta = \frac{\sum_{q=1}^n (qU_D)_{cyc}}{\sum_{q=1}^n 2\pi qU_s} \quad 6.1$$

where  $n$  is the total number of the plies,  $(qU_D)_{cyc}$  is the energy dissipated in the  $q$ th layer during a cycle, and  $qU_s$  is the maximum strain energy stored in the  $q$ th layer.

Detailed expressions of  $(qU_D)_{cyc}$  and  $qU_s$  are given in Appendix E in which the energy expressions for a visco-elastic material given in reference [57] are used.

The analytical expression of the maximum strain energy  $U_s$  for an elastic body is

$$U_s = \frac{1}{2} \int_v \epsilon_j C_{jk} \epsilon_k dv \quad 6.2$$

( $j, k = 1, 2 \dots 6$ )

where  $\epsilon_j$  are the maximum strains, and  $C_{jk}$  are the moduli of the elastic body.

The expressions of  $C_{jk}$  ( $j, k = 1, 2 \dots 6$ ) for orthotropic elastic material are given by Jones [58]; here  $k$  and  $j$  axes are material principal axes. In this study, each layer of fiber composite is considered to be

transversely isotropic material. Therefore, as presented in Appendix F.1, the moduli of  $m$ th layer fiber composite could be defined as functions

$$(C_{jk})_m = f(E_L, E_T, G_{LT}, \nu_{LT}, \nu_{TT'})_m \quad 6.3$$

where  $E_L$ ,  $E_T$ ,  $G_{LT}$ , and  $\nu_{LT}$  are given in Section 3.1 for short-fiber composites, and  $\nu_{TT'}$  is assumed equal to  $\nu_m$ . An analytical expression for  $\nu_{TT'}$  is available in the literature [38], but the assumption that  $\nu_{TT'} = \nu_m$  is believed to be accurate enough in our analysis. According to the elastic-viscoelastic correspondence principle, when the viscoelastic behaviors of the body are considered,  $E_L$ ,  $E_T$ ,  $G_{LT}$ ,  $\nu_{LT}$ ,  $\nu_{TT'}$  should be replaced by  $E_L^*$ ,  $E_T^*$ ,  $G_{LT}^*$ ,  $\nu_{LT}^*$ , and  $\nu_{TT'}^*$ , respectively. For example,

$$C_{12} = \frac{\nu_{TL} E_L}{1 - \nu_{TL} \nu_{LT}} \quad 6.4$$

changes into

$$C_{12}^* = \frac{(\nu_{TL}' + i\nu_{TL}'') (E_L' + iE_L'')}{1 - (\nu_{TL}' + i\nu_{TL}'') (\nu_{LT}' + i\nu_{LT}'')} \quad 6.5$$

or

$$C_{12}^* = C_{12}' + i C_{12}'' \quad 6.6$$

After separating the real and imaginary parts and using matrix rotation (if the material principal axes do not coincide with the global axes), the complex moduli  $\bar{C}^*$  with respect to the global axes (i.e., x, y, and z axes) of the kth layer of fiber composites are then obtained in the form

$$[\bar{C}^*]_k = [\bar{C}']_k + i [\bar{C}'' ]_k \quad 6.7$$

where  $C'$  are storage moduli, and  $C''$  are loss moduli. All three matrices are symmetric matrices.

The storage energy  ${}_qU_s$  and the dissipated energy during a cycle  $({}_qU_s)_{cyc}$  in the qth layer of laminated composites can be expressed as

$${}_qU_s = \frac{1}{2} \int_{v_q} \epsilon_j \quad C'_{jk} \quad \epsilon_k \quad dv \quad 6.8$$

and

$$({}_qU_D)_{cyc} = \pi \int_{v_q} \epsilon_j \quad C''_{jk} \quad \epsilon_k \quad dv \quad 6.9$$

correspondingly. Consequently, the material damping of a n layers laminated composite in the first mode vibration



$$\eta = \frac{\sum_{q=1}^n \int_{V_q} \{\epsilon\}^T [\bar{C}'' ] \{\epsilon\} dv}{\sum_{q=1}^n \int_{V_q} \{\epsilon\}^T [\bar{C}' ] \{\epsilon\} dv} \quad 6.10$$

where strain field  $\{\epsilon\}$  depends on the loading and boundary conditions, and the strain field would be determined in this study through a three-dimensional finite element method.

From Equation 6.10, one may thus arrive that even a highly dissipative modulus cannot contribute significantly to the total loss factor  $\eta$ , if it's associated strain (or stress) does not participate considerably in the total stored energy.

The procedures taken in energy approach are briefly described as follows:

Step 1:

As in the laminated theory approach, the elastic solution is first sought in energy approach. The equation of motion of an elastic body in static case can be derived from the principle of stationary potential energy given in reference [59].

$$\delta(U - W_e) = 0 \quad 6.11$$

where  $U$  and  $W_e$  are the strain energy and the work done by external forces, respectively.

Step 2:

After the assumed displacement function (as a function of nodal displacement  $\bar{q}$ ) is substituted into Equation 6.11, the equations of motion can be expressed as a system of equations (details are given in Appendix F.2).

$$[\bar{k}] \{\bar{q}\} = \{\bar{f}\} \quad 6.12$$

where  $[\bar{k}]$  is the stiffness matrix, and  $\{\bar{f}\}$  is the nodal forces.

Step 3:

After the displacement field is determined by substituting the solution of Equation 6.12 into the assumed displacement function, the strain field  $\{\epsilon\}$  of the elastic body could be obtained through displacement-strain relations.

Step 4:

Once the strain field of an elastic body is known, the material damping of a viscoelastic body under the same loading and boundary conditions can be determined by Equation 6.10.

6.3 Loading and Boundary Conditions

Two sets of loading and boundary conditions are discussed in this study. However, other loading and boundary conditions can also be accommodated in this approach.

Case 1: Uniform in-plane tension load.

In this case, only one quarter of the plate is analyzed by finite element method. External stress  $\sigma$  is applied at one edge.

Case 2: One side clamped plate under  $M_x$  load.

In this case, the plate is clamped at  $x=0$ . The external force  $F$  is applied along  $x=L$ , and the external force  $-F$  is applied along  $x=0.983L$ .

The numerical results are presented in Section 9.5.

## CHAPTER 7 EXPERIMENTAL MEASUREMENT OF DAMPING

### 7.1 Introduction

Free vibration decay [9], band-width method [9], resonant-dwell method [60], forced-vibration techniques [61], and impulse techniques [62, 63, 64] are the very popular experimental techniques used to measure the material damping. All of these tests are subject to the air drag [65, 66], if the tests are not conducted under a vacuum condition. In this study, an improved impulse technique approach [64] is utilized to measure the material damping.

The impulse technique consists of the application of a force pulse at a point on the test structure and the measurement of the response at another point. The input force and response signal are digitally processed by the analyzer to form the frequency response function or transfer function. Damping and natural frequencies can then be extracted from the output of the analyzer. All measures are performed using a digital signal processing technique. It involves filtering and sampling the input wave forms. The sampling process converts a voltage (at a certain point in time) into a numerical representation.

These numbers are then processed digitally to produce the various calculations performed by the analyzer. The primary output from the Fourier analyzer is the frequency response function, which is a measure of system's characteristics. The analyzer also calculates the coherence function, which ranges from 0.0 to 1.0. The larger the potential measurement noise or the system non-linearity, the lower the coherence function will be [67]. A coherence value of unity indicates that the output is completely related to the input. Thus, the coherence function used here is a measure of the "quality" of the data.

## 7.2 Apparatus

The composite plates or beams are fixed by two aluminum blocks at one end. A non-contact probe (KD-2310-3U, Kaman Science Corporation, Colorado Springs, Colorado), known as a motion transducer, is located about 1.5 mm below the tip of each specimen. This motion transducer operates under the principle of eddy current. An aluminum foil target of diameter 20 mm is cemented underneath the tip of the specimen. A force transducer is mounted to the head of the impulse hammer (Model K291A, Piezotronics, Inc., New York), to measure the force input to the specimen. The other tip of the hammer is connected to the fixed spring so that the magnitude, location, and the dwelling time of the impact load can be controlled. To

improve the coherence, an octave filter (4302 dual 24db, Ithaco, Inc., New York), which is connected to the force transducer at the hammer tip on one end and to the Fast Fourier Analyzer (FFT, Model 5420, Hewlett Packard) on the other end, is used to magnify the input signal 100 times. The impact point is near the stiffer portion of the specimen. The excitation and response signals are fed into the FFT analyzer, which displays the frequency response function and coherence function. Each frequency response and each coherence function are based on a statistical analysis of an ensemble of six tests. A schematic drawing of the experimental set-up is shown in Figure 7.1.

The frequency response function is a complex valued function. A typical experimental display of the real and imaginary parts of the frequency response function for a graphite-epoxy composite, according to reference [64], is shown in Figure 7.2 and an enlarged schematic drawing of real part of frequency response function is shown in Figure 7.3. As prescribed in references [62, 63, 64], the peak of the imaginary part determines the resonant frequency, and then from the corresponding real part (see Figure 7.3) the material damping (loss factor,  $\eta$ ) can be calculated by

$$\eta = \frac{(f_a/f_b)^2 - 1}{(f_a/f_b)^2 + 1} \quad 7.1$$

In using the impulse technique to measure the material damping, following precautions, as reported in study [64], must be taken.

1. In order to improve the accuracy of experimental data of damping associated with a particular mode of vibration, the values of natural frequency within the frequency range of interest (say 0 to 1,600 Hz) are first approximately determined. Then a zooming technique to increase the resolution of the response in the neighborhood of this particular frequency is used.
2. It is necessary to avoid measurement of response near a nodal point for the modes to be tested. Such measurements would consist primarily of noise, since the actual response is very small near nodal points.
3. The amplitude of the vibration must be kept below the thickness of the specimen to ensure that air damping (air drag) is negligible, since the air damping is linearly proportional to the amplitude-to-thickness ratio of the beam specimen [66].
4. It is important to optimize the Analog to Digital Converter (ADC) range setting on an FFT analyzer before making a measurement, since an optimized ADC range set will increase resolution in the digitizing process [35].

Recently, Suarez and Gibson [35, 36], did some experiments on material damping of short-fiber composite

through impulse hammer technique. Some of those experimental results for unidirectional short-fiber composites presented in this chapter are compared with the analytical results.



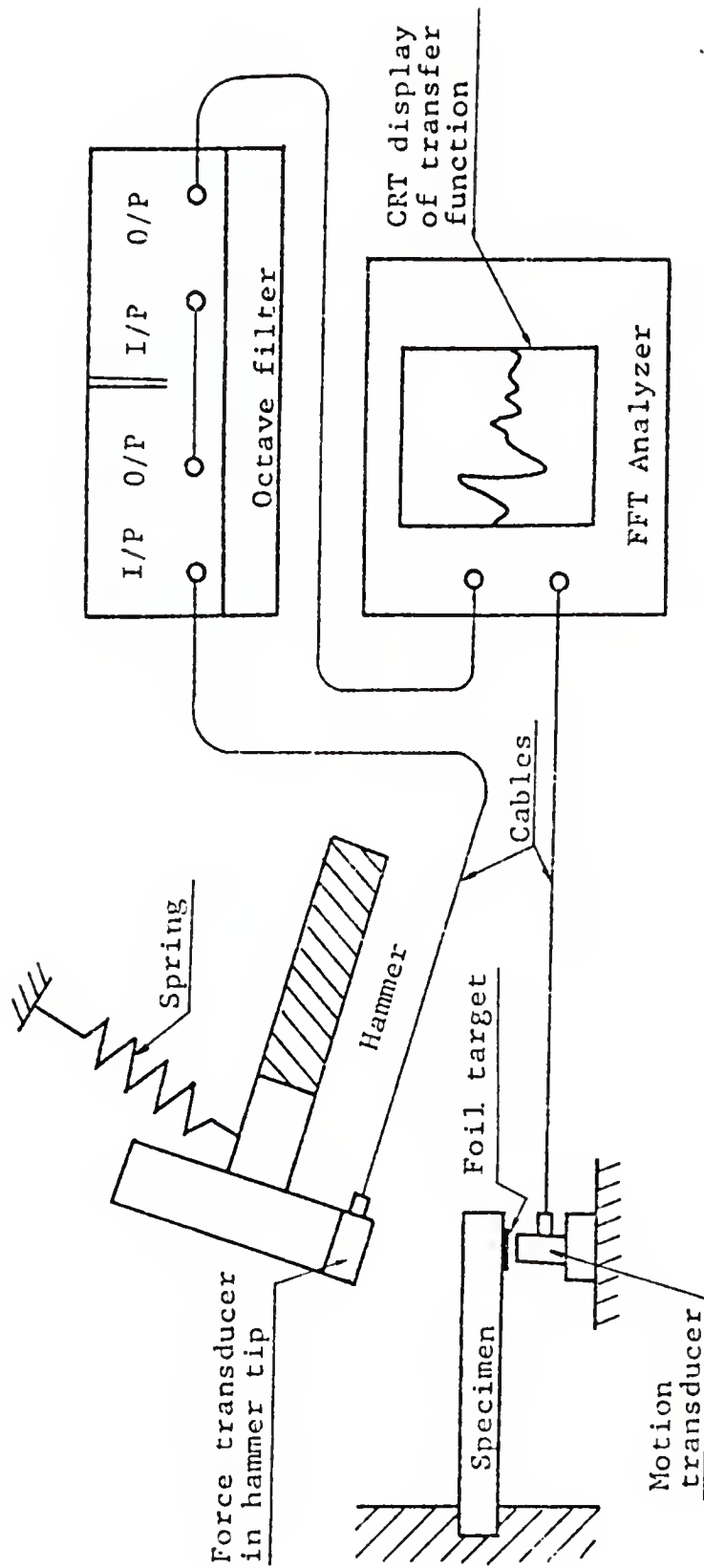


Figure 7.1: Schematic Drawing of the Experimental Set-Up

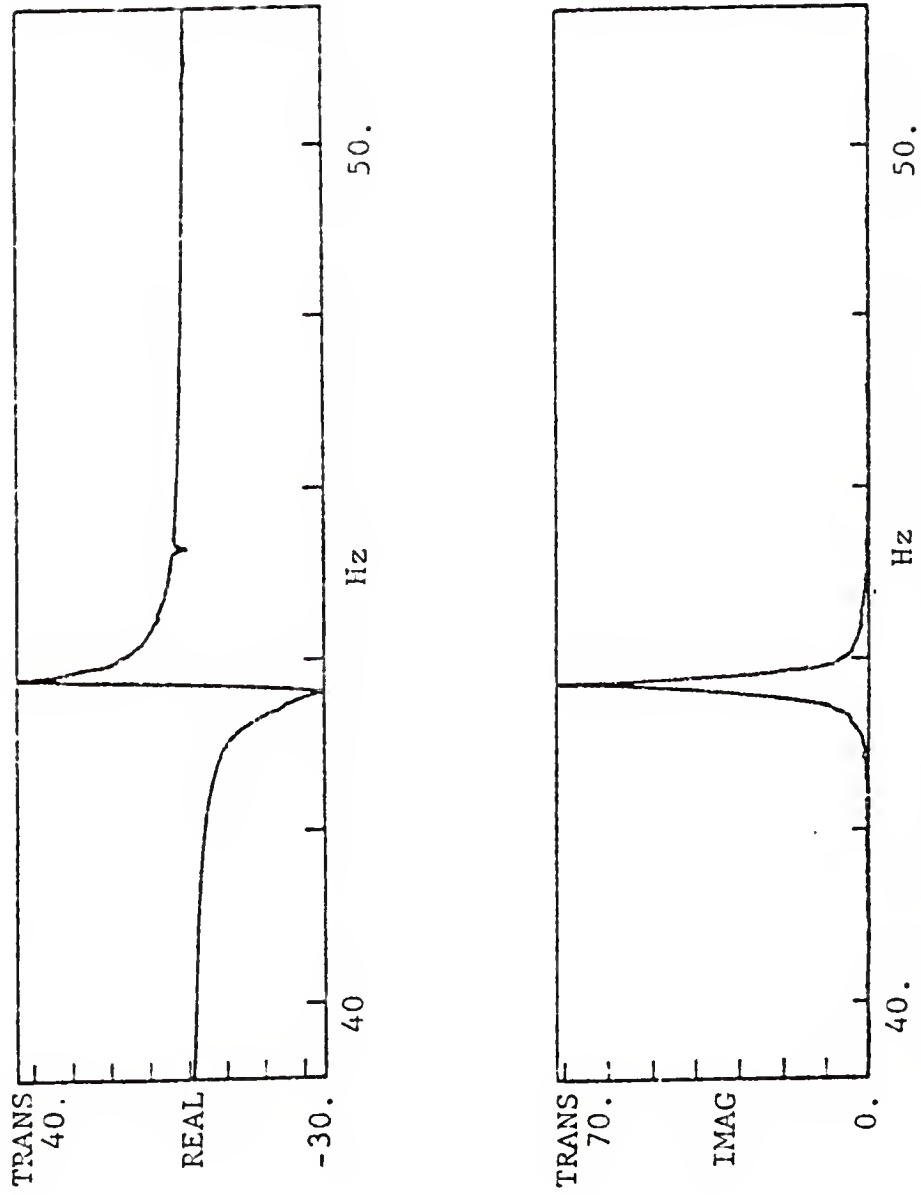


Figure 7.2: Typical Display of Real and Imaginary Parts of Frequency Response Function for a Graphite Epoxy Composite Material

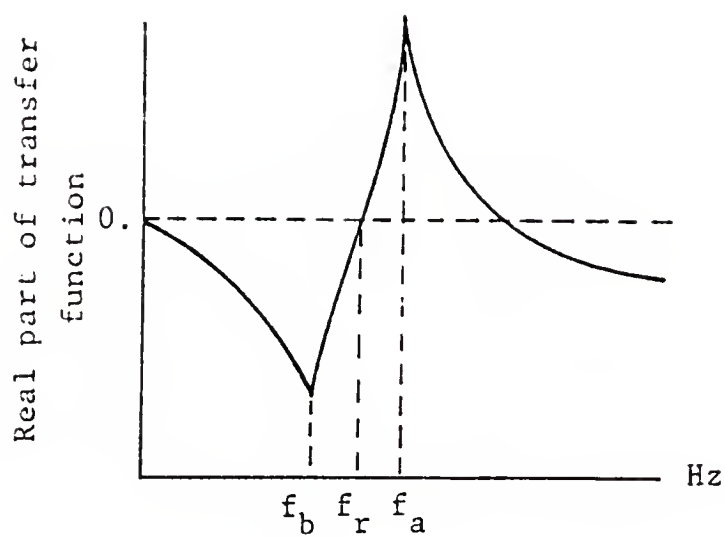


Figure 7.3: Enlarged Schematic Drawing of Real Part of Frequency Response Function

CHAPTER 8  
OPTIMIZATION OF DAMPING AND SPECIFIC STIFFNESS  
FOR FIBER COMPOSITES

8.1 Introduction

Plunkett and Lee [19] pointed out that maximum damping can be obtained through properly choosing the length and spacing of the constraining layers. Those layers are used to constrain the viscoelastic layer (or coating) on the structure surface. In the study presented here, the optimization of damping is based on the composite material itself (i.e., choosing the proper fiber length, fiber direction, the longitudinal distance between fiber tips, etc.). It is known that high damping can reduce the displacement at and near the resonant frequencies, while high stiffness can further reduce the displacement at other frequencies. The best way to optimize both damping and stiffness is to keep them as high as possible. Unfortunately, there exists a general trend that higher damping is mostly coupled with low stiffness and vice versa. Therefore, the idea of the optimization in this study is to try to increase damping without sacrificing the stiffness too much.

From the formulations presented in previous chapters, one can see the complication contained in damping

analysis. It will be a simpler approach for the optimization analysis if no derivative is needed. Consequently, the so-called Sequential Simplex Method [68, 69] has been selected to analyze the optimization.

## 8.2 Brief Introduction to Sequential Simplex Method

The sequential Simplex Method [68, 69] takes a regular geometric figure (known as a simplex) as a base. Thus, in two dimensions (i.e., two-design variables), one should choose an equilateral triangle; and in three dimensions (i.e., three-design variables), one should choose a tetrahedron.

Observations (experiments) are located so that the objective function is evaluated at the points formed by vertices of the geometric figure. One vertex is then rejected as being inferior in value to the others. The general direction of search may then be taken in a direction away from this worst point, the direction being chosen so that the movement passes through the center of gravity of the remaining points. A new point is then selected along this direction so as to preserve the geometric shape of the figure, and the function is evaluated anew at this point. The method proceeds with this process of vertex rejection and regeneration until the figure straddles the optimum. When no subsequent moves would lead to further improvement, the last few geometric figures are essentially repeated. There are three rules

that govern the whole procedure of this method. These rules are explained in the two-dimensional case as follows:

1. Take the point to be rejected where the worst value of the objective function is obtained, and replace it by its reflection in the opposite side of the triangle. See Figure 8.1, where point B is replaced by point D.
2. No return can be made to points which have just been left; see Figure 8.2, where point A is replaced by point D. If point D is still the worst point of triangle BCD, then point B is replaced by point E.
3. If the best valued vertex remains unchanged for more than M iterations, then the simplex size is reduced by, for example, halving the distance of all other vertices from that vertex. The next stage can then start. For example, as in Figure 8.3, point C is sequentially repeated in five triangles ABC, BDC, DEC, EFC, and FGC; and after the size of the fifth triangle FGC is reduced to triangle F'G'C, the rule 1 is applied at the new triangle F'G'C.

The magnitude of M depends on the number of variables. Spendley [68] suggested that

$$M = 1.65n + 0.05 n^2 \qquad 8.1$$

where  $n$  is the total number of design variables. The search can finally be stopped when the simplex is small enough to locate the optimum adequately.

It should be noted that Rule 1 and Rule 2 force the simplexes to circle continuously about an indicated optimum, rather than oscillate over a limited range such as a ridge (see Figure 8.2). If one ensures that at any point violating a constraint, a sufficiently large negative value (or positive value, if one is maximizing) is set for the response at such a point, the system of simplexes will then move along rather than cross the constraints.

The advantages of this method are as follows:

1. It is easy to apply.
2. It is useful when analytical or numerical derivatives of the objective function are not available.

The disadvantage of this method is that it could not guarantee that the global optimum design is obtained. Therefore, several different initial locations (designs) should be considered to get global optimization.

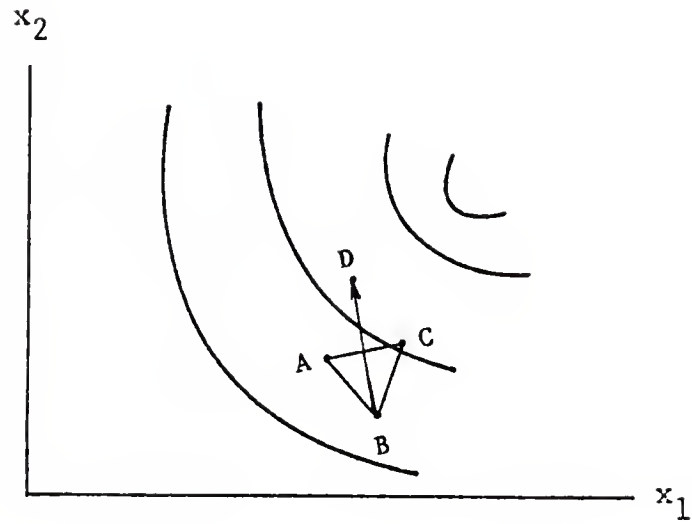


Figure 8.1: Rule 1 of Sequential Simplex method

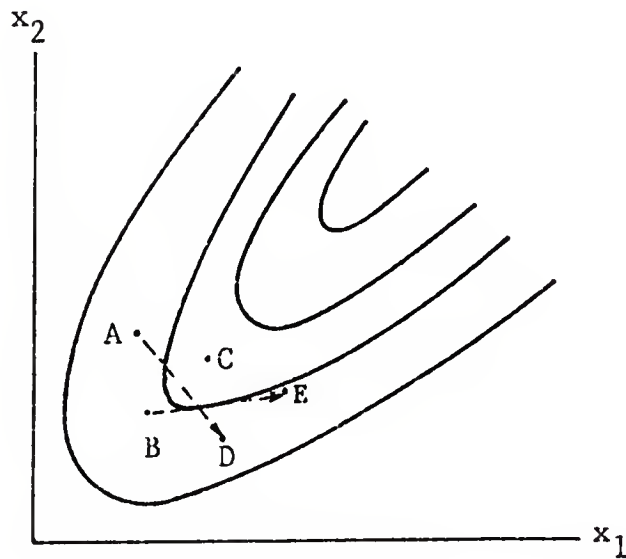


Figure 8.2: Rule 2 of Sequential Simplex method





Generally speaking, the design variables of continuous or discontinuous fiber composites include fiber volume fraction  $V_f$ , fiber moduli  $E_f$ , fiber aspect ratio  $s/d$ , the longitudinal distance between fiber tips  $p$ , and fiber orientation angle  $\theta$  for certain special stacking sequence. Among those six variables, only fiber aspect ratio  $s/d$  and fiber tip longitudinal distance  $p$  are treated as the design variables in the optimization analysis. Since orthotropic materials are utilized in the optimization analysis, the fiber direction  $\theta$  is kept as certain constants. The fiber volume fraction is also set as a constant (0.65) in this study, since the fiber composites are made from prepreg tape. Stacking sequence is fixed and most of this study is concentrated on graphite-epoxy, Kevlar-epoxy and the hybrid of those two composite materials, so that only two sets of fiber moduli are considered.

Two different cases are considered in optimization analysis:

Case one is to optimize the specific stiffness and material damping of an orthotropic square plate simply supported on all four sides under free vibration.

The equation of motion for this case is

$$D_{11} W_{,xxxx} + 2(D_{12} + 2D_{66}) W_{,xxyy} + D_{22} W_{,yyyy} = \rho W_{,tt}$$

where the  $D_{ij}$  are derived from laminated plate theory, and  $W$  is the flexural deformation. Let

$$W = A_{mn} F_m(x) H_n(y) T(t) \quad 8.3$$

By separation of variables, the form (8.4) is obtained for  $T(t)$ ; while  $F_m(x)$  and  $H_n(y)$  satisfy Equation 8.5

$$T(t) = e^{(i \frac{\lambda_k}{\rho})^{\frac{1}{2}} t} \quad k = 1, 2, 3 \dots \quad 8.4$$

$$\begin{aligned} D_{11} F_m^{(iv)} H_n + 2(D_{12} + 2D_{66}) F_m'' H_n'' + D_{22} F_m H_n^{(iv)} \\ = \lambda_k F_m H_n \end{aligned} \quad 8.5$$

where  $\lambda_k$  is the constant to be determined, and  $i$  is  $\sqrt{-1}$  in Equation 8.4.

In accordance with the simple support boundary conditions,  $F_m$  and  $H_n$  functions can be assumed as

$$F_m(x) = \sin \frac{m\pi y}{a} \quad 8.6$$

$$H_n(y) = \sin \frac{n\pi x}{b} \quad 8.7$$

where  $a$  and  $b$  are the lengths of the edges along  $x$  and  $y$  directions, respectively.

By substituting Equations 8.6 and 8.7 into Equation 8.5, one obtains

$$D_{11} \frac{m^4 \pi^4}{a^4} + 2(D_{12} + 2D_{66}) \frac{m^2 n^2 \pi^4}{a^2 b^2} + D_{22} \frac{n^4 \pi^4}{b^4} = \lambda_k \quad 8.8$$

Letting  $b=a$  for a square plate and considering only the first mode of vibration (i.e.,  $m=n=1$ ), one can obtain  $\lambda_1$  as

$$\lambda_1 = \frac{\pi^4}{a^4} (D_{11} + 2D_{12} + 4D_{66} + D_{22}) \quad 8.9$$

The natural circular frequency of the first mode,  $\omega_1$ , is defined as

$$\omega_1 = \left( \frac{\lambda_1}{\rho} \right)^{\frac{1}{2}} \quad 8.10$$

Then the first mode solution of Equation 8.2 is

$$W = a_{11} \sin \frac{\pi x}{a} \sin \frac{\pi y}{a} e^{i\omega_1 t} \quad 8.11$$

If the viscoelastic behavior of the materials is considered, the complex form of  $D_{ij}$  should be included, i.e.

$$\omega^* = \frac{\pi^2}{a^2} \frac{1}{\rho} (D_{11}^* + 2D_{12}^* + 4D_{66}^* + D_{22}^*)^{\frac{1}{2}} \quad 8.12$$

After separating the real and imaginary parts and neglecting the higher-order terms of the binomial expansion of the quantity on the right-hand side in Equation 8.12, the following expression is obtained.

$$\omega_1^* = \omega_1' + i \omega_1'' \quad 8.13$$

where

$$\omega_1' = \frac{\pi^2}{a^2} \frac{1}{\rho} (D_{11}' + 2D_{12}' + 4D_{66}' + D_{22}')^{\frac{1}{2}} \quad 8.14$$

$$\omega_1'' = \frac{\pi^2}{2a^2} \frac{D_{11}'' + 2D_{12}'' + 4D_{66}'' + D_{22}''}{\rho (D_{11}' + 2D_{12}' + 4D_{66}' + D_{22}')^{\frac{1}{2}}} \quad 8.15$$

Hence, for viscoelastic material, Equation 8.11 should be rewritten as

$$W = (a_{11} \sin \frac{\pi x}{a} \sin \frac{\pi y}{a} e^{i\omega_1' t}) e^{-\omega_1'' t} \quad 8.16$$

Equation 8.16 is similar to the mathematical model of logarithmic decrement [42], and the logarithmic decrement  $\delta$  can be approximated by

$$\delta = \frac{2\pi \frac{\omega_1''}{\omega_1'}}{1 - \left(\frac{\omega_1''}{\omega_1'}\right)^2} \approx 2\pi \frac{\omega_1''}{\omega_1'} \quad 8.17$$

for light damping, i.e. when  $\omega_1''/\omega_1' < \ll 1$ .

By using Equation 2.22, the loss factor of this system is then determined as

$$\eta = 2 \frac{\omega_1''}{\omega_1'} = \frac{D_{11}'' + 2D_{12}'' + 4D_{66}'' + D_{22}''}{D_{11}' + 2D_{12}' + 4D_{66}' + D_{22}'} \quad 8.18$$

The value of  $A_{mn}$  depends on the stiffness. High stiffness reduces the deflection at resonance; the material damping can further reduce the displacement at resonance. Gibson [61] shows that flexural vibration for a double cantilever beam under forced vibration at resonant frequency depends inversely on the product of material damping, area moment of inertia of cross section and Young's modulus. It should be noted that his result is based on the equation of motion for free vibration and

the boundary conditions of forced vibration. For the case considered here, the product of the area moment of inertia and Young's modulus corresponds to the generalized stiffness  $\tilde{D}$ , which is defined as

$$\tilde{D}^* = \tilde{D}' + i \tilde{D}'' \quad 8.19$$

$$\tilde{D}' = D' + 2D'_{12} + 4D'_{66} + D'_{22} \quad 8.20$$

$$\tilde{D}'' = D''_{11} + 2D''_{12} + 4D''_{66} + D''_{22} \quad 8.21$$

Equation 8.18 can be rewritten as

$$\eta = \tilde{D}''/\tilde{D}' \quad 8.22$$

In order to have small resonant deformation, a high value of the product of stiffness and material damping is required. But high specific stiffness is the major property of fiber composites to be widely used in space vehicle and aircraft. Therefore, the mathematical formulation of optimization on damping and specific stiffness is to seek the maximum value of the objective function

$$f_1 (p/d, s/d) \quad 8.23$$

of two variables  $p/d$  and  $s/d$ , where  $f_1$  is assumed in the form

$$f_1(p/d, s/d) = T_1 \frac{\frac{\tilde{D}'}{\rho}}{\frac{\tilde{D}'_0}{\rho_0}} + T_2 \frac{\frac{\tilde{D}'}{\rho} \cdot \eta}{\frac{\tilde{D}'_0}{\rho_0} \cdot \eta_m} \quad 8.24$$

or

$$f_1(p/d, s/d) = \frac{\tilde{D}'}{\rho} \frac{\rho_0}{\tilde{D}'_0} (T_1 + T_2 \frac{\eta}{\eta_m}) \quad 8.25$$

The ranges for design variables  $p/d$  and  $s/d$  are

$$0 \leq p/d \leq 0.05 s/d \quad 8.26$$

$$25 \leq s/d \leq 10000 \quad 8.27$$

where  $T_1$  and  $T_2$  are weighting constants,  $\eta_m$  is the damping value of epoxy,  $\rho$  is the density of designed composite,  $\tilde{D}'$  and  $\eta$  of design composite are defined in equations 8.20 and 8.22, respectively, and  $\tilde{D}'_0$  and  $\rho_0$  are the corresponding values of  $\tilde{D}'$  and density of continuous graphite reinforced epoxy having the same stacking sequence and fiber volume fraction. If high specific stiffness is important in structures,  $T_1$  could be chosen as a high value.



Alternatively, if small resonant deformation is the major consideration,  $T_2$  should be a high value.

Case two is to optimize the specific stiffness and material damping of an orthotropic square plate clamped on all four sides under free vibration.

The equation of motion is just the same as Equation 8.2. The first mode solution is assumed, according to reference [70]

$$W = A_{11} F(x) H(y) T(t) \quad 8.28$$

where

$$F(x) = \beta_1 \cos \lambda_1 x - \beta_1 \cosh \lambda_1 x + \sin \lambda_1 x - \sinh \lambda_1 x \quad 8.29$$

$$H(y) = \beta_1 \cos \lambda_1 y - \beta_1 \cosh \lambda_1 y + \sin \lambda_1 y - \sinh \lambda_1 y \quad 8.30$$

$$\beta_1 = \frac{\sin \lambda_1 a - \sinh \lambda_1 a}{-\cos \lambda_1 a + \cosh \lambda_1 a} \quad 8.31$$

and  $\lambda_1$  is the constant to be determined.

The natural frequency of first mode vibration of a clamped square plate was given in reference [70] as

$$\omega_1 = \frac{\pi^2}{a^2} \frac{1}{\rho} [5.14D_{11} + 1.55(2D_{22} + 4D_{66}) + 5.14D_{22}]^{\frac{1}{2}} \quad 8.32$$

By a similar approach to that prescribed in case one, one will obtain the loss factor of the system for case two as

$$\eta = \frac{5.14D_{11}'' + 1.55 (2D_{12}'' + 4D_{66}'') + 5.14D_{22}''}{5.14D_{11}' + 1.55 (2D_{12}' + 4D_{66}') + 5.14D_{22}'} \quad 8.33$$

The mathematical formulation of optimization for this case is to seek the maximum value of the objective function

$$f_2 (p/d, s/d) \quad 8.34$$

of two variables  $p/d$  and  $s/d$ , where  $f_2$  is defined in Equation 8.37

The ranges of design variables are

$$0 \leq p/d \leq 0.05 \quad s/d \quad 8.35$$

$$25 \leq s/d \leq 10000 \quad 8.36$$

where

$$f_2 (p_1, s/d) = T_1 \frac{\frac{\tilde{D}'}{\rho}}{\frac{\tilde{D}'_0}{\rho_0}} + T_2 \frac{\frac{\tilde{D}'}{\rho} \cdot \eta}{\frac{\tilde{D}'_0}{\rho_0} \cdot \eta_m} \quad 8.37$$

and

$$\tilde{D}' = 5.14D'_{11} + 1.55(2D'_{12} + 4D'_{66}) + 5.14D'_{22} \quad 8.38$$

$$\tilde{D}'' = 5.14D''_{11} + 1.55(2D''_{12} + 4D''_{66}) + 5.14D''_{22} \quad 8.39$$

$$\eta = \tilde{D}''/\tilde{D}' \quad 8.40$$

## CHAPTER 9 RESULTS AND CONCLUSIONS

### 9.1 Preliminary Remarks

The damping analyses presented in Chapters 3 to 6 are applicable to all kinds of fiber composites, including continuous fiber composites, discontinuous fiber composites, symmetrically or unsymmetrically laminated or laminar composites, randomly oriented fiber composites, etc. The optimization analysis on damping and specific stiffness presented in Chapter 8 is based on orthotropic material. However, a similar approach is applicable for more general anisotropic materials. Since most widely- and practically-used fiber composites are symmetrically laminated fiber composites, the numerical analysis of this study is concentrated on certain kinds of symmetrically laminated fiber composites, unidirectional laminar composites, and in-plane randomly oriented short-fiber composites.

As mentioned before (see Chapters 3 and 5), damping  $\eta_x$  is defined as  $E''_x/E'_x$  (or  $D''_x/D'_x$ ). Since both  $E'_x$  and  $E''_x$  (or  $D'_x$  and  $D''_x$ ) are functions of  $\underline{E}_f$ ,  $\underline{E}_m$ ,  $s/d$ ,  $\theta$ ,  $P$  (the longitudinal distance between fiber tips),  $V_f$  and  $\eta_f$ , etc., the variations of  $\eta_x$  and  $E'_x$  (or  $D'_x$ ) may not follow the same pattern. Consequently, in the numerical results,

three dependent variables (i.e.,  $\eta'_x$ ,  $E'_x$ , and  $E''_x$ ) are discussed in laminar composites, while more dependent variables are involved in other composites. Among the independent variables, most interest is focused on  $E_f$ ,  $E_m$ ,  $s/d$ , and  $\theta$ .  $P$  is treated as an independent variable only for optimization, and  $V_f$  is set as a constant in most cases.

The numerical results presented in this chapter are based on the following assumptions:

1. The matrix epoxy behaves as a linear, isotropic, viscoelastic material [15].
2. All fibers are also linear viscoelastic materials, and damping of fibers is independent of direction.
3. The dependence of modulus on frequency is not considered at the present time.

## 9.2 Damping and Stiffness of Unidirectional Fiber Composites

The numerical results of damping and stiffness analysis presented in Chapter 3 are discussed in this section. It should be noted that the modified Cox's model (i.e. Equations 3.8 and 3.13) is used to calculate the longitudinal modulus of composite materials.

Figures 9.1, 9.2, and 9.3 present the nondimensional plots of  $E'_x/E'_m$ ,  $E''_x/E''_m$ , and  $\eta_x/\eta_m$  of graphite epoxy composite as functions of fiber aspect ratio  $s/d$ , using  $\theta$

(the angle between fiber direction and loading direction) as parameter. For small angle, say  $\theta < 10^\circ$ , the storage modulus sharply increases as fiber aspect ratio increases; the loss modulus reaches its maximum around  $s/d=130$  and then reduces as  $s/d$  increases, while damping apparently decreases as  $s/d$  increases. Comparing  $0^\circ$  curves with the  $30^\circ$  curves in those drawings, one can notice that when  $\theta=0^\circ$  low damping at large  $s/d$  is caused mainly by high storage modulus. Comparing the  $60^\circ$  curves with the  $90^\circ$  curves in those drawings, it is recognized that for large angles, the differences in loss moduli have more influence on damping. Alternatively, Figures 9.4, 9.5, and 9.6 show the nondimensional plots of  $E'_x/E'_m$ ,  $E''_x/E''_m$ , and  $\eta_x/\eta_m$  of graphite epoxy composites as functions of  $\theta$ , using  $s/d$  as parameter. It is clearly observed that the shorter the fiber, the stronger is the dependence of  $E'_x/E'_m$ ,  $E''_x/E''_m$ , and  $\eta_x/\eta_m$  on  $s/d$  for small angles, say  $\theta < 10$ . When  $\theta \geq 45$ , there is not any change of  $E'_x/E'_m$ ,  $E''_x/E''_m$ , and  $\eta_x/\eta_m$  caused by changing  $s/d$ . In addition, Figure 9.5 shows that the maximum value of  $E''_x/E''_m$  occurred between  $\theta=0^\circ$  and  $\theta=15^\circ$  for fiber aspect ratio ranging from 25 to 10000.

Similar properties of unidirectional boron epoxy composite and glass epoxy composites are observed. But, for  $\theta=0$ , the maximum values of  $E''_x/E''_m$  occur around  $s/d=500$  and  $s/d=50$  for boron epoxy composite and glass epoxy composite, respectively. Also, the damping of boron epoxy composite is, in general, higher than that of graphite

epoxy composite. This is because boron itself has higher damping than graphite does.

The corresponding drawings of Figures 9.1, 9.2, and 9.3 for unidirectional Kevlar epoxy composite are given in Figures 9.7, 9.8, and 9.9, respectively. It is observed that Kevlar epoxy composite has the highest material damping among those four kinds of composite. This is due to the fact that Kevlar (aramid) is a kind of polymer which usually has high damping. It is interesting to notice that  $E''_X/E''_m$  of Kevlar epoxy composite monotonically increases with respect to  $s/d$  when  $\theta=0^\circ$ . All other properties of Kevlar epoxy composite are similar to those of graphite epoxy composite.

Figure 9.10 presents the plots of  $E'_X/E'_m$ ,  $E''_X/E''_m$ , and  $\eta_X/\eta_m$  of Kevlar epoxy composite as functions of  $\theta$  with  $s/d=100$ . This figure shows that high damping of such material is induced by the fact that the values of  $E'_X/E'_m$  and  $E''_X/E''_m$  are very close. The damping of Kevlar epoxy composite is insensitive to angle change because the reduction rates of  $E'_X/E'_m$  and  $E''_X/E''_m$  are very close. Figure 9.11 shows the plots of  $E'_X/E'_m$  and  $E''_X/E''_m$ , and  $\eta_X/\eta_m$  of Kevlar epoxy composite and graphite epoxy composite as functions of  $\theta$ , while  $s/d$  is kept as 100. This suggests idea that if a hybrid composite (graphite epoxy and Kevlar epoxy composite) is made, damping of this hybrid composite will be higher than that of graphite composite, while the

stiffness of the hybrid composite will be greater than that of Kevlar epoxy composite.

Figure 9.12 presents  $E'_x/E'_m$  of graphite epoxy composite as function of  $\theta$  for different fiber volume fractions  $V_f$ , when  $s/d=100$ . Differences in  $E'_x/E'_m$  caused by different volume fractions decreases when angle increases. It is also observed that an apparent reduction in  $E'_x/E'_m$  occurs when angle increases from  $0^\circ$  to  $15^\circ$ . Figure 9.13 exhibits the plots of  $\eta_x/\eta_m$  for graphite epoxy composite versus  $\theta$  for different fiber volume fractions, when  $s/d=100$ . The peak value of damping moves from about  $50^\circ$  to  $30^\circ$  when the volume fraction changes from 0.1 to 0.6.

Three-dimensional plots using  $E'_x$  and  $\eta_x$  as vertical axis, and  $s/d$  and  $\theta$  as two base axes of Kevlar epoxy composites are given in Figures 9.14 and 9.15, respectively. The associated contour curves are presented in Figures 9.16 and 9.17.

### 9.3 Damping and Stiffness of Randomly Oriented Short-Fiber Composites

Figure 9.18 gives the nondimensional plots of  $\eta_r/\eta_m$ ,  $E'_r/E'_m$ , and  $E''_r/E''_m$  of glass epoxy composite as functions of  $s/d$ . It is observed that damping reaches its maximum value at small values of  $s/d$  and decreases as  $s/d$  increases. The storage modulus  $E'_r/E'_m$  monotonically increases as  $s/d$  increases. However, loss modulus  $E''_r/E''_m$  almost remains unchanged. In Figures 9.19 and 9.20, nondimensional plots of  $\eta_r/\eta_m$ ,  $E'_r/E'_m$  and  $E''_r/E''_m$  for graphite epoxy composite



and Kevlar epoxy composite are presented separately. The variations of  $\eta_r/\eta_m$  and  $E'_r/E'_m$  for Kevlar epoxy composite or graphite epoxy composite are similar to those of glass epoxy composite. But, for Kevlar epoxy composite,  $E''_r/E''_m$  increases as  $s/d$  increases, while graphite epoxy composite,  $E''_r/E''_m$  has its maximum value around  $s/d=120$ . Figures 9.21, 9.22 and 9.23 show similar plots of  $\eta_{Gr}/\eta_{Gm}$ ,  $G'_r/G'_m$ , and  $G''_r/G''_m$  as functions of  $s/d$  for glass epoxy composite, graphite epoxy composite, and Kevlar epoxy composite, respectively. Variations of  $\eta_{Gr}/\eta_{Gm}$ ,  $G'_r/G'_m$  and  $G''_r/G''_m$  are almost the same as those of  $\eta_r/\eta_m$ ,  $E_r/E_m$ , and  $E''_r/E''_m$  of corresponding composite, respectively.

Figure 9.24 shows the nondimensional plots of  $\eta_r/\eta_m$  as function of fiber volume fraction  $V_f$ , using  $s/d$  as parameter. It is observed that  $\eta_r/\eta_m$  decreases as  $V_f$  increases for small  $s/d$  as well as for large  $s/d$ .

Three-dimensional plots, using  $E'_r$  and  $\eta'_r$  as vertical axis, and  $E_f$  and  $s/d$  as two base axes, of four kinds of fiber composite are given in Figures 9.25 in 9.26, separately. The associated contour curves are presented in Figures 9.27 and 9.28.

#### 9.4 Damping and Stiffness of Laminated Composite-- Laminated Plate Theory Approach

The numerical results of the damping and stiffness analysis described in Chapter 5 are presented in this section. Five types of lamination (quasi-isotropic lamination, angle ply lamination, cross ply lamination,

unidirectional lamination, and a special kind of lamination  $[\theta_n/-\theta_{4n}]_s$  of graphite Epoxy composites are considered in numerical examples.

Figure 9.29 exhibits nondimensional plots of  $D'_{11}$  and  $F\eta_{11}$  (flexural normal damping) for  $[0_2/90_2/45_2/-45_2]_s$ ,  $[45_2/0_2/-45_2/90_2]_s$ , and  $[45_2/-45_2/90_2/0_2]_s$  as functions of  $s/d$ . It should be noted that all those three kinds of lamination have the same values of in-plane longitudinal stiffness  $A'_{11}$  and in-plane longitudinal damping  $I\eta_{11}$ . But Figure 9.29 shows, as expected, that for the same  $s/d$ ,  $[0_2/90_2/45_2/-45_2]_s$  has the highest value of  $D'_{11}$  and the lowest value of  $F\eta_{11}$ ,  $[45_2/-45_2/90_2/0_2]_s$  has the lowest value of  $D'_{11}$  and the highest value of  $F\eta_{11}$ , while  $[45_2/0_2/-45_2/90_2]_s$  has almost the average values of  $D'_{11}$  and of  $F\eta_{11}$  of the other two kinds of lamination. Alternatively, Figure 9.30 shows the nondimensional plots of  $D'_{66}$  and  $F\eta_{66}$  (twisting damping) for those three kinds of lamination as functions of  $s/d$ . In this drawing for same  $s/d$ ,  $[0_2/90_2/45_2/-45_2]_s$  has the lowest value of  $D'_{66}$  and the highest value of  $F\eta_{66}$ ,  $[45_2/-45_2/0_2/90_2]_s$  has the highest value of  $D'_{66}$  and the lowest value of  $F\eta_{66}$ , and  $[45_2/0_2/-45_2/90_2]_s$  still remains around the average values of those other two kinds of lamination. Figures 9.29 and 9.30 actually show us how to design the quasi-isotropic laminated plate for either maximum damping or maximum stiffness purpose.

Figures 9.31 and 9.32 show the nondimensional plots of  $E'_{11}$  and  $I\eta_{11}$  (in-plane longitudinal damping) of angle ply

laminated graphite epoxy composite as function of  $\theta$ , using  $s/d$  as a parameter.  $E'_{11}$  increases with  $s/d$  for small angles, say  $\theta < 20^\circ$ . The variation of  $E'_{11}$  with  $s/d$  reduces as  $\theta$  increases, and very small differences exist for  $\theta > 60^\circ$ . The  $I\eta_{11}$  distinctively decreases as  $s/d$  increases for small angles (say,  $\theta < 30^\circ$ ), while the variation of  $I\eta_{11}$  with  $s/d$  reduces as  $\theta$  increases. Figures 9.31 and 9.32 are comparable to Figures 9.4 and 9.6 correspondingly. The reduction in  $I\eta_{11}$  (or the increment in  $E'_{11}$ ) of angle ply laminated composite is not as sharp as that of unidirectional composite, when  $s/d$  is increased and the angle is small.

In-plane shear stiffness  $E'_{66}$  and in-plane shear damping  $I\eta_{66}$  of angle ply graphite epoxy composite as function of  $\theta$ , using  $s/d$  as parameter are shown in Figures 9.33 and 9.34, separately. Maximum  $E'_{66}$  and minimum  $I\eta_{66}$  occur at  $\theta = 45^\circ$ . Larger dependences of  $E'_{66}$  and  $I\eta_{66}$  on  $\theta$  are observed for larger  $s/d$ . The reason why  $D'_{11}/D'_m$ ,  $D'_{66}/D'_{Gm}$ ,  $F\eta_{11}/\eta_m$ , and  $F\eta_{66}/\eta_{Gm}$  are not presented in drawings is that those values are very close to the values of  $E'_{11}/E'_m$ ,  $E'_{66}/G'_m$ ,  $I\eta_{11}/\eta_m$ , and  $I\eta_{66}/\eta_{Gm}$  separately.

Figures 9.35-9.38 present the nondimensional plots of  $D'_{11}$ ,  $F\eta_{11}$ ,  $D'_{66}$ , and  $F\eta_{66}$  of graphite epoxy composite laminated with four kinds of lamination ( $[45/-45]_{4s}$ ,  $[45_2/0_2/-45_2/90_2]_s$ ,  $[0/90]_{4s}$ , and  $[0_8]_s$ ) as functions of  $s/d$ . It is observed that for the same  $s/d$ ,  $[45/-45]_{4s}$  has the highest values of  $D'_{66}$  and  $F\eta_{11}$  and the lowest values

of  $D'_{11}$  and  $F\eta_{66}$ . The values of  $D'_{66}$  and  $F\eta_{66}$  for  $[0/90]_{4s}$ , and for  $[0_8]_s$  are same, and those values are almost independent of  $s/d$ . This is because  $E_T$  and  $G_{LT}$  of fiber composites are assumed to be independent of the fiber length.  $D'_{11}$  of  $[0_8]_s$  is, as expected, higher than  $D'_{11}$  of  $[0/90]_{4s}$  at the same  $s/d$ , but  $F\eta_{11}$  of those two kinds of lamination are surprisingly close. The  $D'_{11}$ ,  $F\eta_{11}$ ,  $D'_{66}$  and  $F\eta_{66}$  of  $[45_2/0_2/-45_2/90_2]_{4s}$  are just somewhere near the middle range of those of  $[45/-45]_{4s}$  and  $[0/90]_{4s}$ .

The characteristic property of  $[\theta_n/-\theta_{4n}]_s$  is that its  $D'_{16}$  and  $D'_{26}$  are very close to zero. For example,  $D'_{16}/D'_{11}$  or  $D'_{26}/D'_{11}$  of this lamination for graphite epoxy composite is less than 0.02 for all angles, while those of angle ply lamination are less than about 0.11 for all angles. Numerical results show that  $D'_{11}$ ,  $F\eta_{11}$ ,  $D'_{66}$ , and  $F\eta_{66}$  of  $[\theta_2/-\theta_8]_s$  are very close (difference within 2%) to those of  $[\theta/-\theta]_{5s}$ . But  $E'_{11}$  and  $E'_{66}$  (or  $I\eta_{11}$  and  $I\eta_{66}$ ) are in general less (or greater) than those of  $[\theta/-\theta]_{5s}$  (maximum differences ranging from 13% to 30%).

#### 9.5 Damping and Stiffness of Laminated Fiber Composite-- Energy Approach

There are twenty-one different kinds of material damping induced from  $C''_{ij}/C'_{ij}$  ( $i, j = 1, 2 \dots 6$ ) for anisotropic materials. In the energy approach, material damping of structure is just the ratio of the sum of  $\frac{1}{2} \epsilon_{ij}^2 C''_{ij}$  to the sum of  $\frac{1}{2} \epsilon_{ij}^2 C'_{ij}$ . Therefore, different values of material damping could be observed for one

material under different kinds of loading and boundary conditions. In the author's opinion, damping analysis through the energy approach is more acceptable than laminated plate approach, because the energy approach considers the influence of all stresses on the dissipated energy, while laminated plate approach considers one stress at a time. The results of damping analysis through the energy approach presented in Chapter 6 are discussed in this section.

Figure 9.39 shows the difference between material damping through the energy approach and through the laminated plate approach for a  $60 \times 60 \times 10$  cross plied ( $0_5/90_5/0_5$ ) graphite epoxy composite under uniform in-plane tension load along x direction. The difference is mainly caused by the fact that there exists some stress other than  $\sigma_x$ ; for example,  $\tau_{xz}$  is not negligible in certain regions. The difference increases when the value of  $s/p$  is increased. In other words, continuous fiber composites have more apparent difference of damping values through those two approaches than discontinuous (short-fiber) composites do.

Figure 9.40 presents the influence of plate thickness and of the lamination on the damping value by the energy approach under in-plane uniform tension load. It is noticed that either increasing the number of interfaces or reducing the total plate thickness will, in general, reduce the difference between damping values of those two

approaches. It should also be noted that, for an isotropic material under tensional load along x direction, the damping value of the energy approach is same as the value of  $\Gamma_{11}$  through the laminated plate theory approach.

When a flexural bending load is considered, a pair of couple forces are applied around one edge; while a fixed boundary condition is presumed at the opposite edge.

Figure 9.41 shows that reducing the total thickness makes the damping values of the energy approach closer to those of the laminated plate approach. It is also indicated by Figure 9.41 that for the flexure bending load case, increasing the total number of interfaces would somehow help those two approaches to obtain more consistent damping results.

#### 9.6 Experimental Results of Damping and Stiffness

Figure 9.42 presents some experimental results by the impulse hammer technique [35, 36] about material damping and stiffness of graphite epoxy composite beams. Experimental results of stiffness are very close to those of the analytical results, while experimental results of damping are not so close to the analytical results. A similar trend is also presented in Figure 9.42 where experimental results [35, 36] about damping and stiffness of off-axis unidirectional continuous graphite epoxy composite beams are compared with analytical results. Table 9.1 shows the experimental results of damping and of the first mode



nature frequency (this quantity is proportional to the stiffness of the structure) of five cross ply short-fiber glass epoxy composite plates. It is observed that high value of  $s/p$  (either increase fiber length,  $s$ , or reduce the gap between fiber tips,  $p$ ) will increase the nature frequency and decrease the damping.

### 9.7 Optimization of Damping and Specific Stiffness of Fiber Composites

According to the prescription about optimizing damping in Chapter 8, some optimum designs are discussed in this section for graphite epoxy composites and for hybrid composites keeping  $V_f$  equal to 0.65. The design variables include the fiber aspect ratio,  $s/d$ , and the ratio of the longitudinal distance between fiber tips,  $p$ , to the fiber diameter,  $d$ .

Table 9.2 shows the influence of weighting constants,  $T_1$  and  $T_2$ , on the optimum design for 0/90/0 graphite epoxy composites under situations of case one. By increasing  $T_2$ ,  $s/p$  is reduced; while by increasing  $T_1$ ,  $s/p$  is increased. These imply that to have smaller resonant deformation, larger distance between fiber tips is preferred; while to have higher specific stiffness, smaller distance between fiber tips is required.

Table 9.3 shows the optimum design for cross ply graphite epoxy composites and hybrid composites under case one situation and having the same total thickness, with  $T_1=1$  and  $T_2=5$ . There is no difference in the optimum

values of design variables  $s/d$  and  $p/d$  for 0/90/0 and 0/90/0/90/0 graphite epoxy composites. For the same total thickness, with  $T_1=1$  and  $T_2=5$ , discontinuous fibers give a high value of objective function in the stacking sequence  $0^G/90^G/0^K/90^K/s$ ; while continuous fibers give high value of the objective function in the stacking sequence  $0^K/90^K/0^G/90^G/90^G/s$  where the superscripts G and K represent graphite and Kevlar, respectively, and the fiber composites having  $s/p=2593$ . can be treated as continuous fiber reinforced composites. When comparing the value of objective function of each optimum design for each case, one can discover that  $0^K/90^K/0^G/90^G/s$  has the highest value of objective function. This indicates that the continuous hybrid fiber composite plate with the stacking sequence  $0^K/90^K/0^G/90^G/s$  is the optimum design for case one.

Figure 9.44 shows the contour curves of objective function of case one vs  $s/d$  and  $s/p$  (keeping  $T_1=1$ ,  $T_2=5$ ). It is observed that there probably exists an acceptable region as optimum design. In fact, the term  $(s/p)_{ave}$  in Tables 9.2, 9.3 and 9.4 is the average value of ratio  $s$  to  $p$  at all points whose objective value is within 99.95% and 100.05% times of the objective value of the optimum design shown in  $s/d$  and  $p/d$  items. Numerical results show this region ranging from  $s/d=2000$  to  $s/d$  over 9000 for case one. That means, as long as  $s/p$  is kept equal to 53.1 and  $s/d$  over 2000, one will get an acceptable optimum design



(when  $T_1=1$  and  $T_2=5$ ) for 0/90/0 or 0/90/0/90/0 cross ply graphite epoxy composite plates under case one conditions.

The optimum designs of case two (see Table 9.3) is very close to those of case one, although  $\tilde{D}$  for those two cases are different. It is because  $D_{12}$  and  $D_{66}$  are too small relative to  $D_{11}$  and  $D_{22}$  (see Equation 8.20 and Equation 8.38).

### 9.8 Conclusions

Since the material damping and stiffness of continuous or discontinuous fiber composites depends upon many quantities such as stiffness ratio  $E_f/E_m$ , fiber aspect ratio  $s/d$ , longitudinal distance between fiber tips  $p$ , loading (or fiber) angle  $\theta$ , fiber volume fraction  $V_f$ , fiber and matrix damping values, and stacking sequence, it is not feasible to discuss the material damping and stiffness by considering all the possible variations of all the independent quantities simultaneously. However, based upon the numerical results presented in this study, we can make the following conclusions:

#### A. About Unidirectional Fiber Composites

1. High damping could be achieved by small  $\theta$ , small  $s/d$ , and high  $p$ ; while high stiffness could be obtained through high  $V_f$ , small  $\theta$ , large  $s/d$ , and low  $p$ .
2. Damping of discontinuous fiber composites is no less than that of continuous fiber composites.

3. For small angle, high  $s/d$  gives high stiffness; while low  $s/d$  brings high damping. For large angles, damping and stiffness are independent of  $s/d$ .

B. About In-Plane Randomly Oriented Fiber Composites

1. Relative to unidirectional fiber composites, in-plane randomly oriented fiber composites have lower stiffness at the price of keeping high damping in all directions parallel to the plane.
2. Variations of shear damping and shear modulus vs  $s/d$  are very close to those of normal damping and normal stiffness, respectively.
3. Influence of  $V_f$  on normal damping becomes less when  $s/d$  is smaller.

C. About Laminated Fiber Composites

1. For different kinds of lamination, high stiffness lamination has low damping and vice versa.
2. The properties of damping and stiffness of angle ply lamination are very similar to those of unidirectional fiber composites, when  $\theta$  is the same.
3. Damping of cross ply lamination is close to that of aligned fiber composite ( $\theta=0^\circ$ ). But the cross ply keeps equal stiffness in both  $x$  and  $y$  directions rather than high stiffness in  $x$  direction and low stiffness in  $y$  direction of the aligned fiber composite.

D. About the Energy Approach and Laminated Plate Theory Approach

1. Damping analysis through the energy approach is loading condition, boundary condition and geometry (of the body) dependent. It gives more reliable results on damping, while the laminated plate theory approach can give quick estimation about damping.
2. Fortunately, the variations of the material damping vs those variables in these two approaches, in general, follow a similar pattern, if the dimension in the thickness direction is one order less than the dimensions in the other two directions.

E. About Optimization

Optimumization of damping and specific stiffness depends on the preference of high specific stiffness or high damping ( $T_1$  or  $T_2$ ), material property of fiber, the stacking sequence for hybrid composite, and boundary conditions. A continuous fiber reinforced hybrid orthotropic composite plate with stacking sequence  $0^K/90^K/0^G/90^G$  is the optimum design for clamped (or simply supported) square plate under the free vibration.

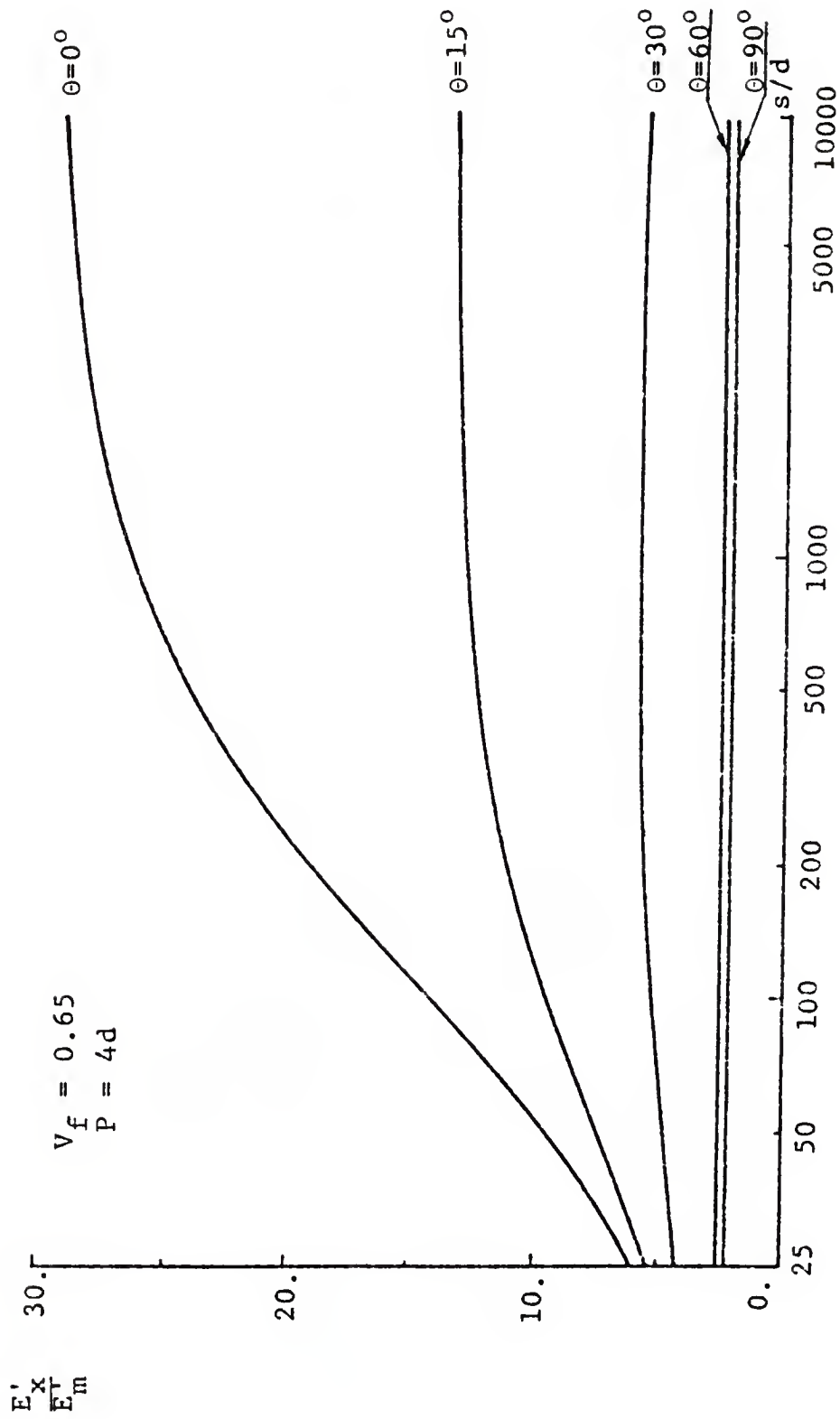


Figure 9.1: Plots of  $E'_x/E'_m$  vs  $s/d$  Using  $\theta$  as a Parameter for Graphite Epoxy Composites

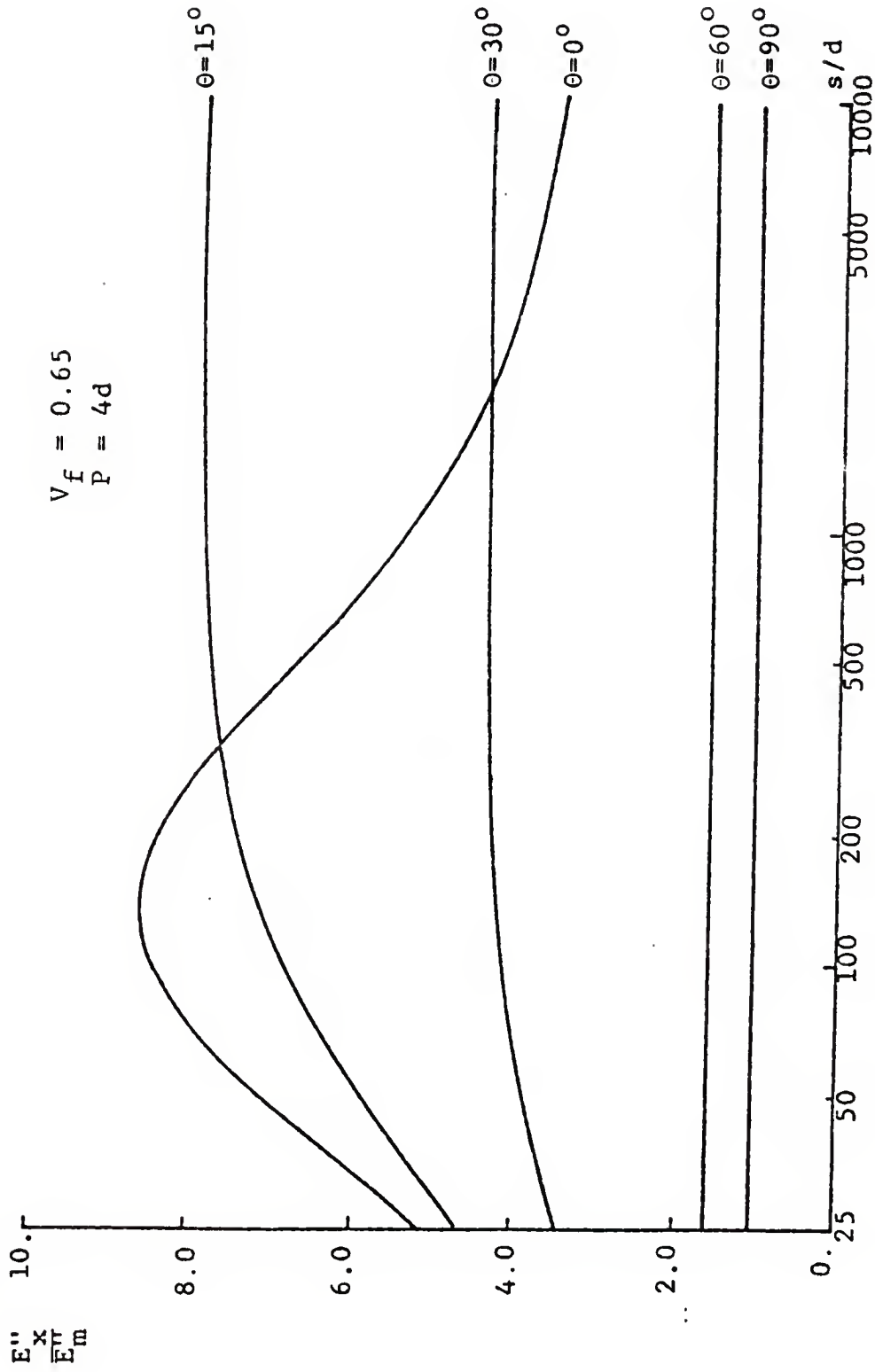


Figure 9.2: Plots of  $E''_x/E''_m$  vs  $s/d$  Using  $\theta$  as a Parameter for Graphite Epoxy Composites

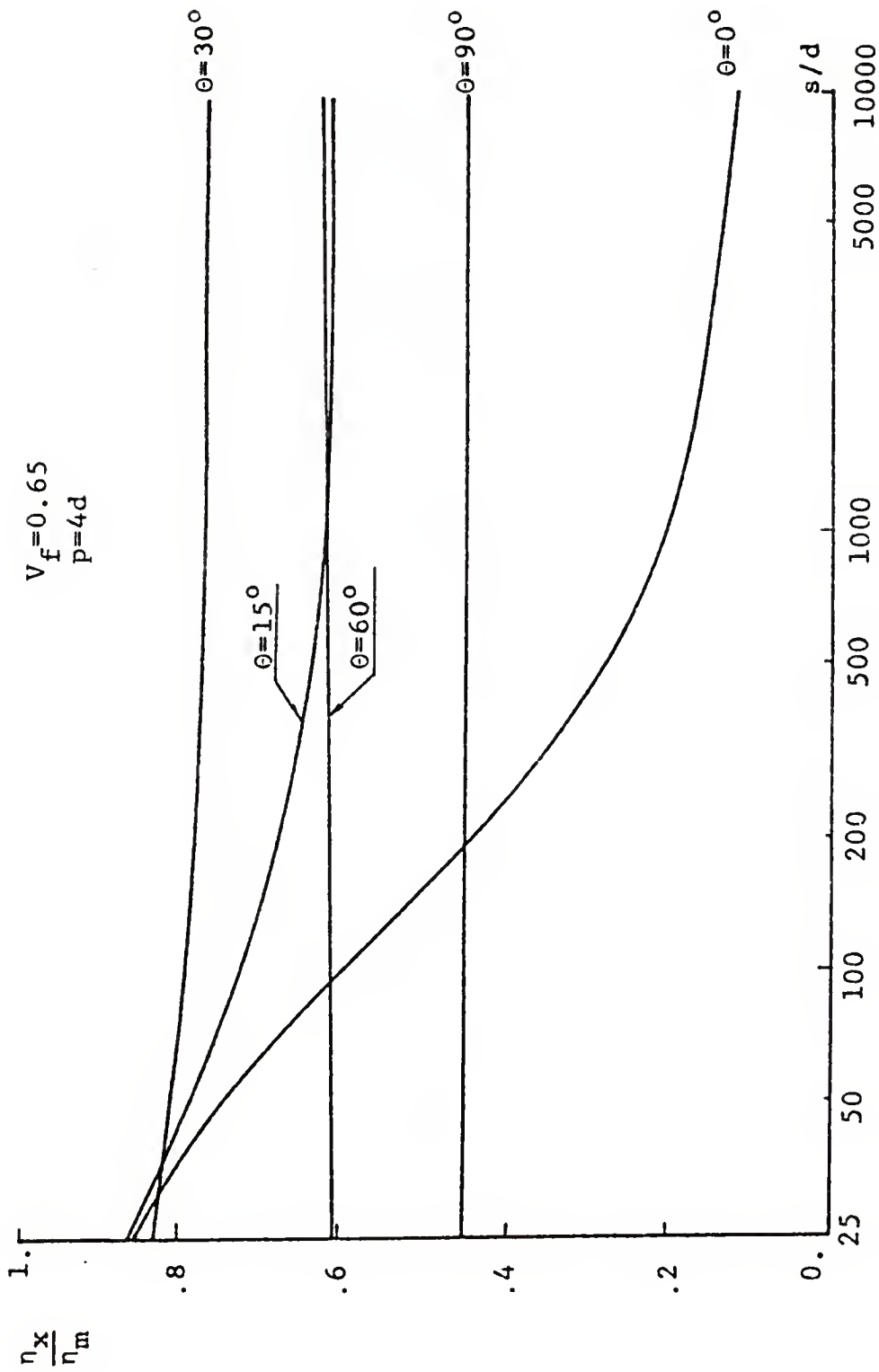


Figure 9.3: Plots of  $\eta_x/\eta_m$  vs  $s/d$  Using  $\theta$  as a Parameter for Graphite Epoxy Composites

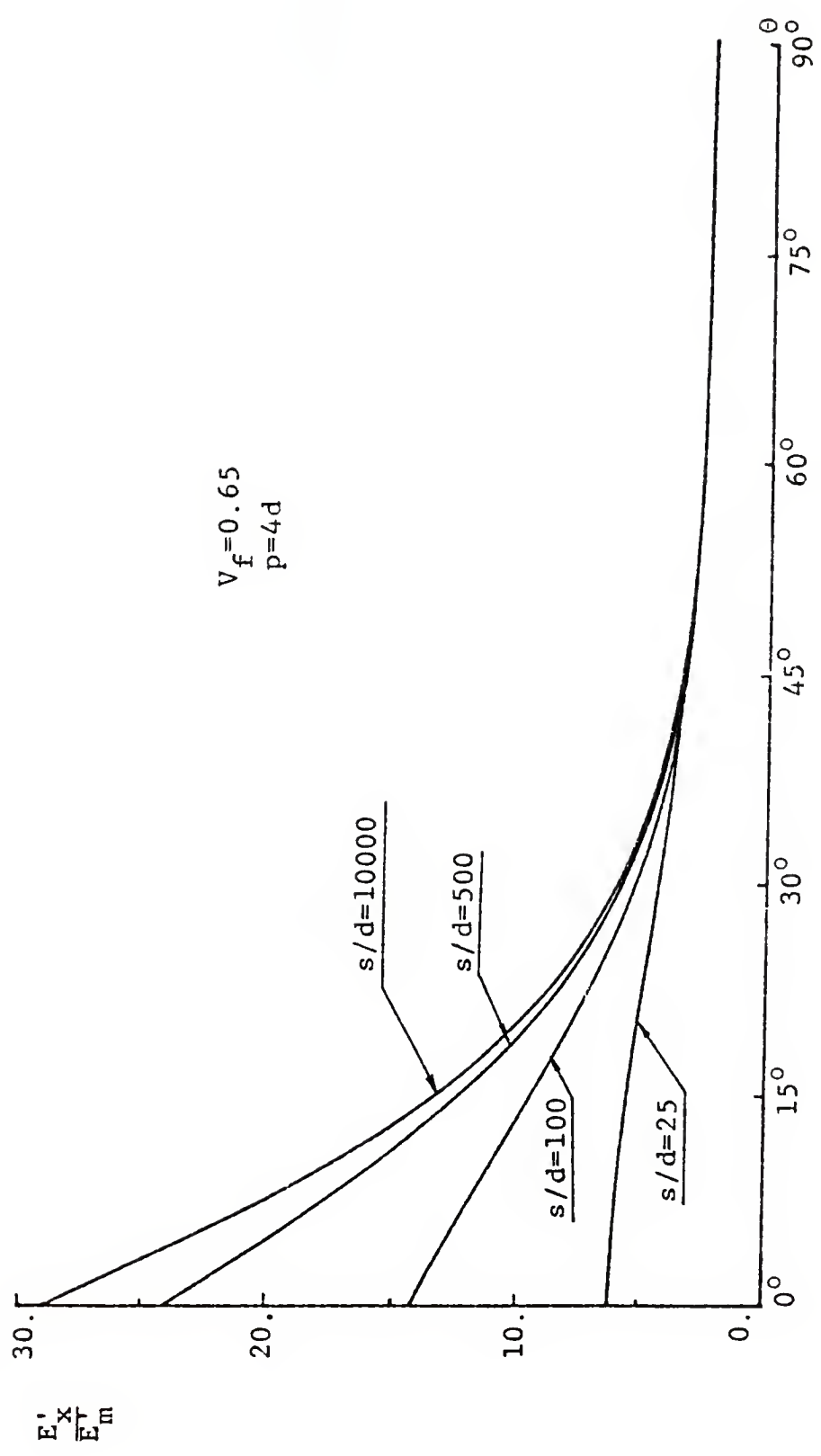


Figure 9.4: Plots of  $E'_x/E'_m$  vs  $\theta$  Using  $s/d$  as a Parameter for Graphite Epoxy Composites

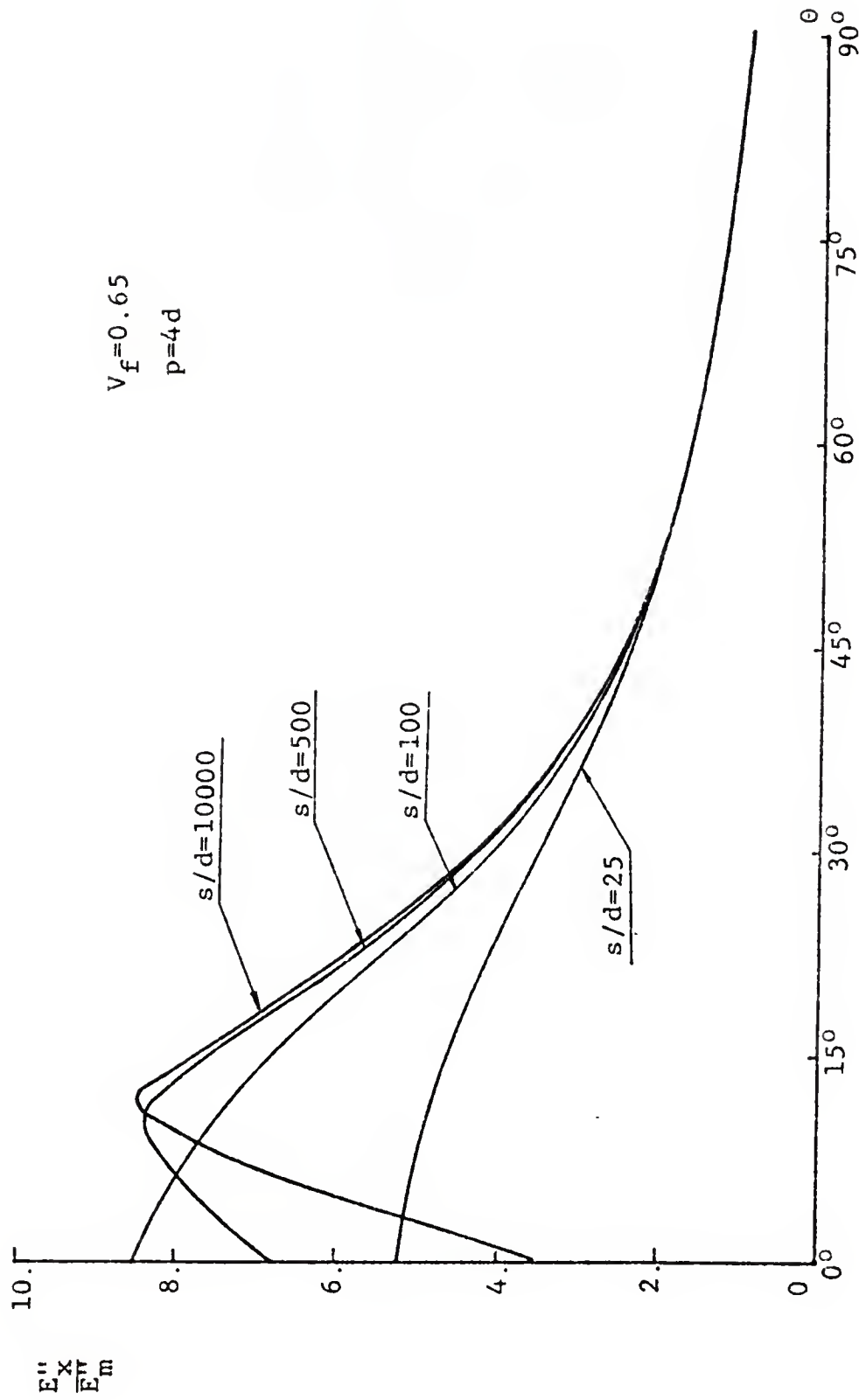


Figure 9.5: Plots of  $E''_x/E''_m$  vs  $\theta$  Using  $s/d$  as a Parameter for Graphite Epoxy Composites



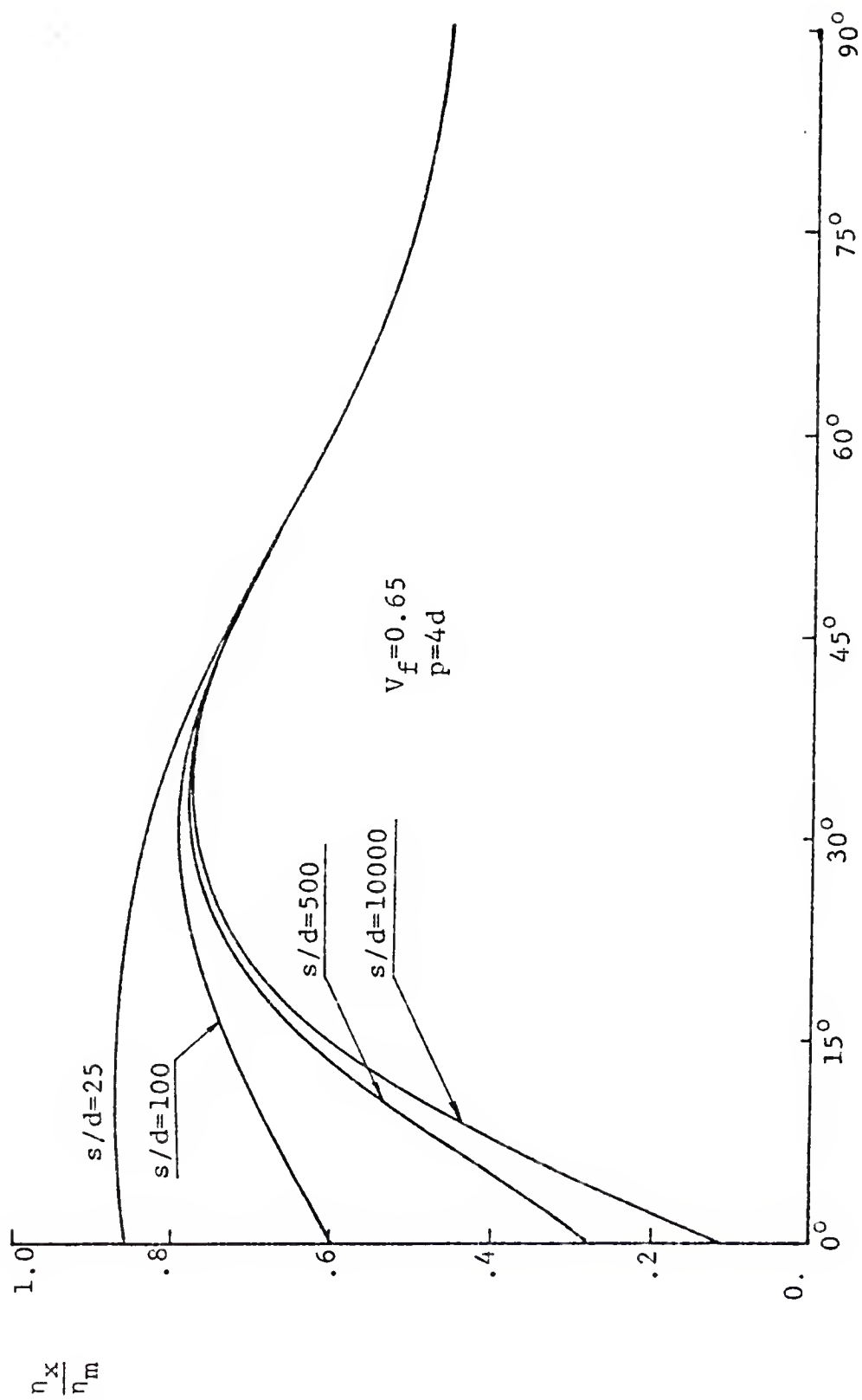


Figure 9.6: Plots of  $\eta_x/\eta_m$  vs  $\theta$  Using  $s/d$  as a Parameter for Graphite Epoxy Composites

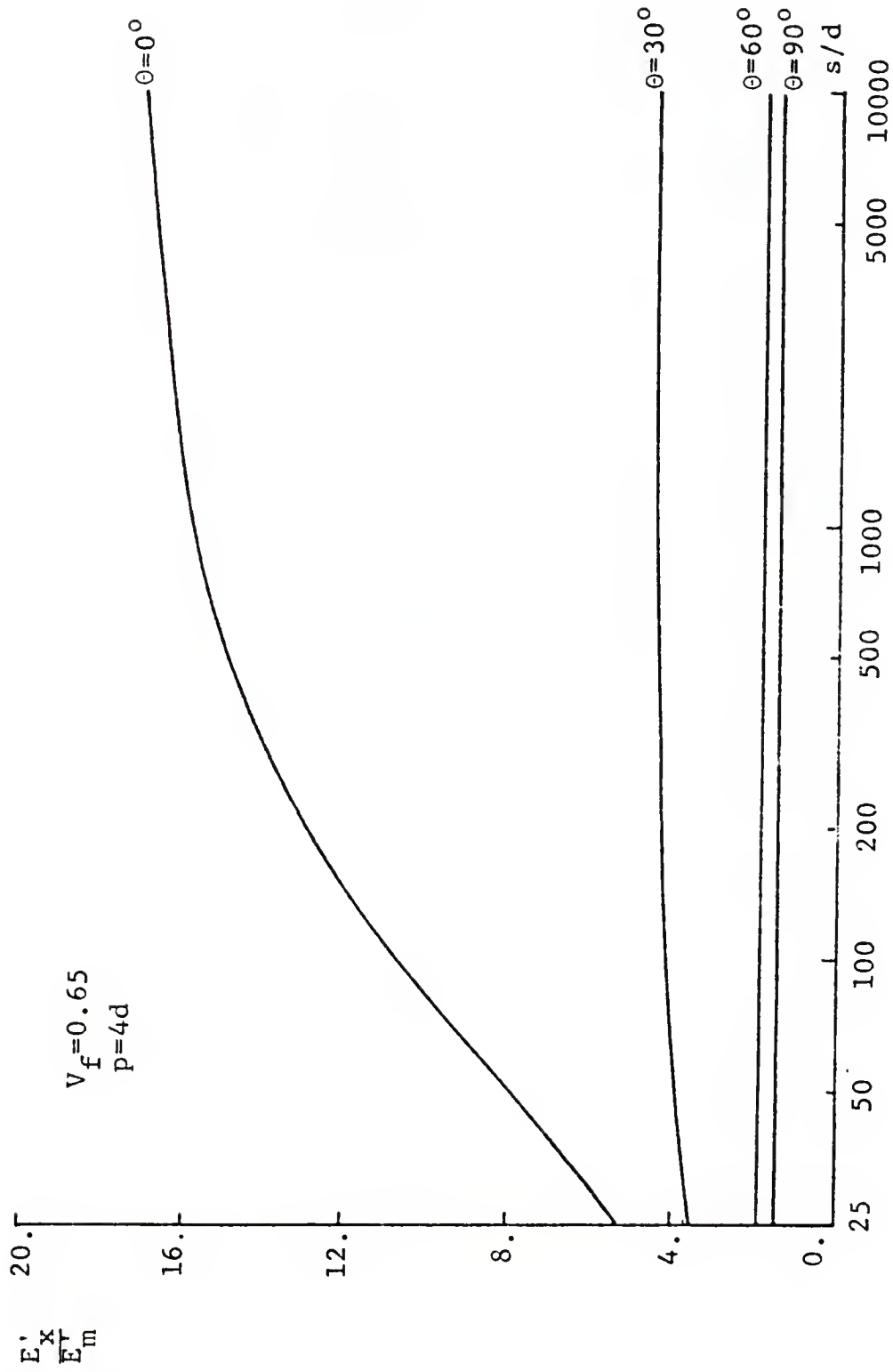


Figure 9.7: Plots of  $E'_x/E'_m$  vs  $s/d$  Using  $\theta$  as a Parameter for Kevlar Epoxy Composites

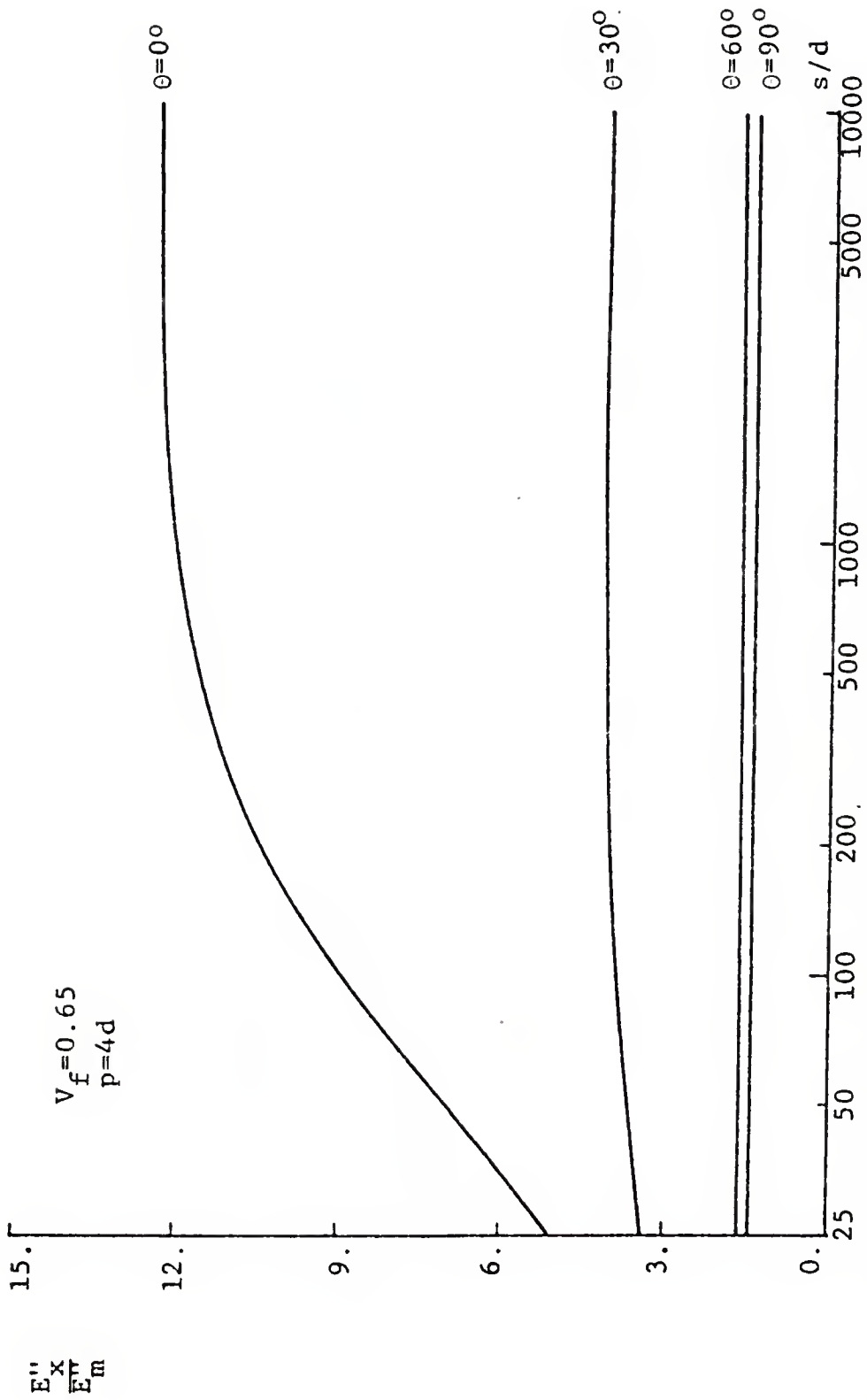


Figure 9.8: Plots  $E''_x/E''_m$  vs  $s/d$  Using  $\theta$  as a Parameter for Kevlar-Epoxy Composites

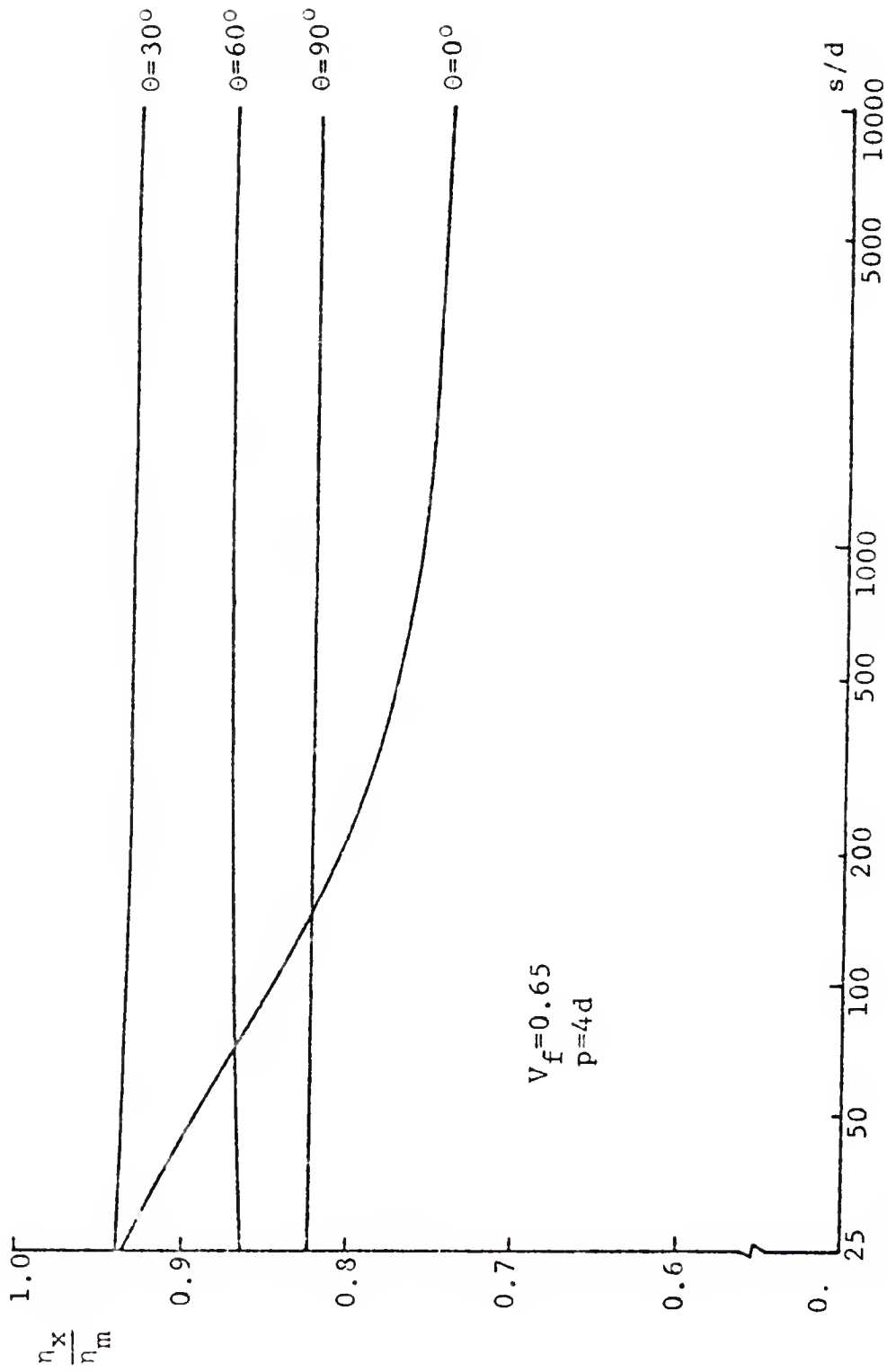


Figure 9.9: Plots of  $\eta_x / \eta_m$  vs  $s/d$  Using  $\theta$  as a Parameter for Kevlar Epoxy Composites

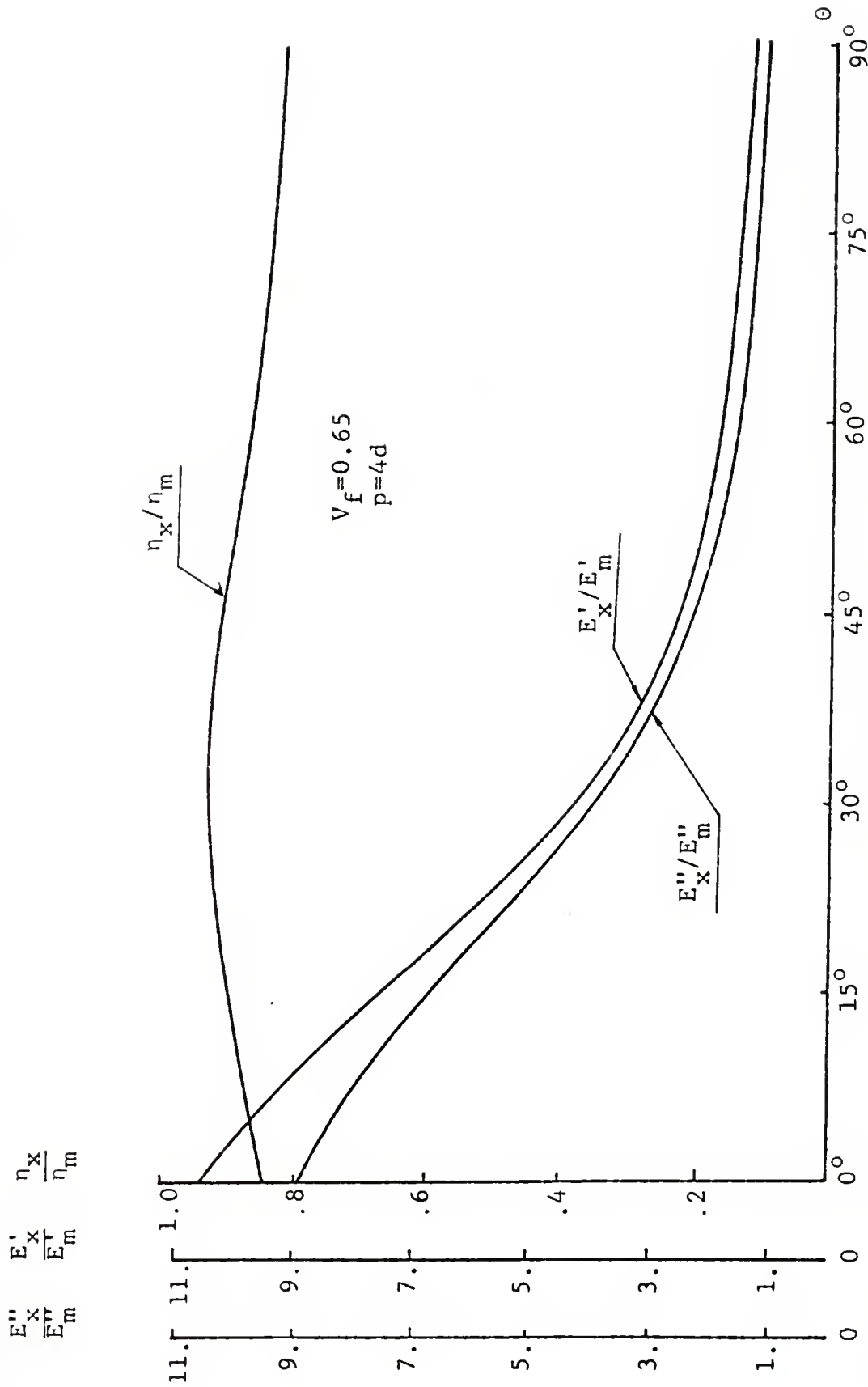


Figure 9.10: Plots of  $\eta_x/\eta_m$ ,  $E'_x/E'_m$  and  $E''_x/E''_m$  vs  $\theta$  Keeping  $s/d=100$  for Kevlar Epoxy Composites

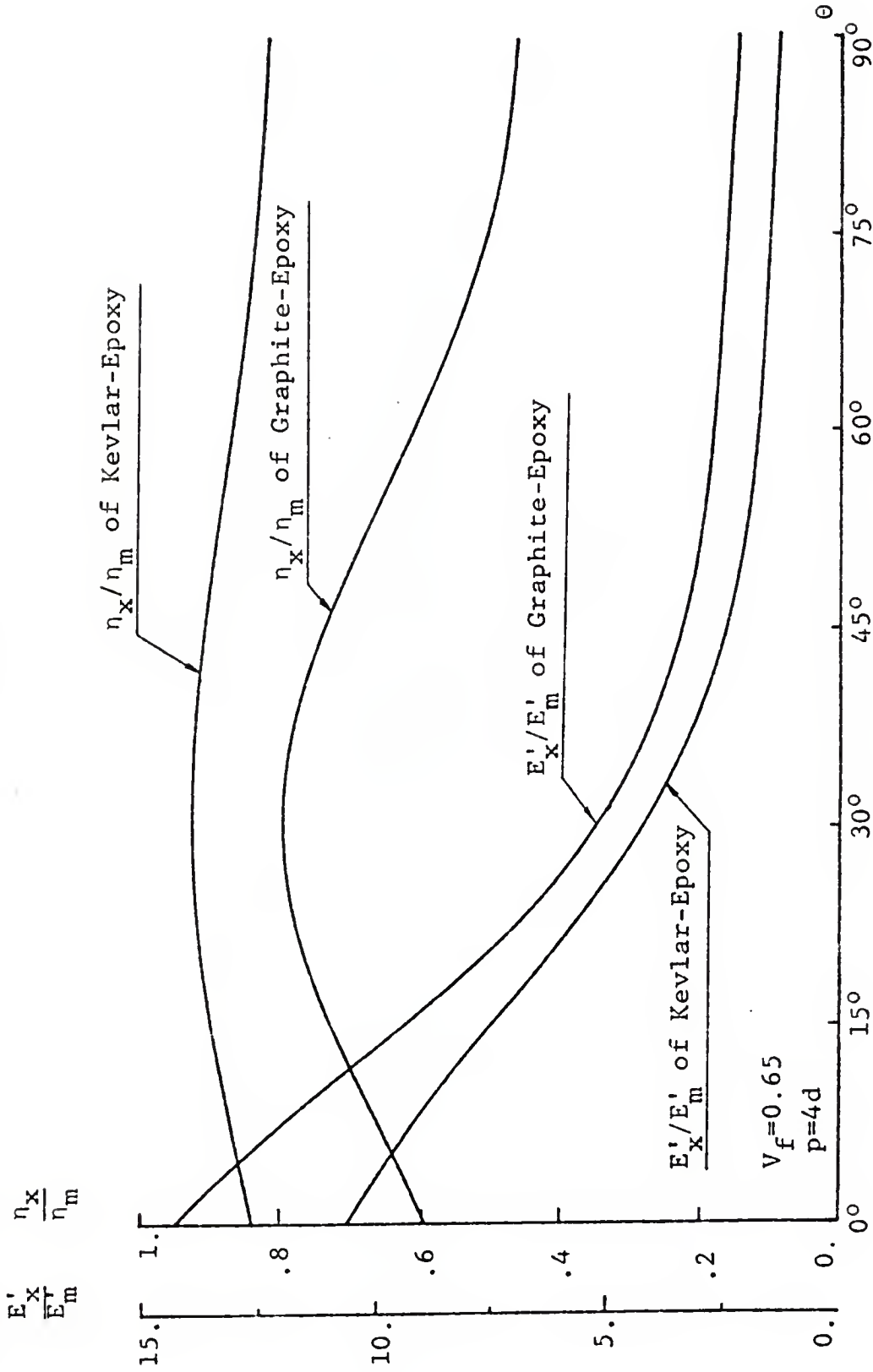


Figure 9.11: Plots of  $\eta_x/\eta_m$  and  $E'_x/E'_m$  vs  $\theta$  Keeping  $s/d=100$  for Graphite Epoxy Composites and Kevlar Epoxy Composites

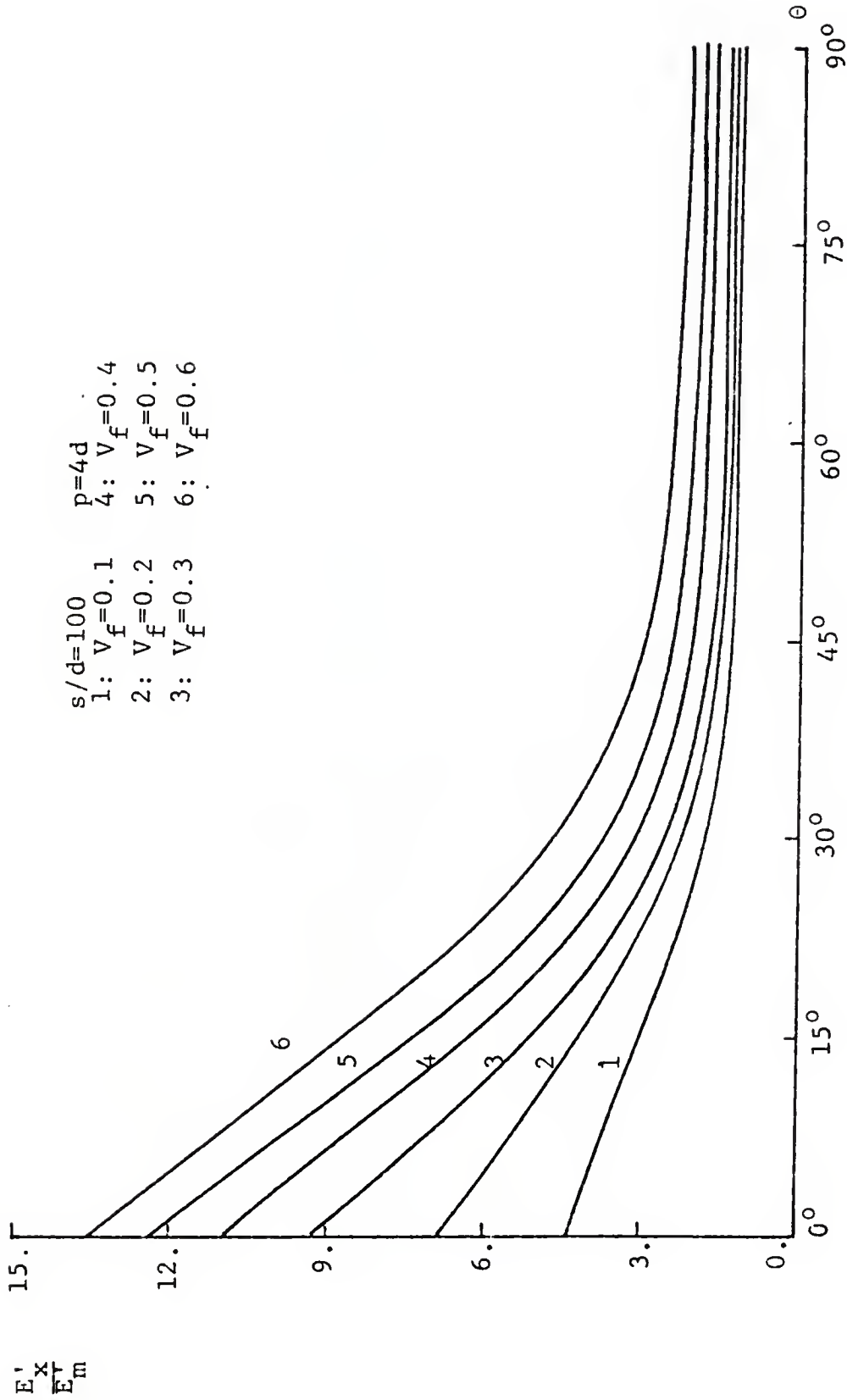


Figure 9.12: Plots of  $E'_x/E'_m$  vs  $\theta$  Using  $V_f$  as a Parameter for Graphite Epoxy Composites

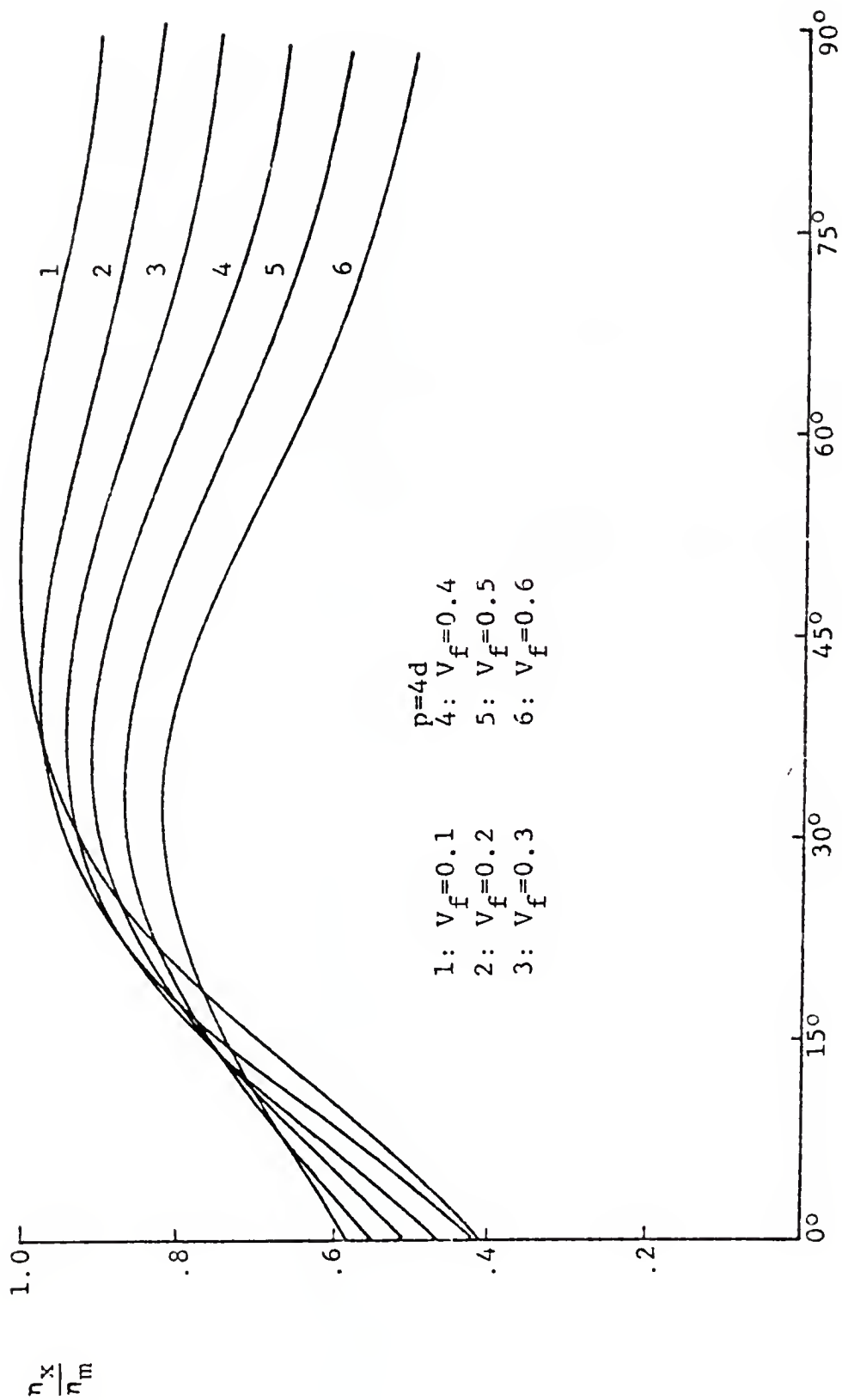


Figure 9.13: Plots of  $\eta_x/\eta_m$  vs  $\theta$  Using  $V_f$  as a Parameter for Graphite Epoxy Composites



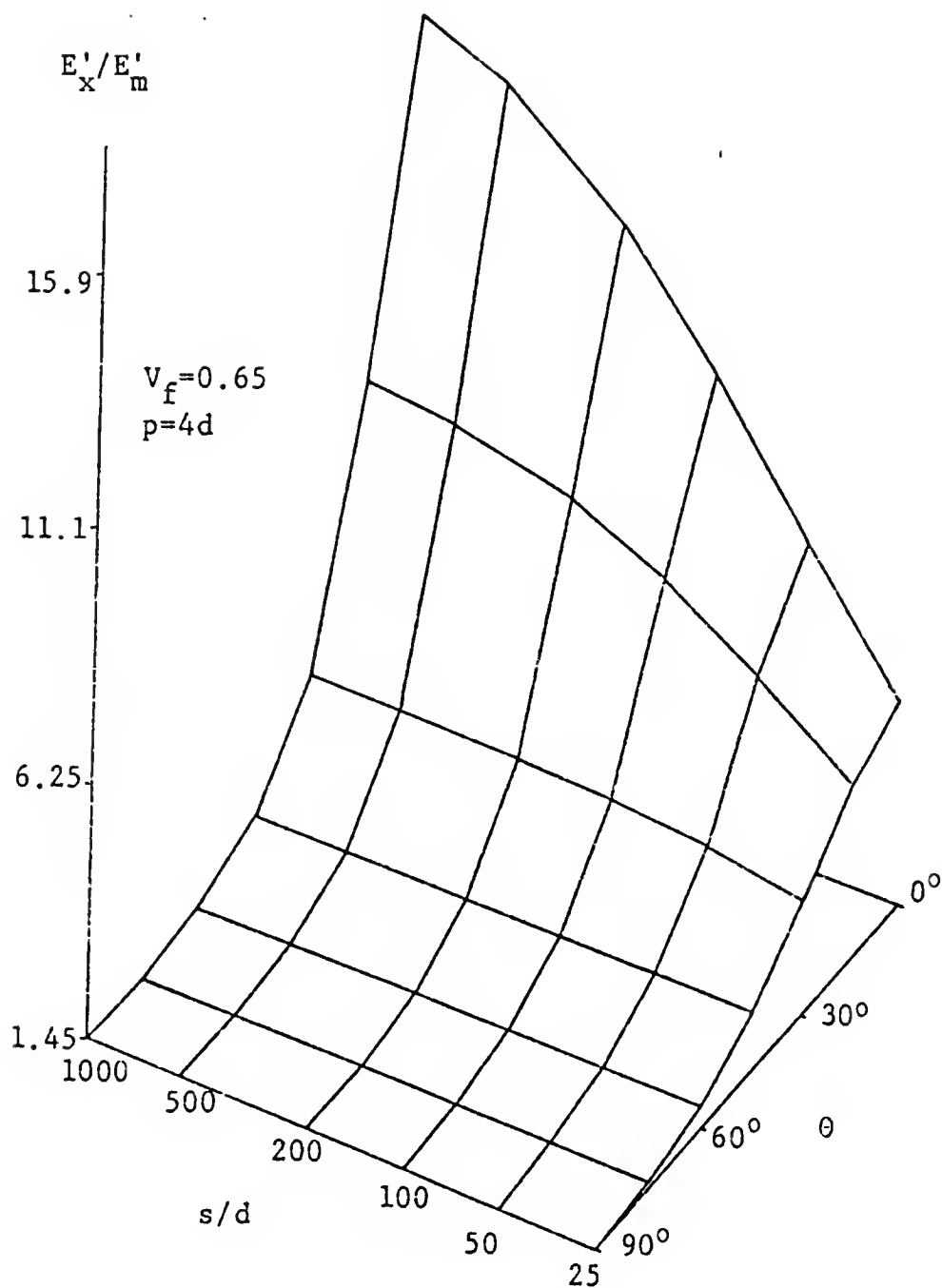


Figure 9.14: Three-Dimensional Plots of  $E'_x/E'_m$  vs  $\theta$  and  $s/d$  for Unidirectional Kevlar Epoxy Composites

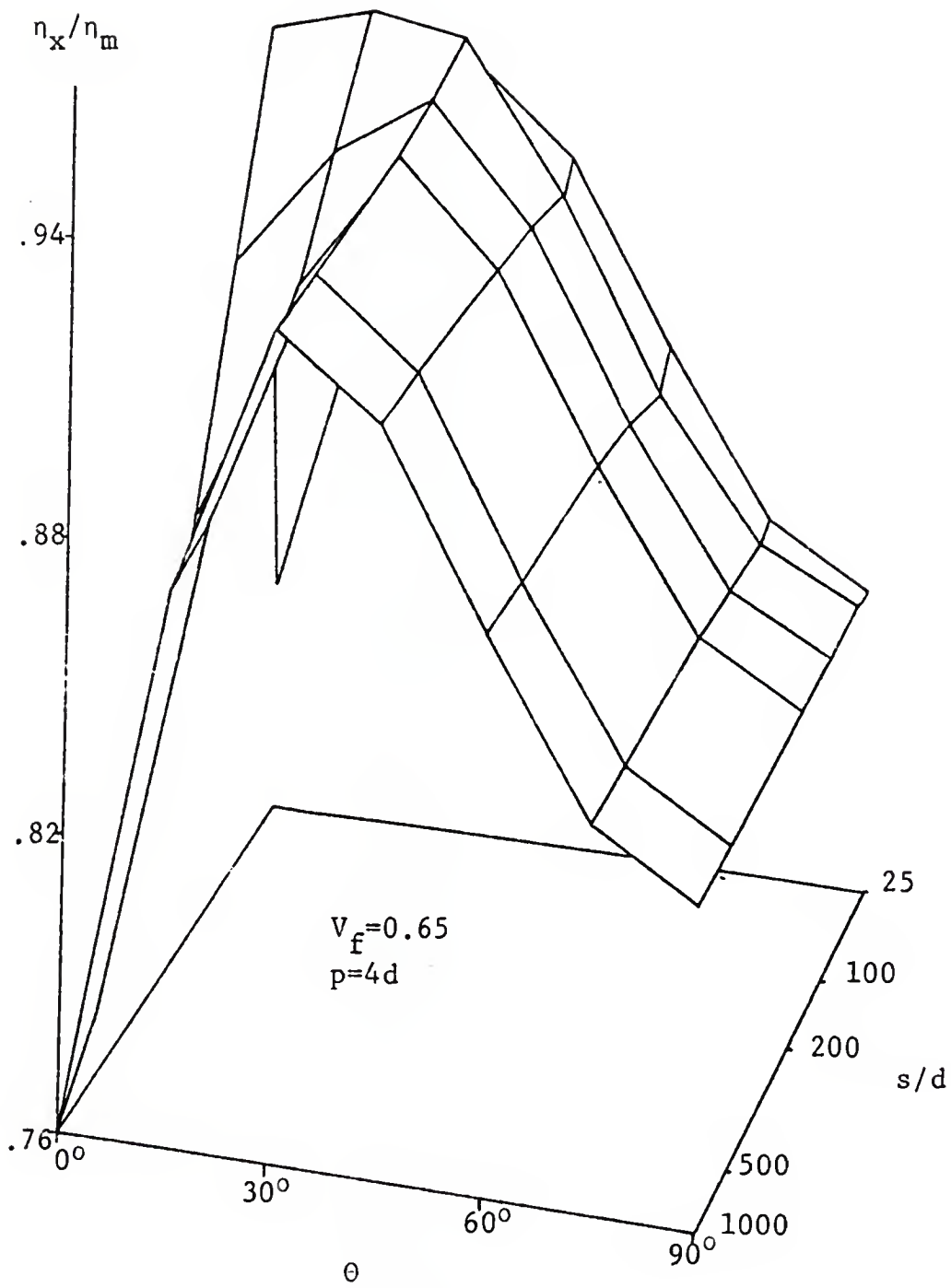


Figure 9.15: Three-Dimensional Plots of  $\eta_x/\eta_m$  vs  $\theta$  and  $s/d$  for Unidirectional Kevlar Epoxy Composites

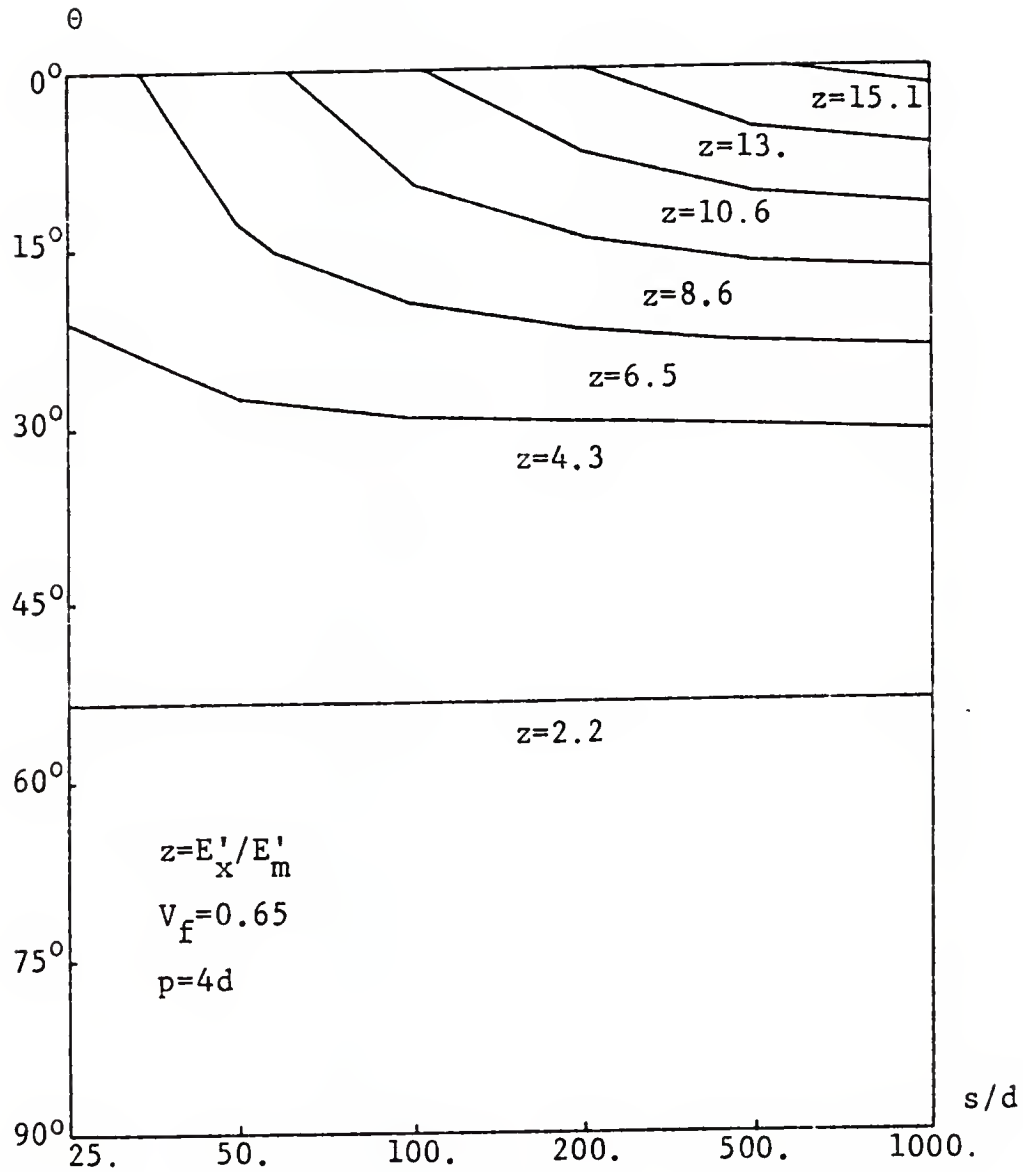


Figure 9.16: Contour Curves of  $E'_x/E'_n$  vs  $\theta$  and  $s/d$  for Unidirectional Kevlar Epoxy Composites

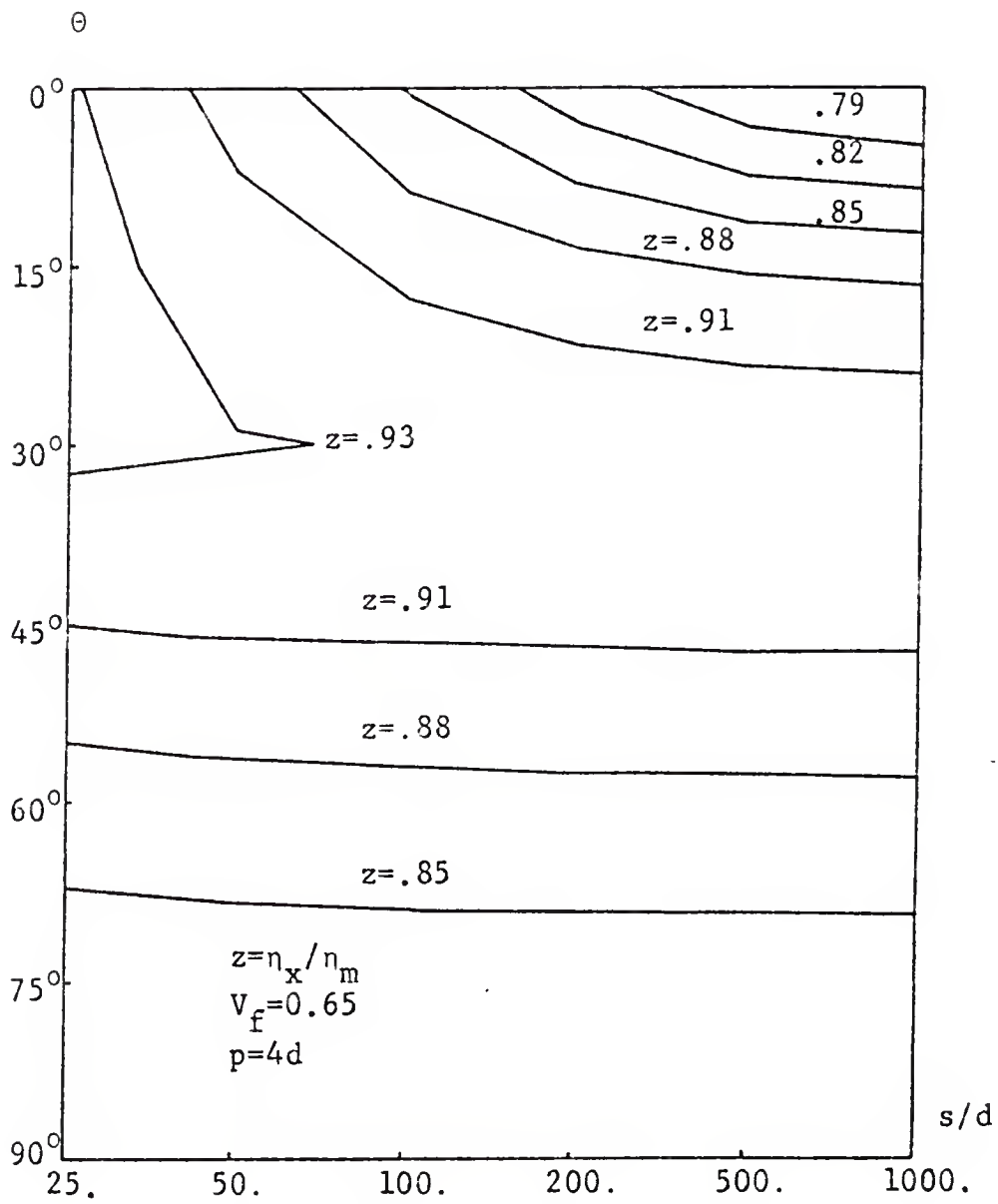


Figure 9.17: Contour Curves of  $\eta_x/\eta_m$  vs  $\theta$  and  $s/d$  for Unidirectional Kevlar Epoxy Composites

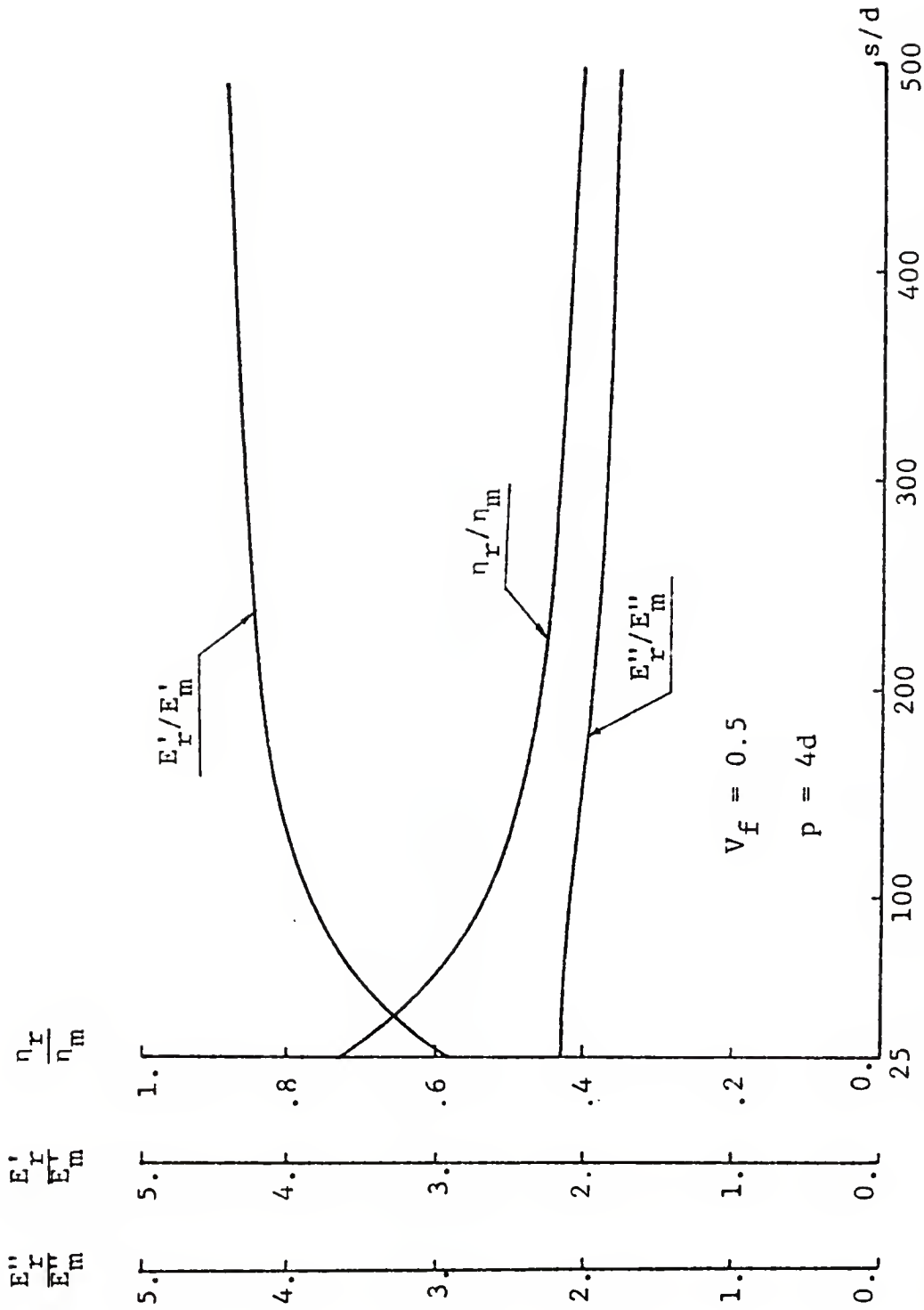


Figure 9.18: Plots of  $\eta_r/\eta_m$ ,  $E'_r/E'_m$  and  $E''_r/E''_m$  vs  $s/d$  for Randomly Oriented Glass Epoxy Composites

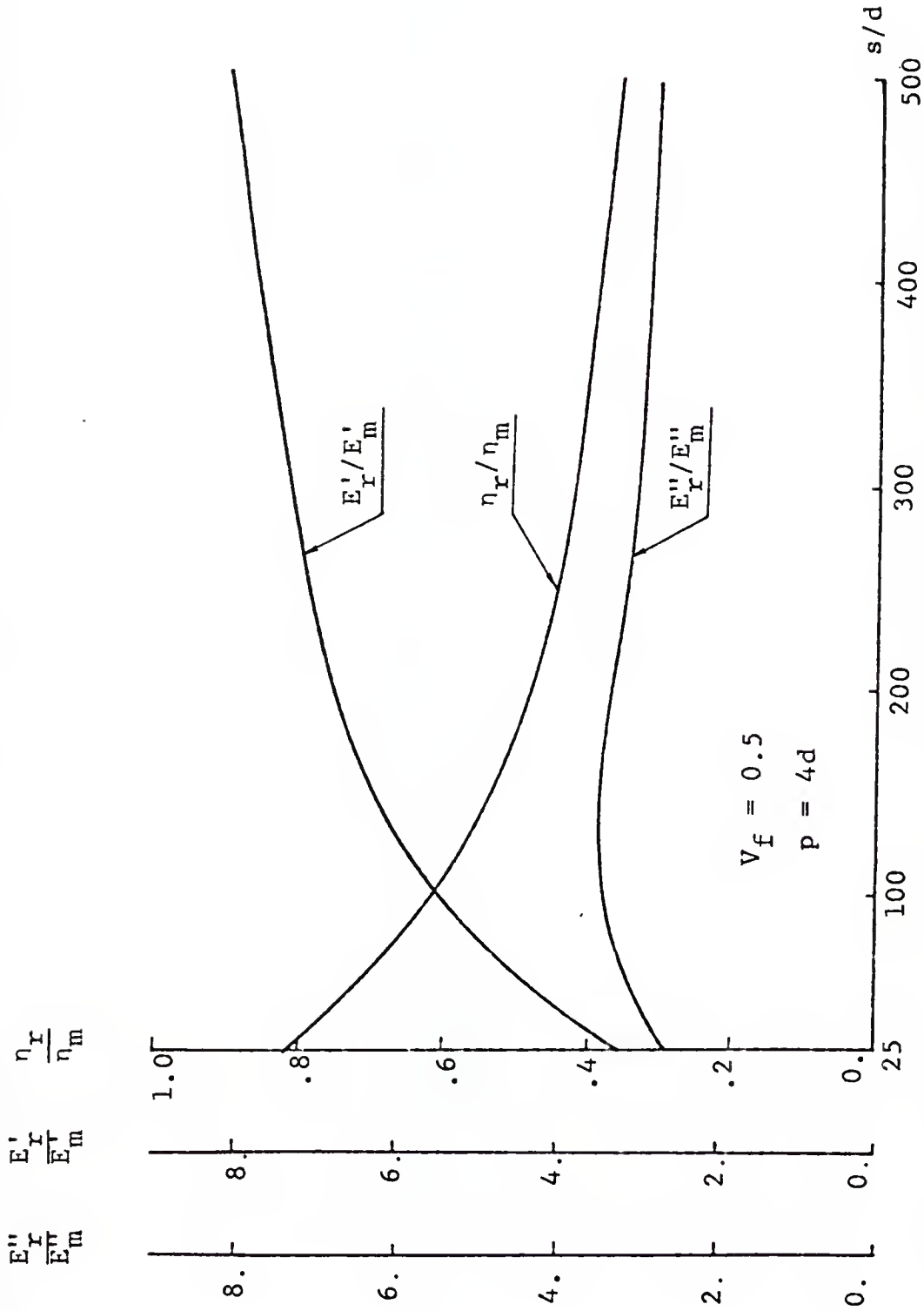


Figure 9.19: Plots of  $\eta_r/\eta_m$ ,  $E'_r/E'_m$  and  $E''_r/E''_m$  vs  $s/d$  for Randomly Oriented Graphite Epoxy Composites

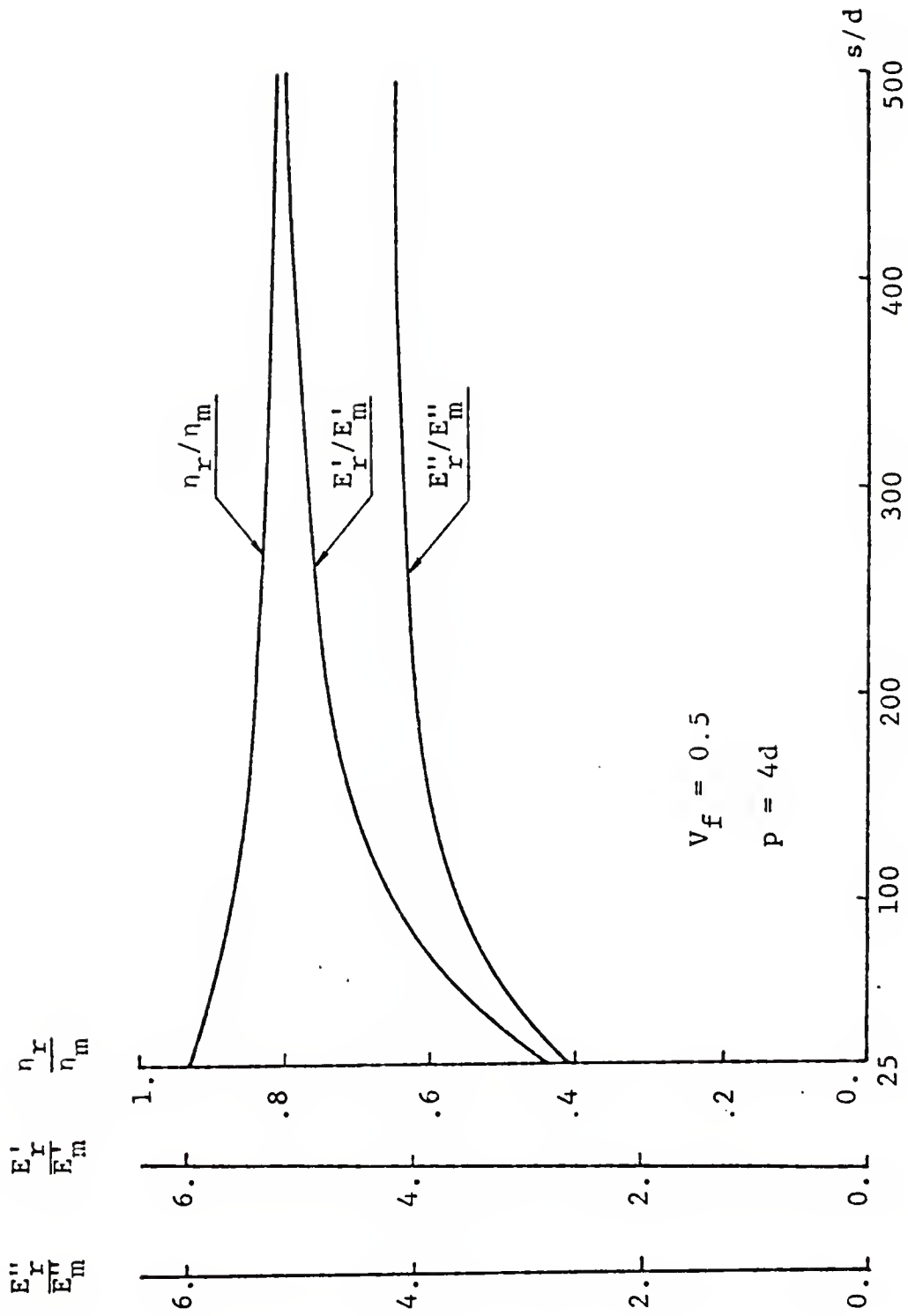


Figure 9.20: Plots of  $\eta_r / \eta_m$ ,  $E'_r / E'_m$  and  $E''_r / E''_m$  vs  $s/d$  for Randomly Oriented Kevlar Epoxy Composites

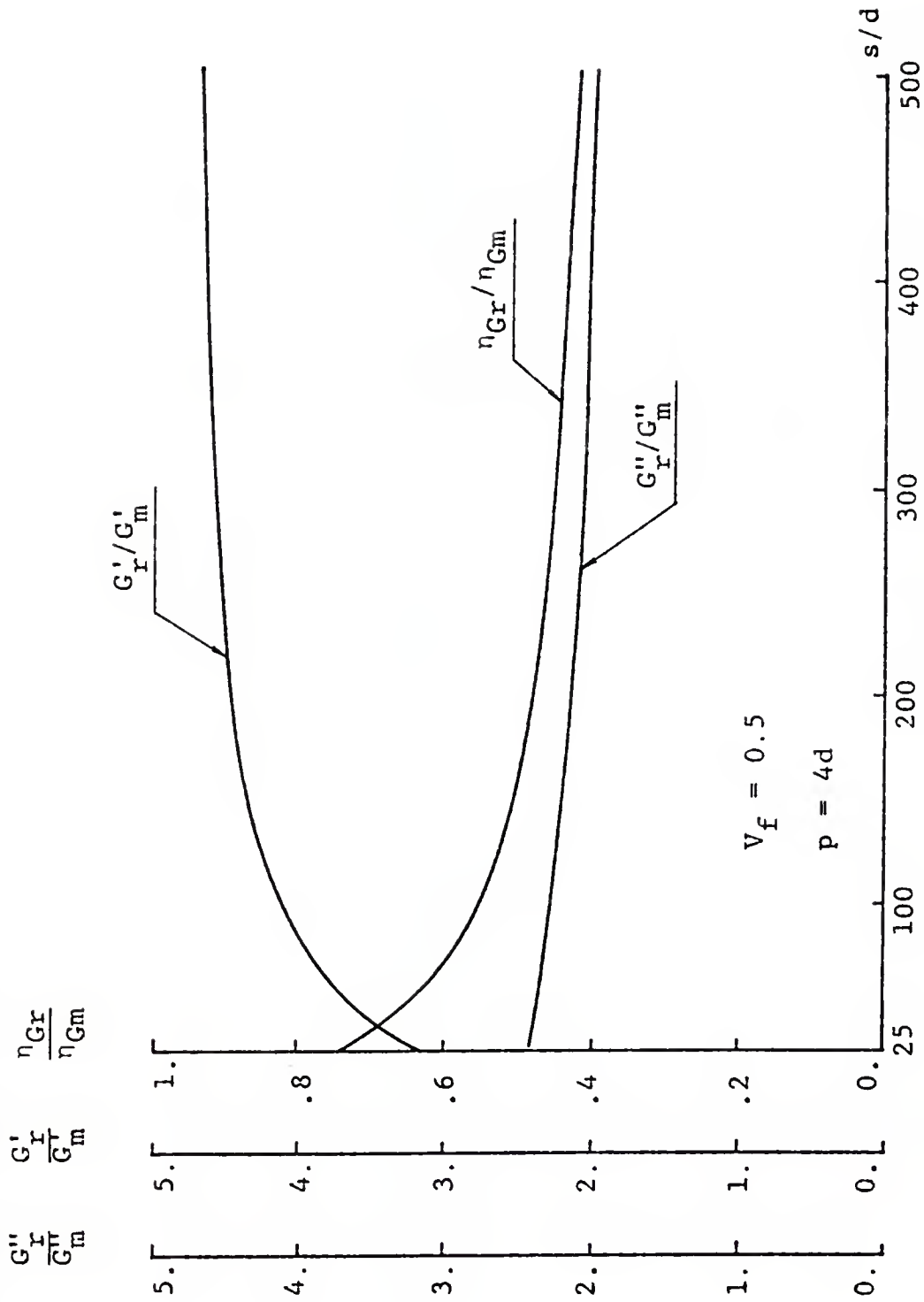


Figure 9.21: Plots of  $\eta_{Gr}/\eta_{Gm}$ ,  $G'_r/G'_m$  and  $G''_r/G''_m$  vs  $s/d$  for Randomly Oriented Glass Epoxy Composites



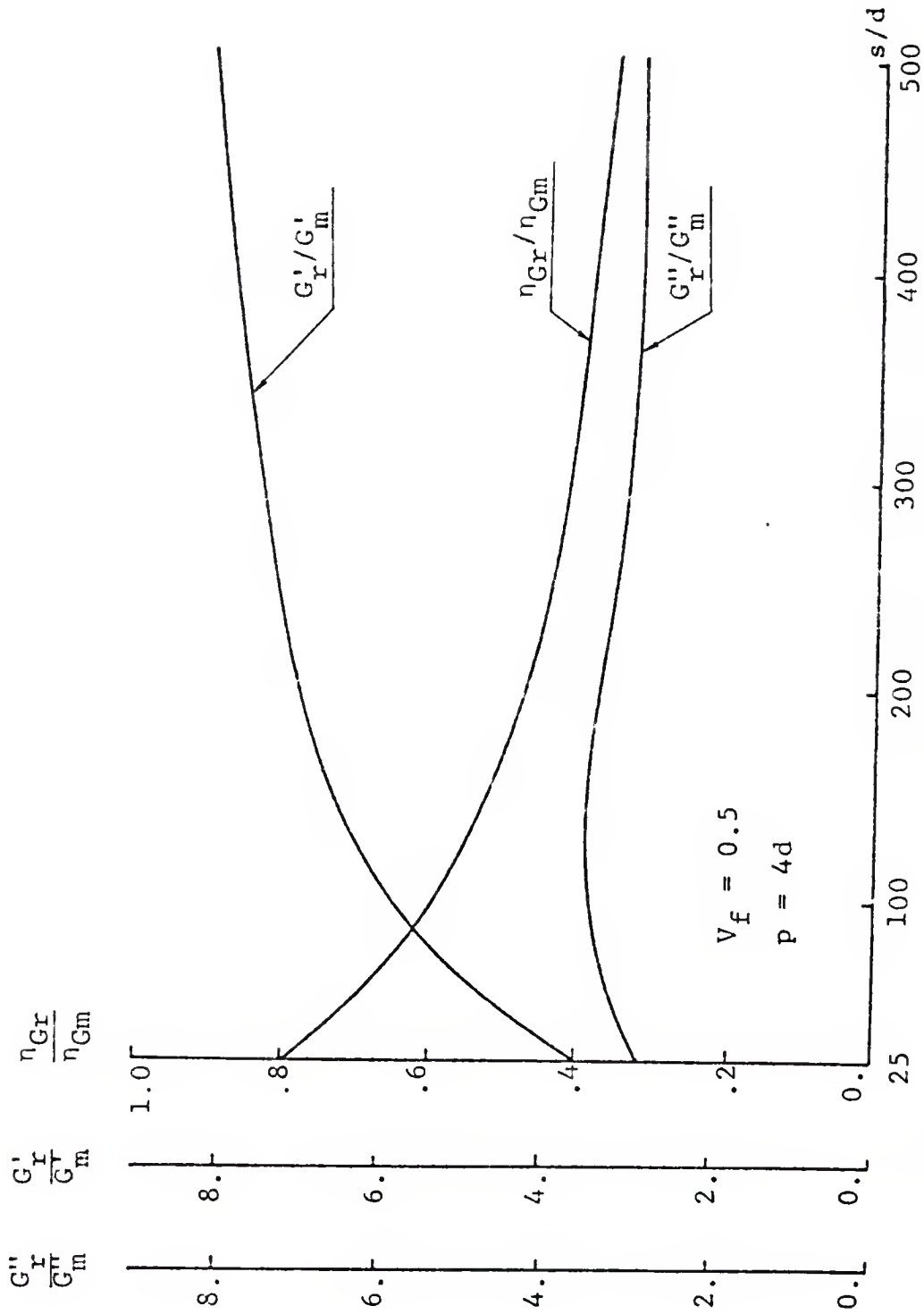


Figure 9.22: Plots of  $\eta_{Gr}/\eta_{Gm}$ ,  $G'_r/G'_m$  and  $G''_r/G''_m$  vs  $s/d$  for Randomly Oriented Graphite Epoxy Composites

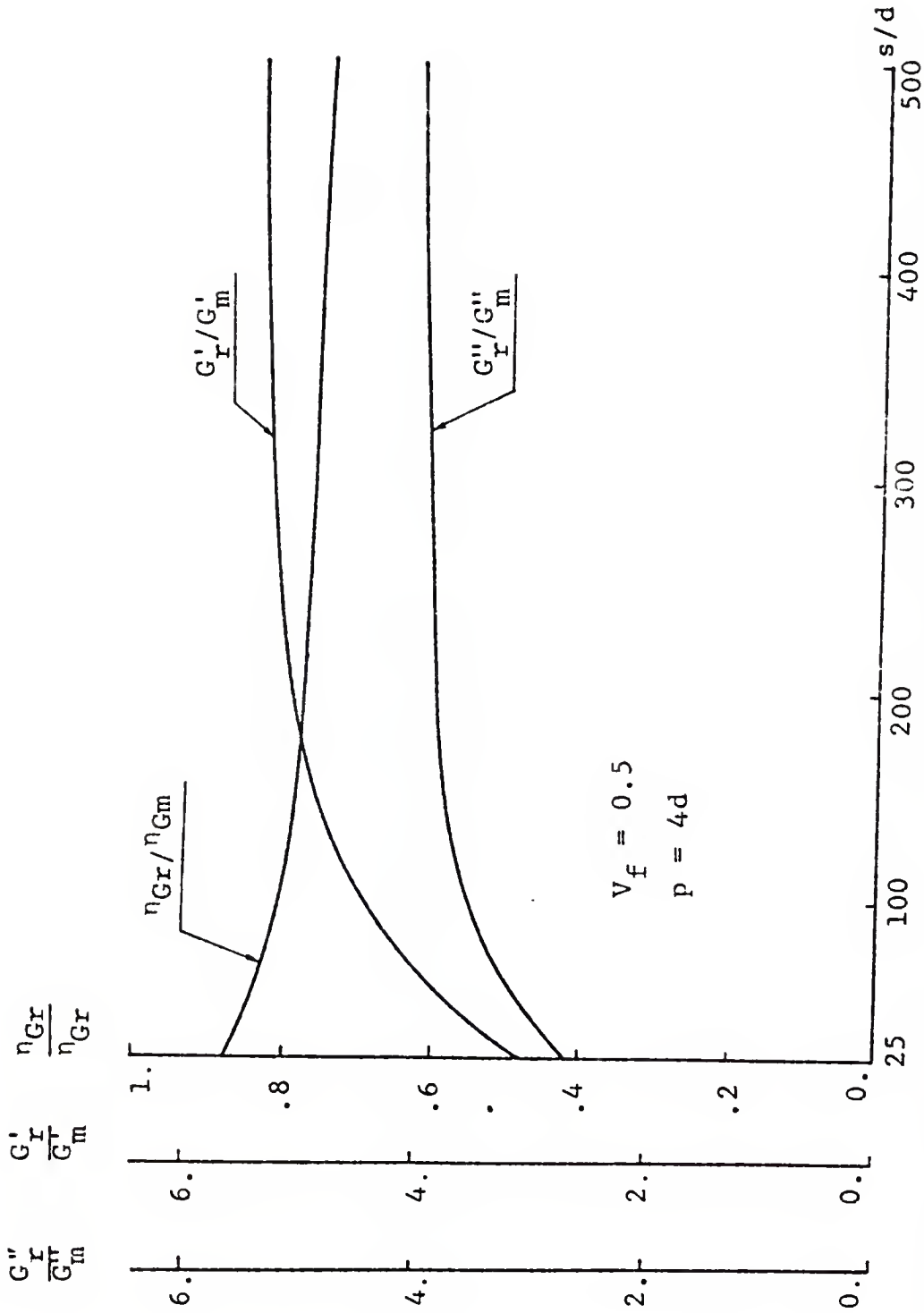


Figure 9.23: Plots of  $\eta_{Gr}/\eta_{Gm}$ ,  $G'_r/G'_m$  and  $G''_r/G''_m$  vs  $s/d$  for Randomly Oriented Kevlar Epoxy Composites

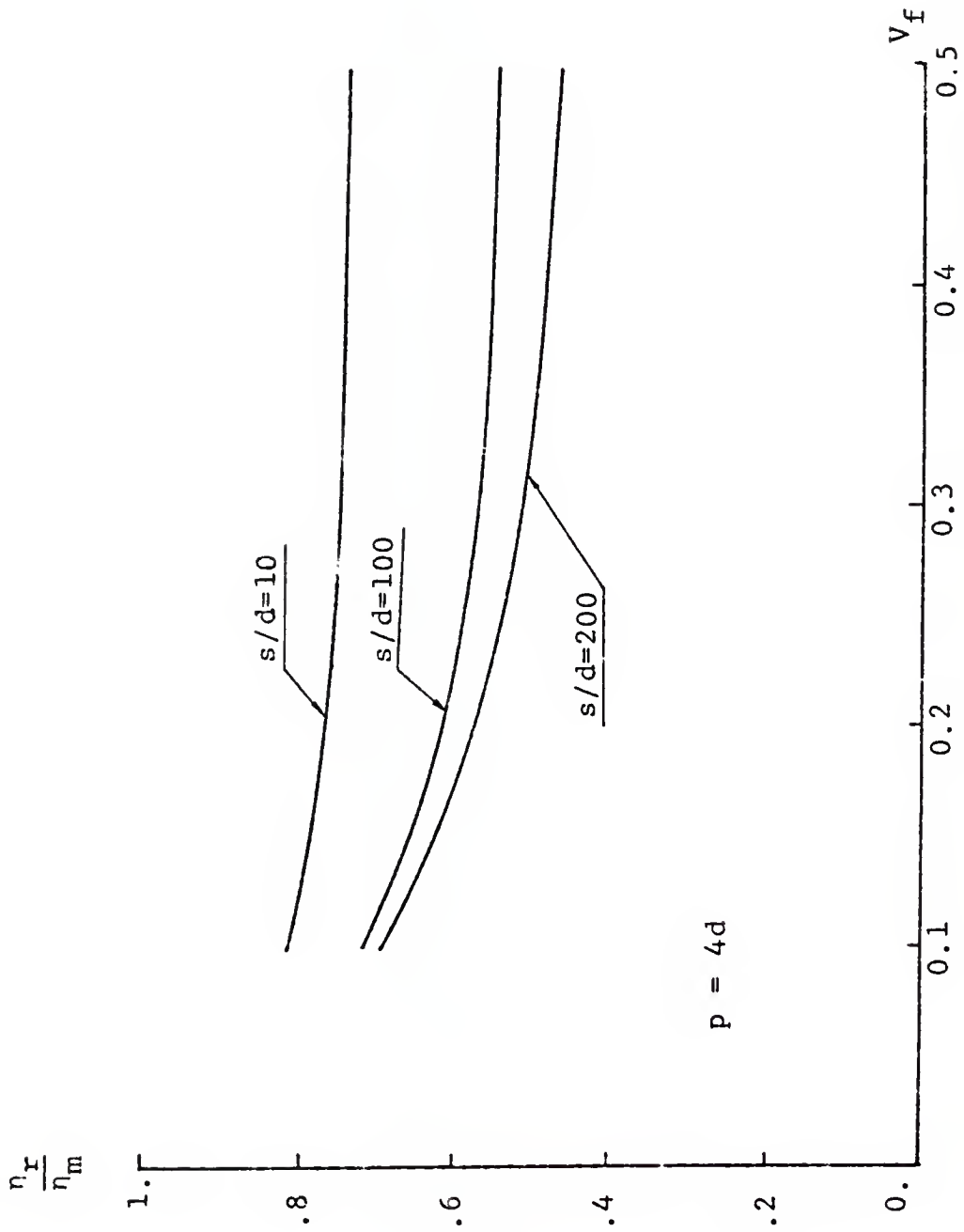


Figure 9.24: Plots of  $\eta_I/\eta_m$  vs  $V_f$  Using  $s/d$  as a Parameter for Randomly Oriented Glass Epoxy Composites

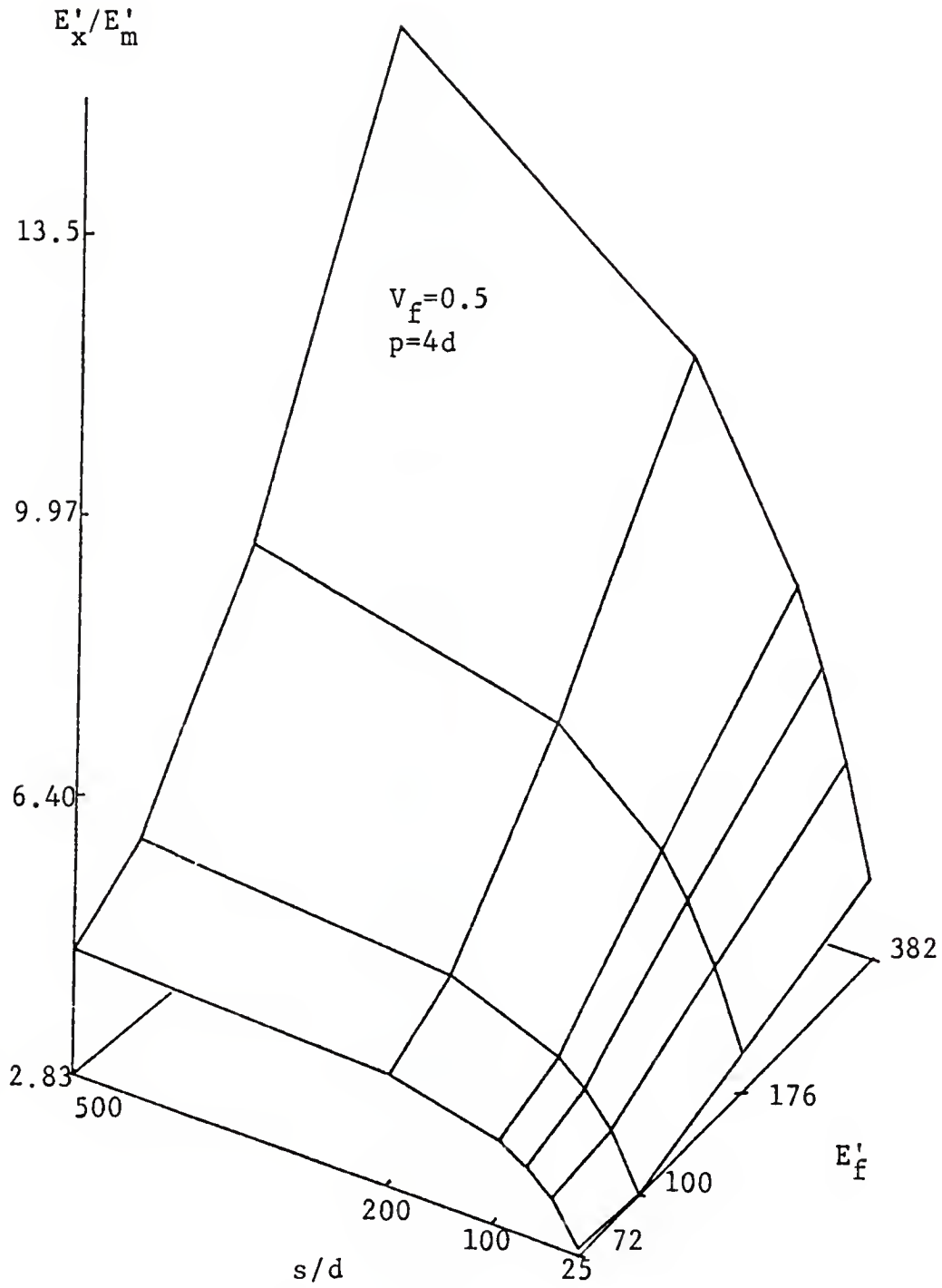


Figure 9.25: Three-Dimensional Plots of  $E'_x/E'_m$  vs  $s/d$  and  $E'_f$  for Randomly Oriented Fiber Composites

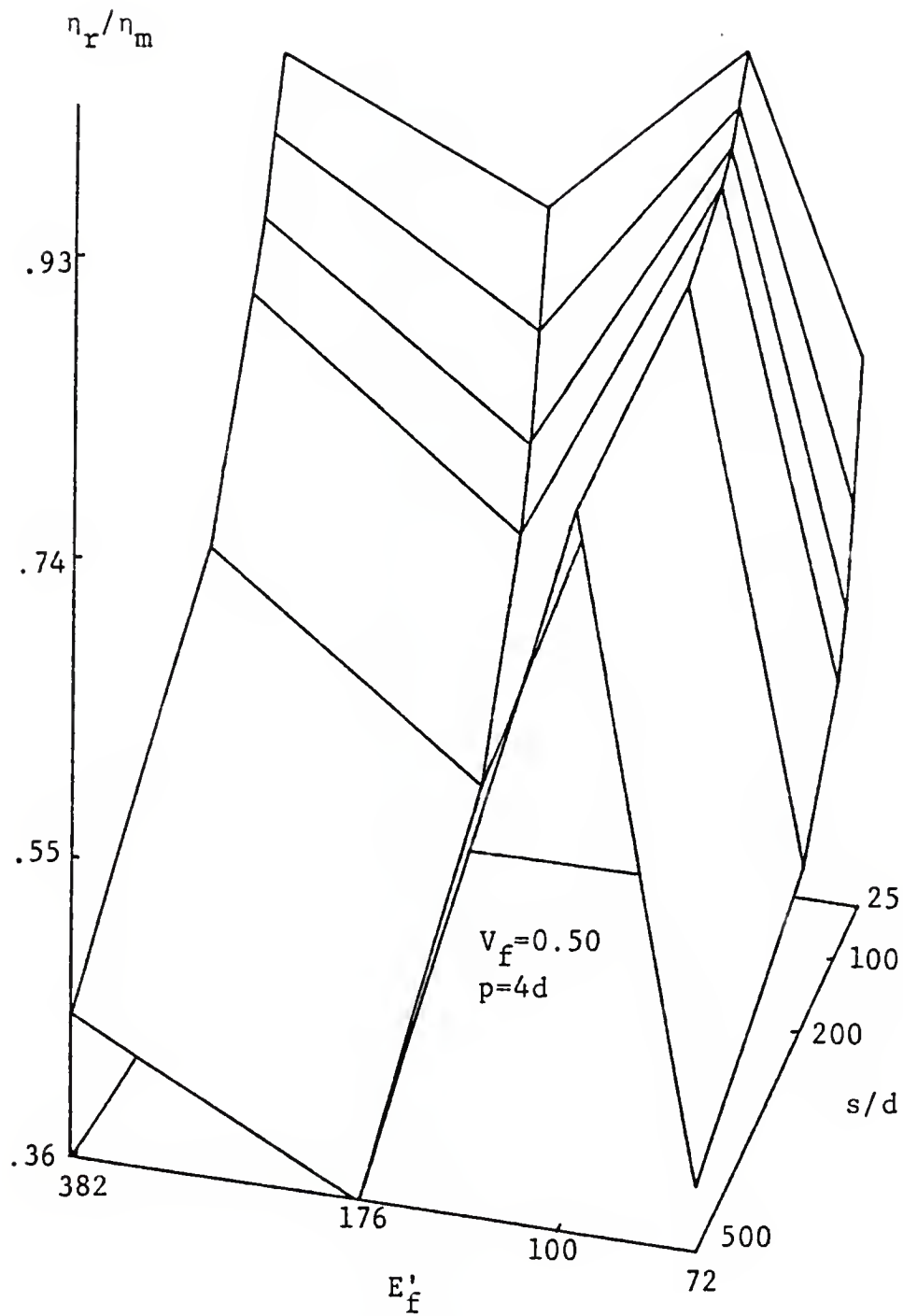


Figure 9.26: Three-Dimensional Plots of  $\eta_r/\eta_m$  vs  $s/d$  and  $E'_f$  for Randomly Oriented Fiber Composites

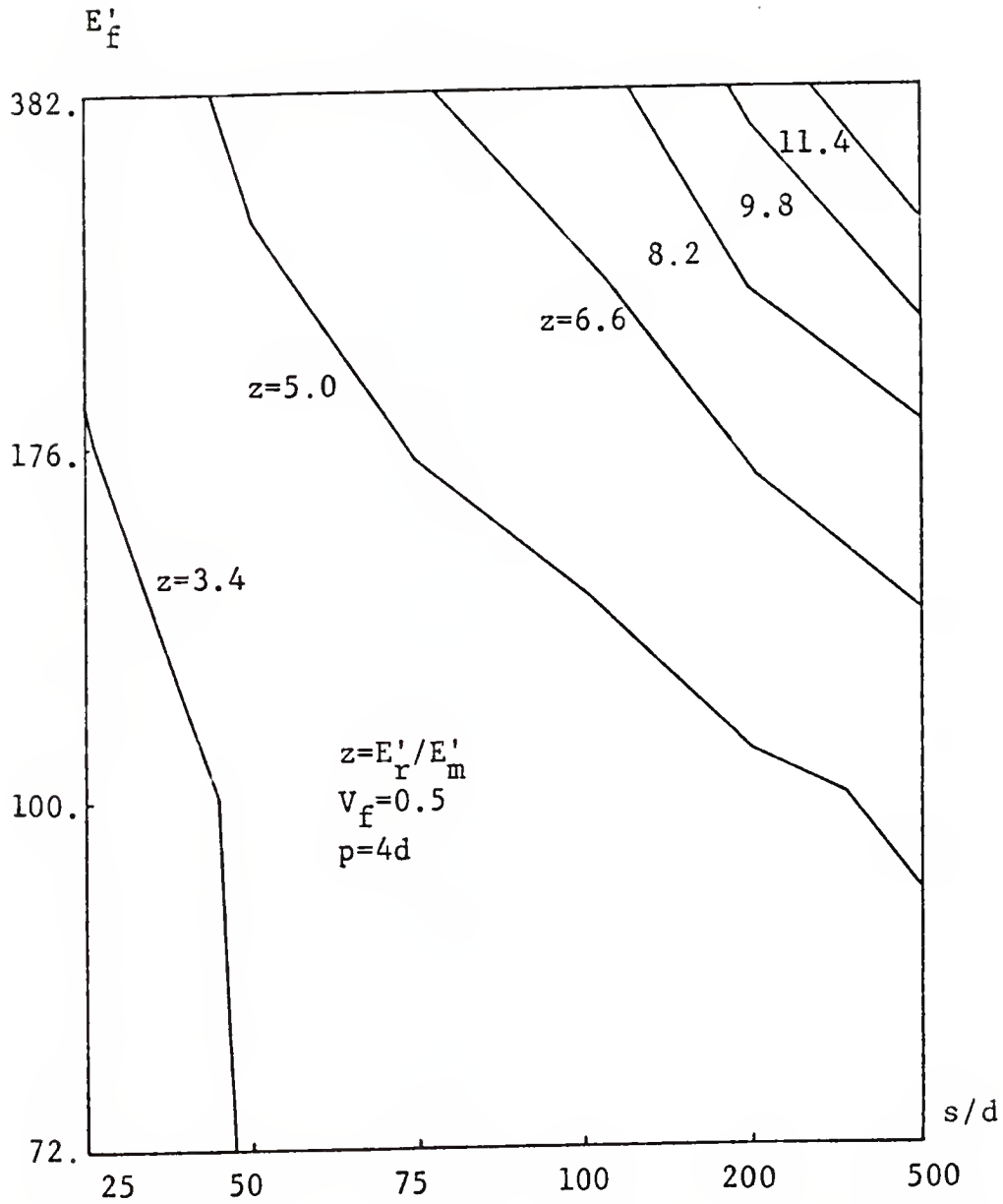


Figure 9.27: Contour Curves of  $E'_r/E'_m$  vs  $s/d$  and  $E'_f$  for Randomly Oriented Fiber Composites

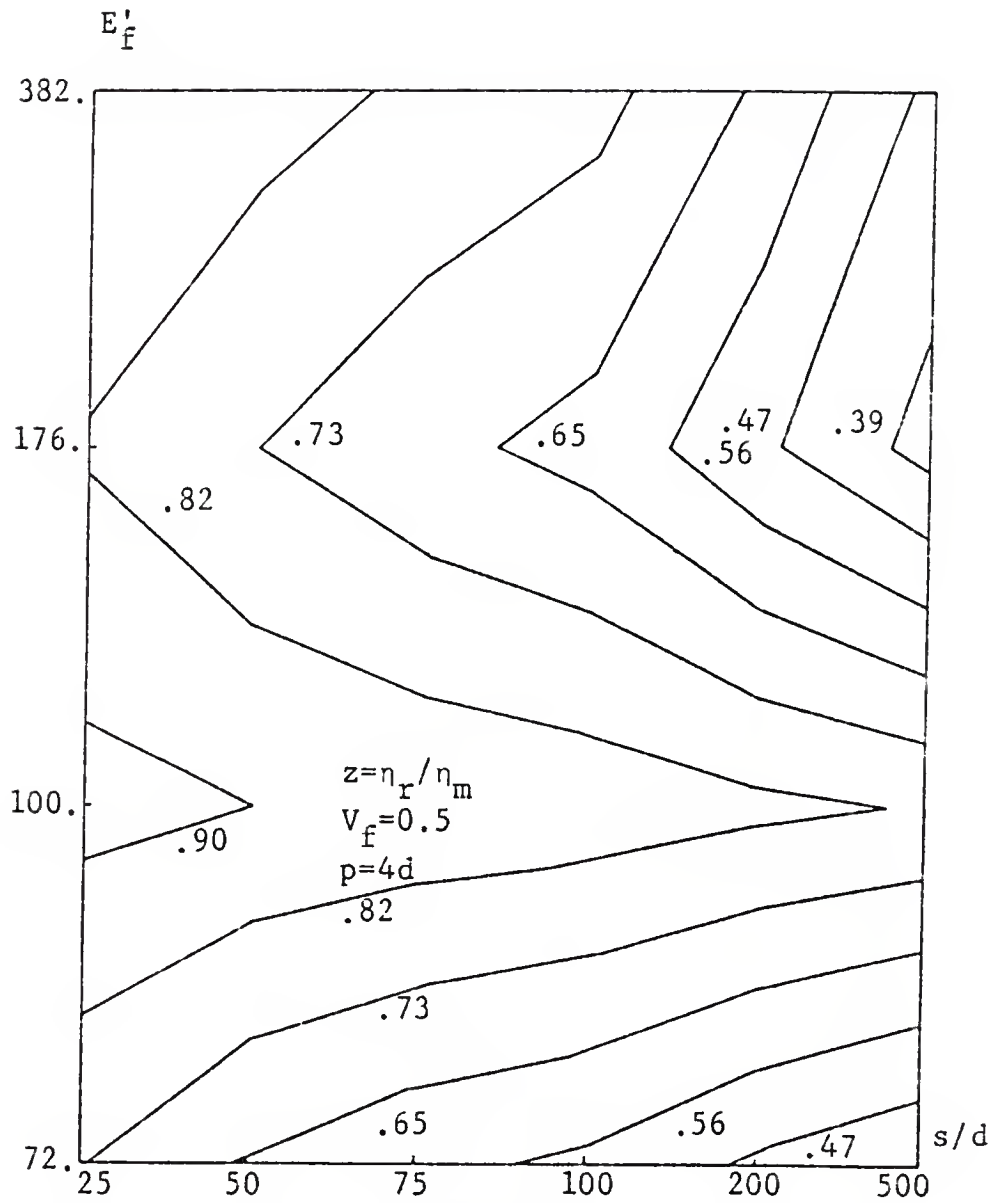


Figure 9.28: Contour Curves of  $\eta_r / \eta_m$  vs  $s/d$  and  $E'_f$  for Randomly Oriented Fiber Composites

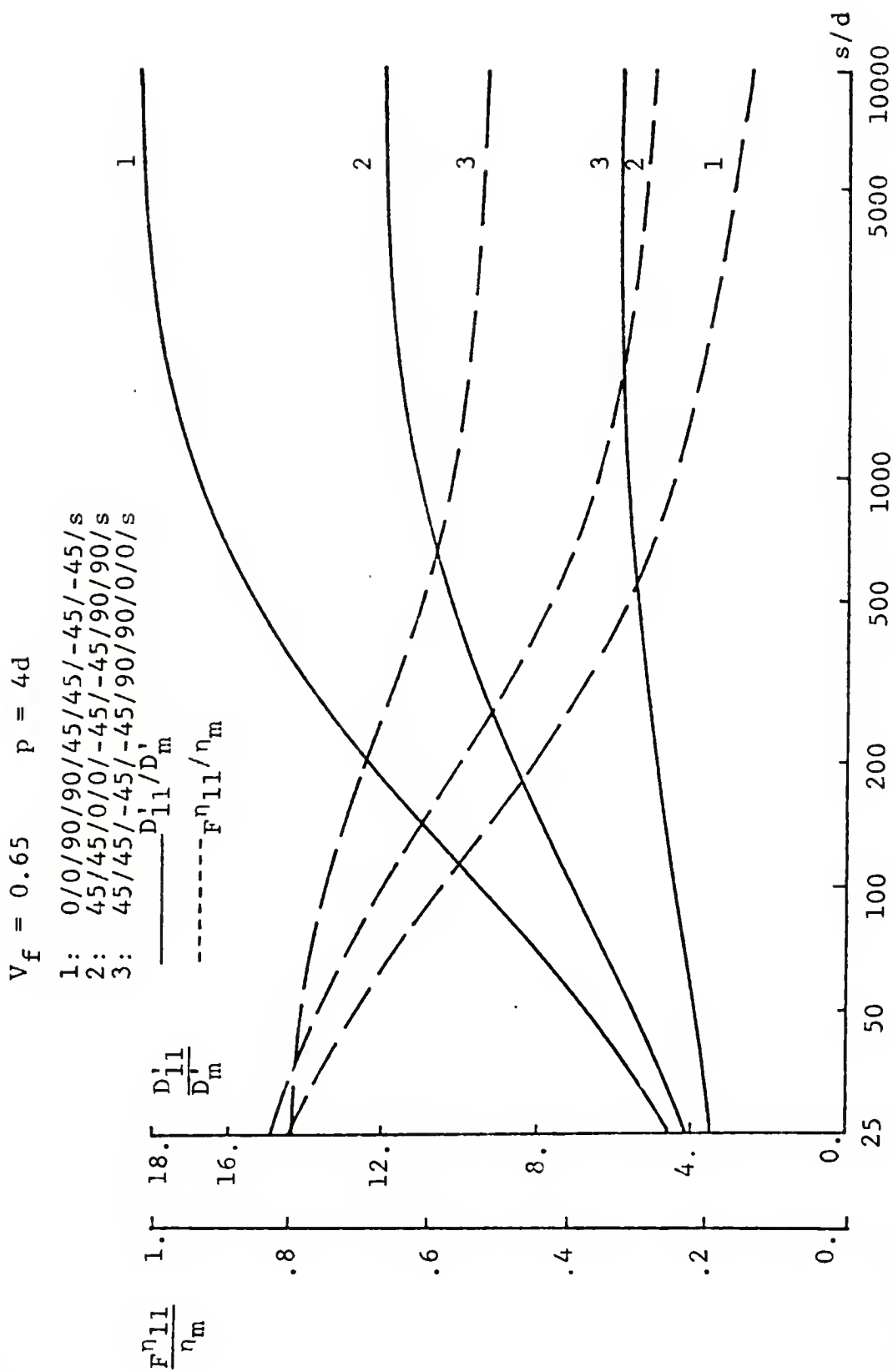


Figure 9.29: Plots of  $D'_{11}/D'_m$  and  $F^{\eta}_{11}/\eta_m$  vs  $s/d$  for Quasi-Isotropic Graphite Epoxy Composites



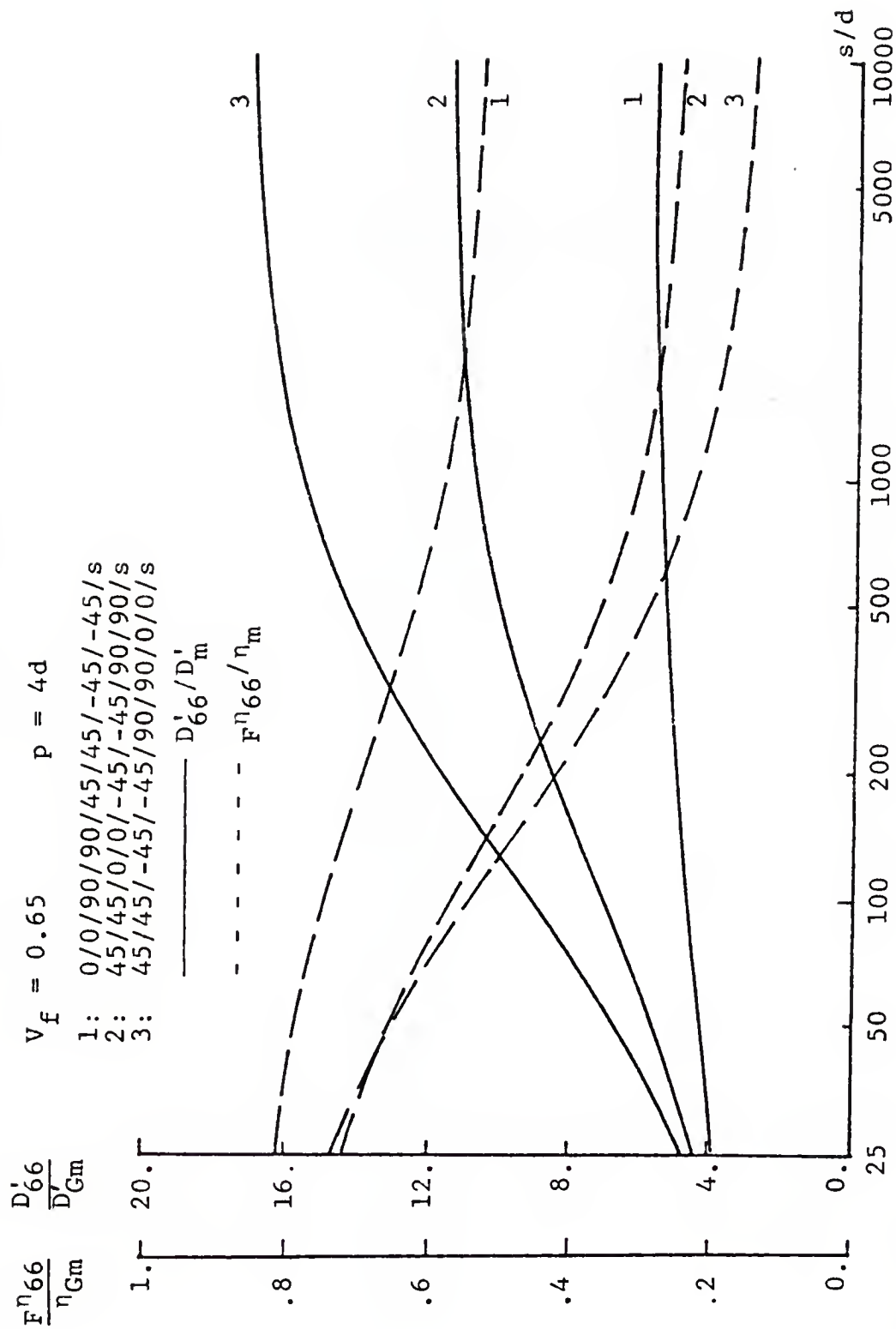


Figure 9.30: Plots of  $D'_{66}/D_m$  and  $F^{\eta}_{66}/\eta_m$  vs  $s/d$  for Quasi-Isotropic Graphite Epoxy Composites

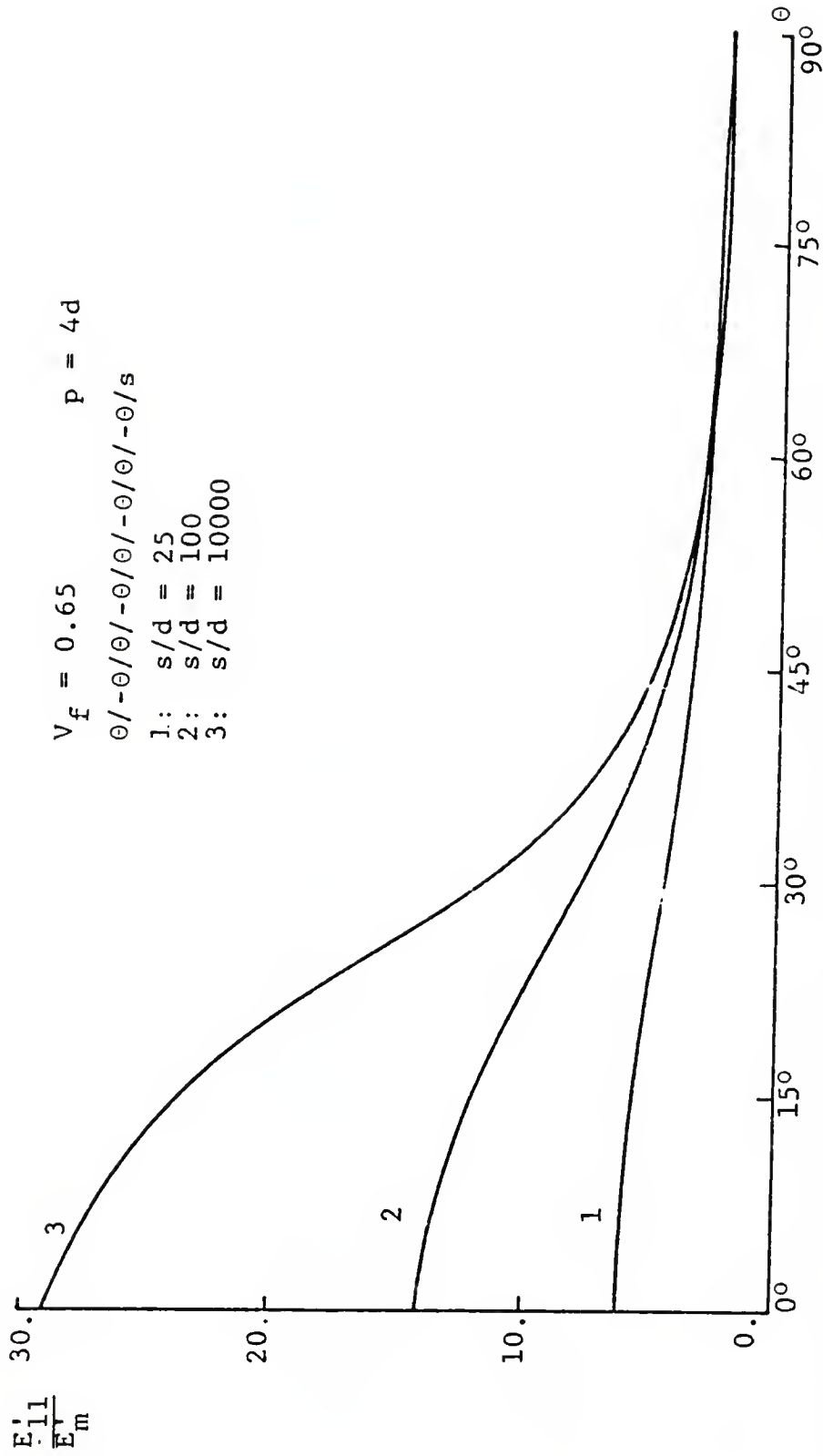


Figure 9.31: Plots of  $E'_{11}/E'_m$  vs  $\theta$  Using  $s/d$  as a Parameter for Angle Ply Graphite Epoxy Composites

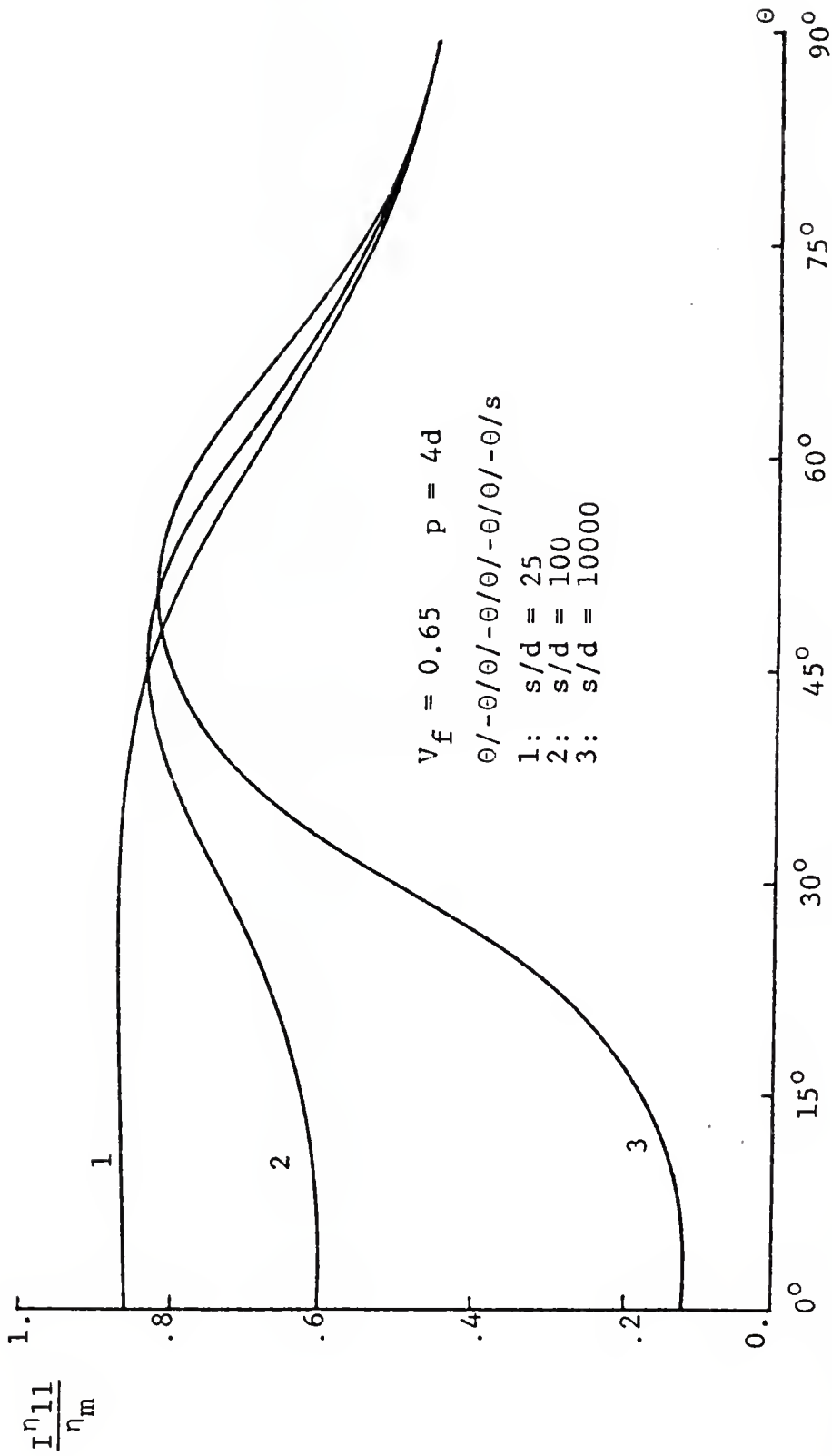


Figure 9.32: Plots of  $I_{\eta_{11}}/\eta_m$  vs  $\theta$  Using  $s/d$  as a Parameter for Angle Ply Graphite Epoxy Composites

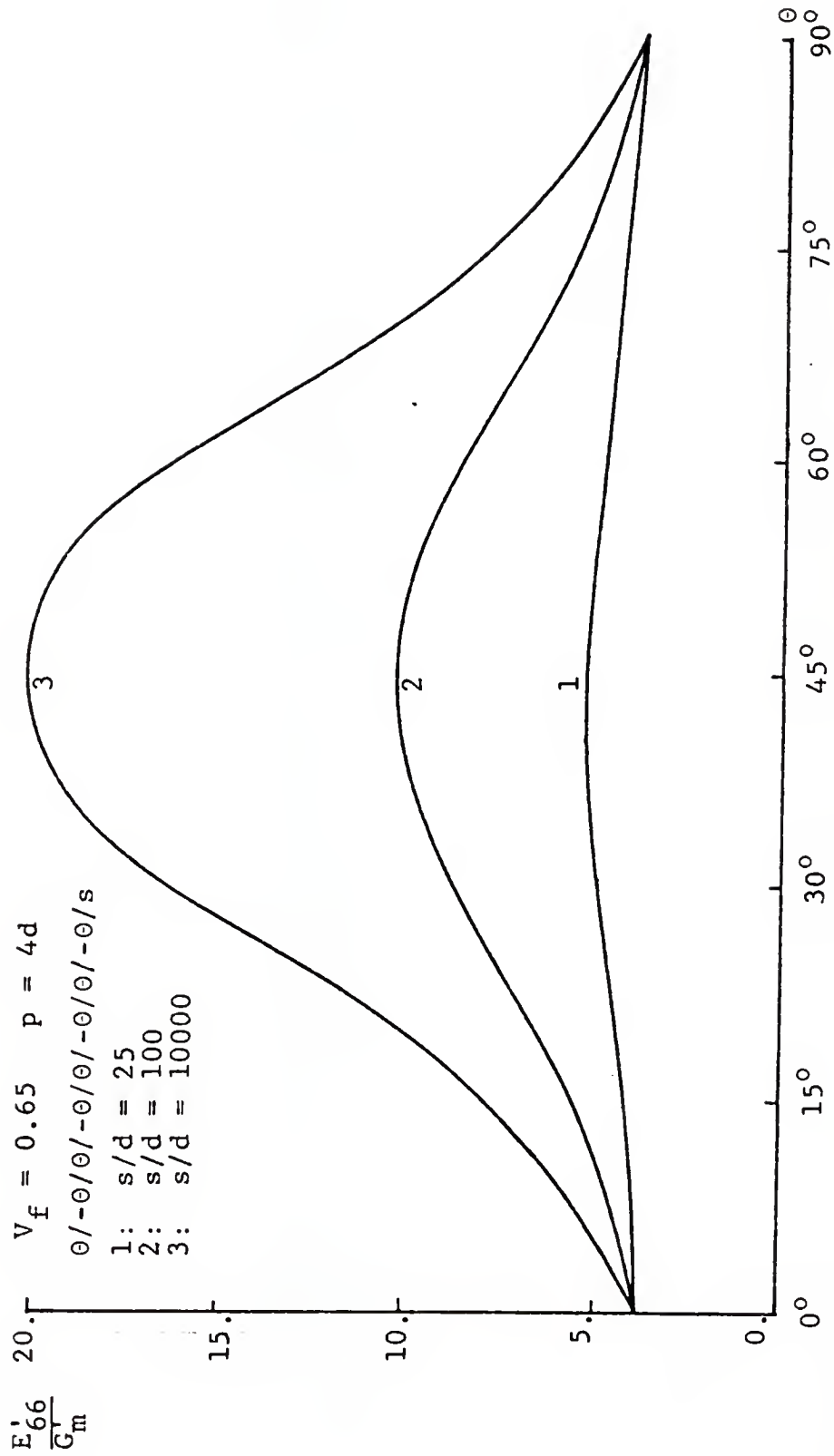


Figure 9.33: Plots of  $E'_{66}/G'_m$  vs  $\theta$  Using  $s/d$  as a Parameter for Angle Ply Graphite Epoxy Composites

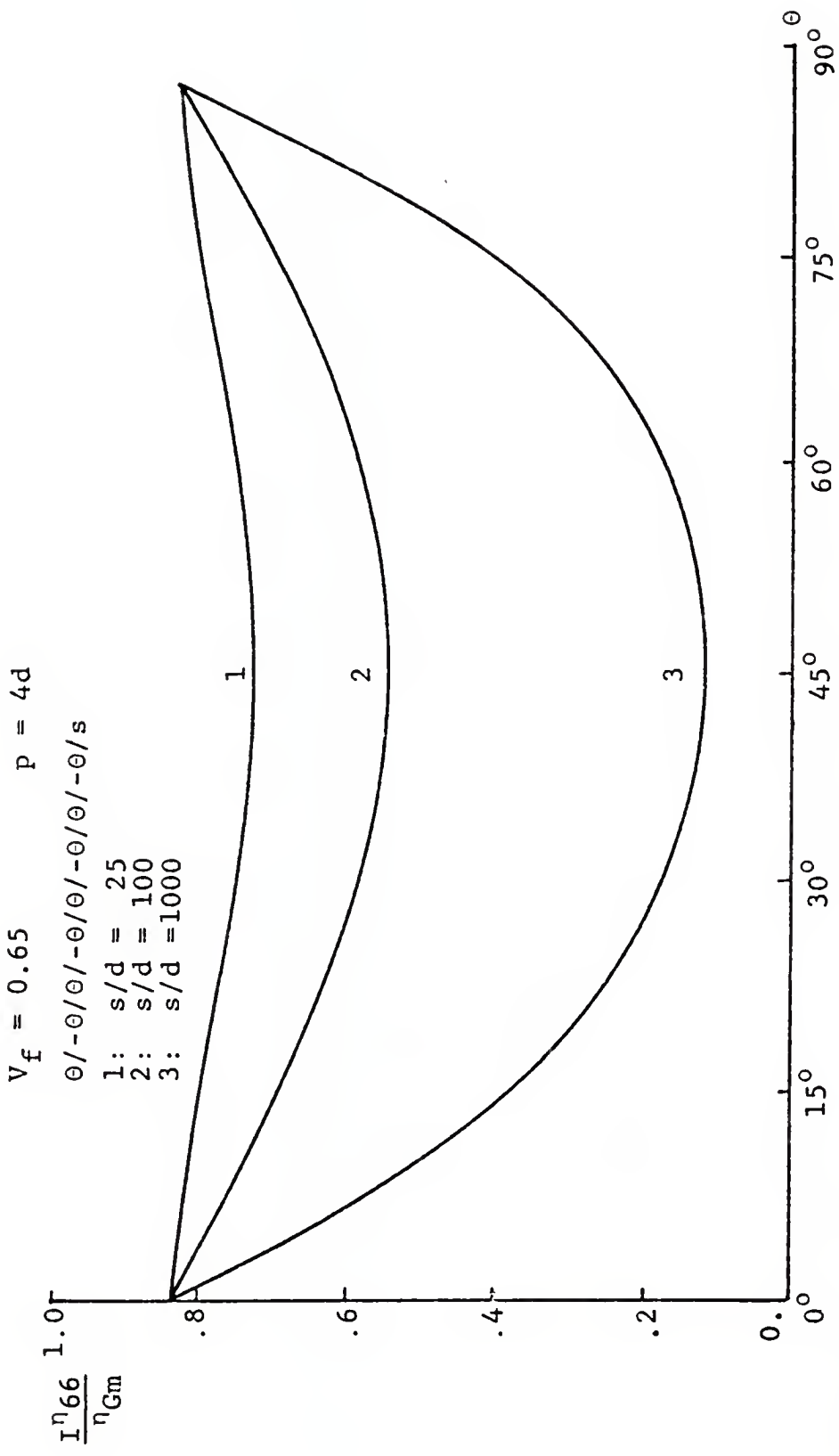


Figure 9.34: Plots of  $I^{66}_{Gm}$  vs  $\theta$  Using  $s/d$  as a Parameter for Angle Ply Graphite Epoxy Composites

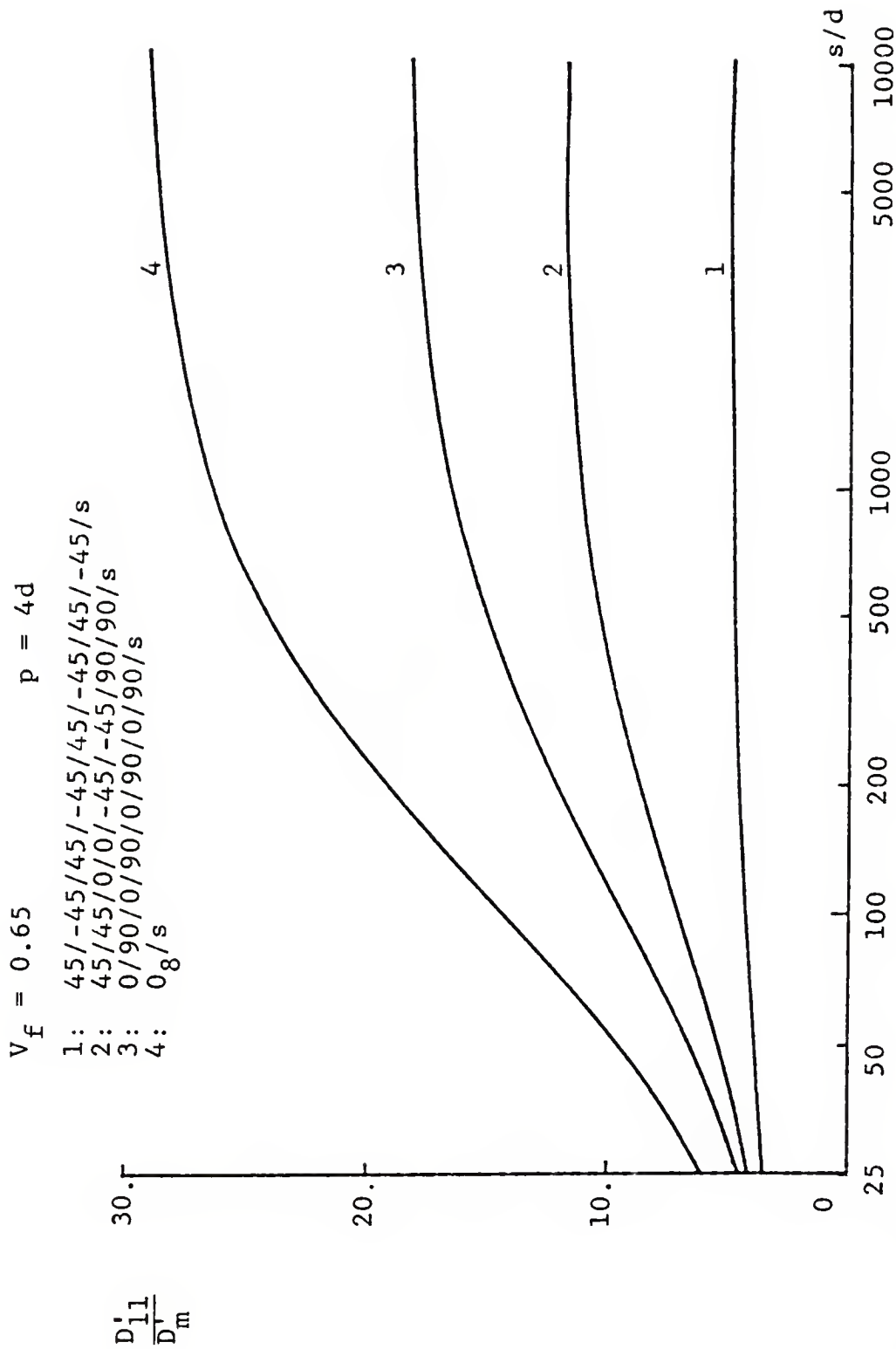


Figure 9.35: Comparisons of  $D'_{11}/D'_m$  vs  $s/d$  for Four Kinds of Laminated Graphite Epoxy Composites

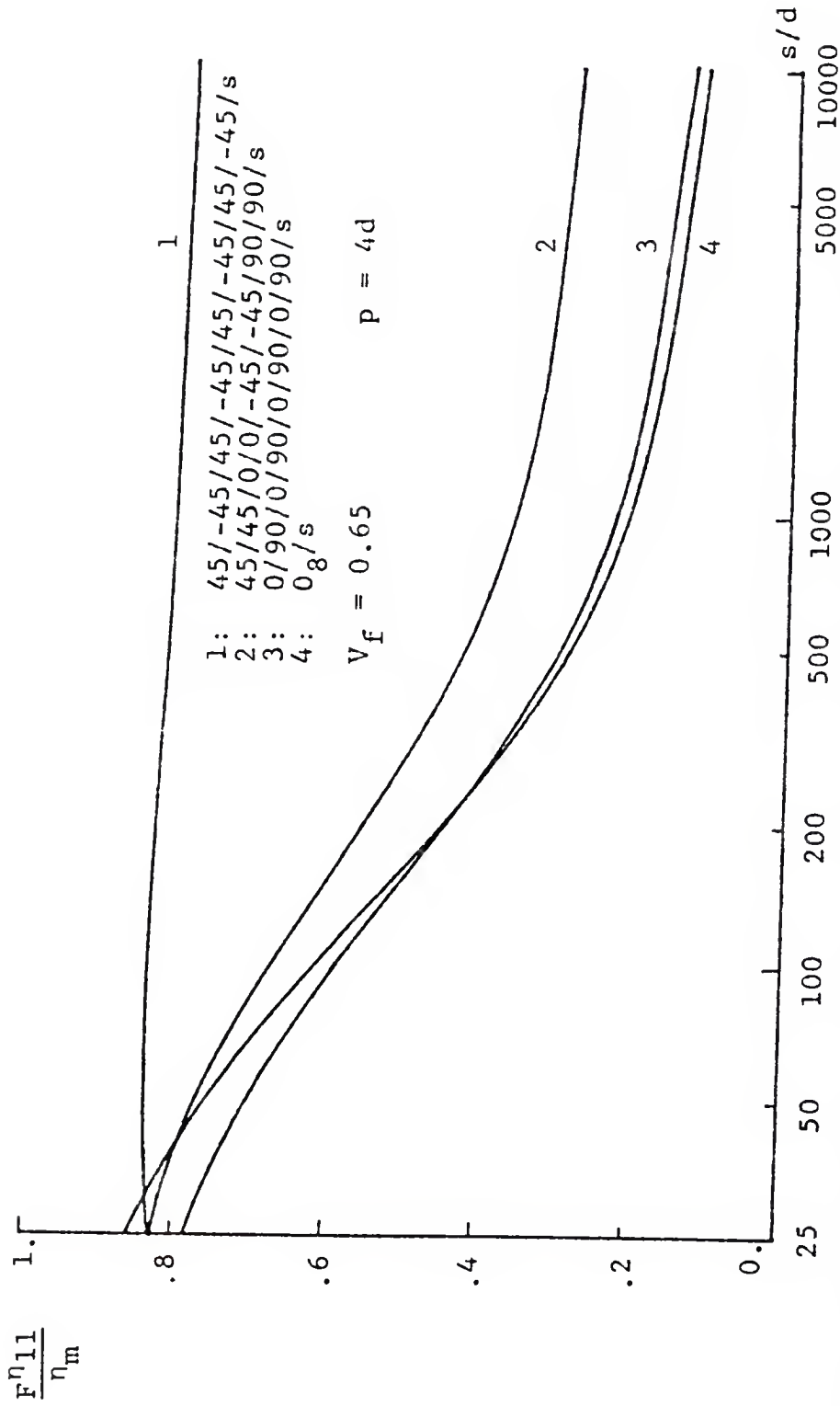


Figure 9.36: Comparison of  $F^{\eta_{11}}/\eta_m$  vs.  $s/d$  for Four Kinds of Laminated Graphite Epoxy Composites

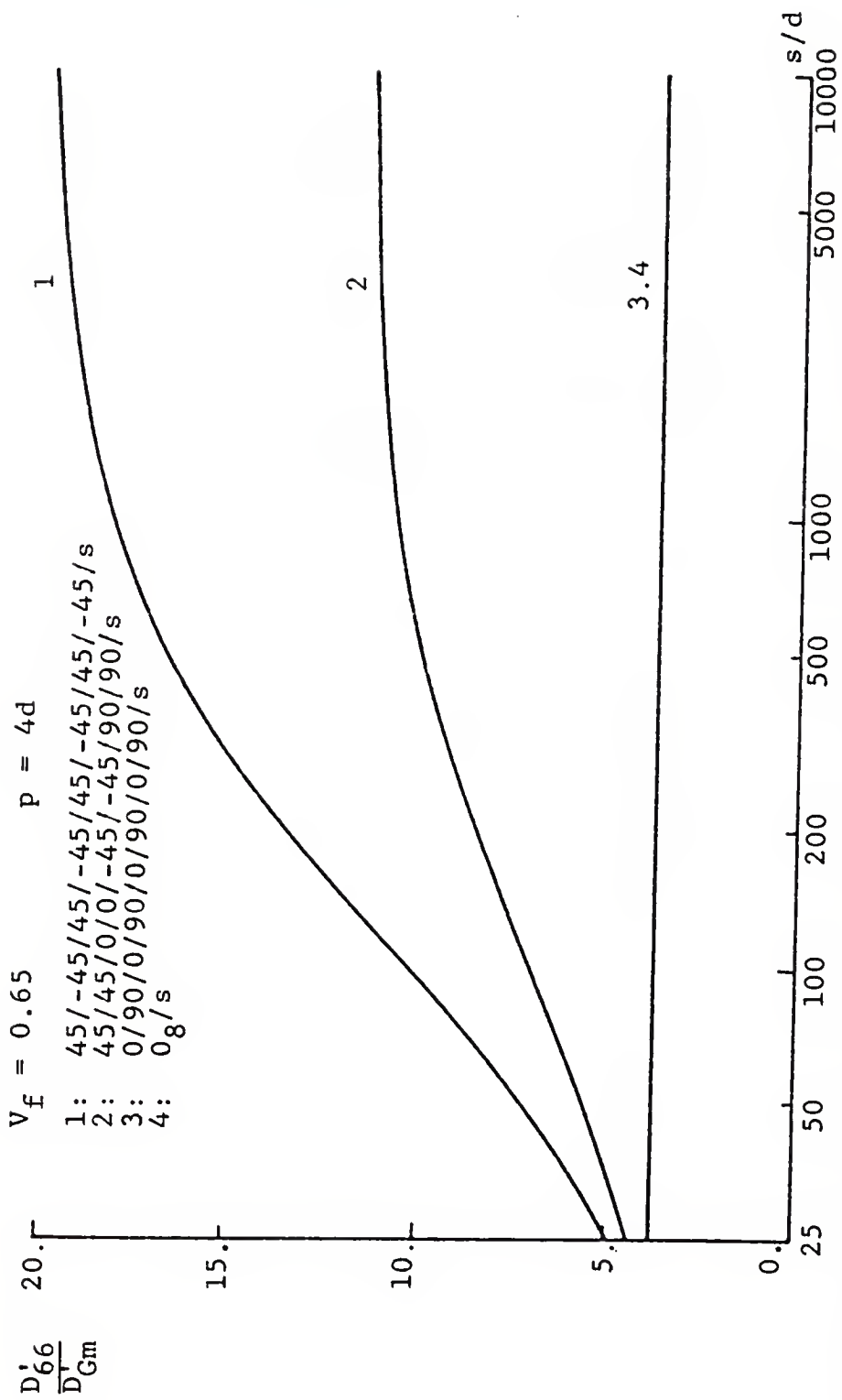


Figure 9.37: Comparisons of  $D'_{66}/D'_{Gm}$  vs  $s/d$  for Four Kinds of Laminated Graphite Epoxy Composites



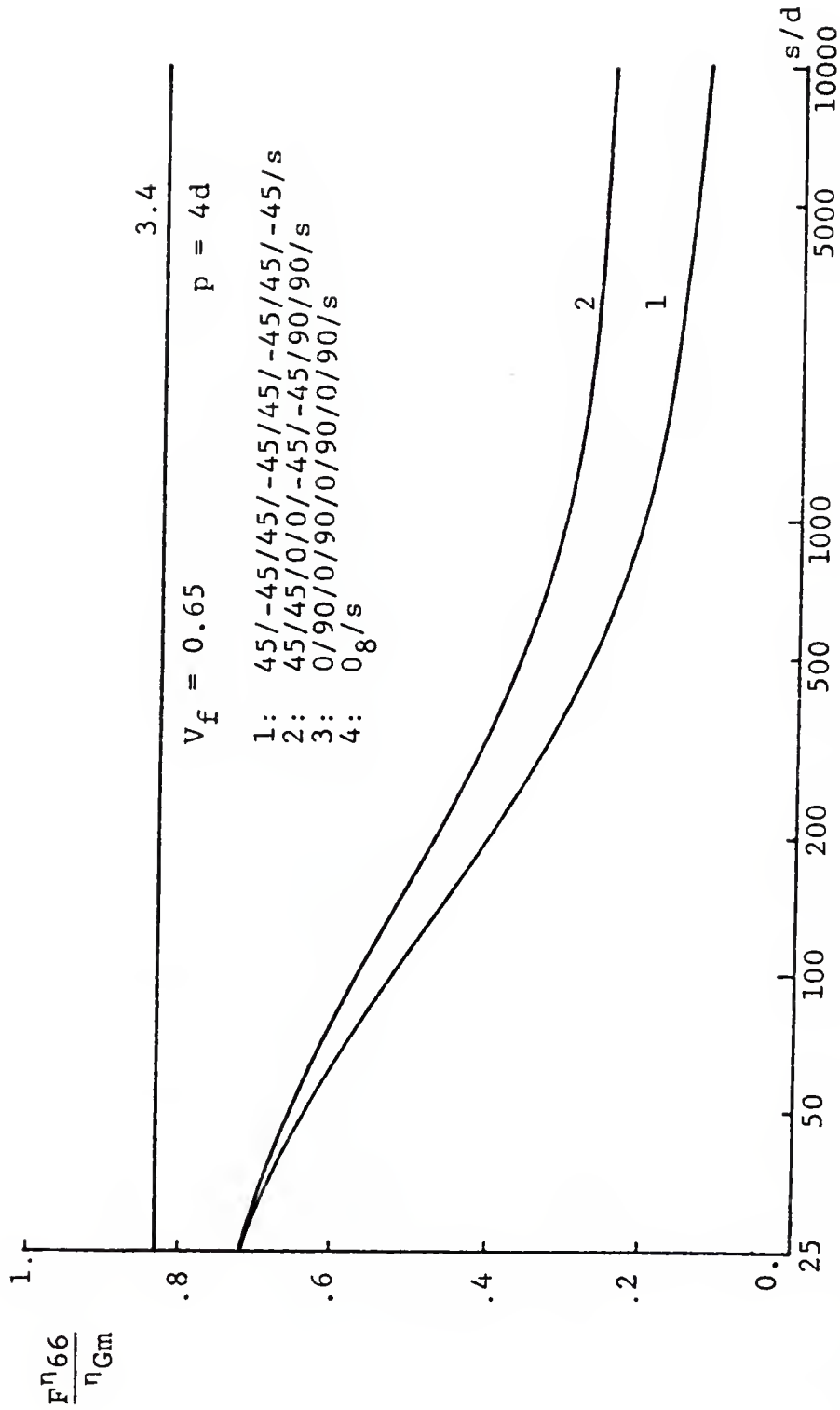


Figure 9.38: Comparisons of  $F^{n66}/\eta_{Gm}$  vs  $s/d$  for Four Kinds of Laminated Graphite Epoxy Composites

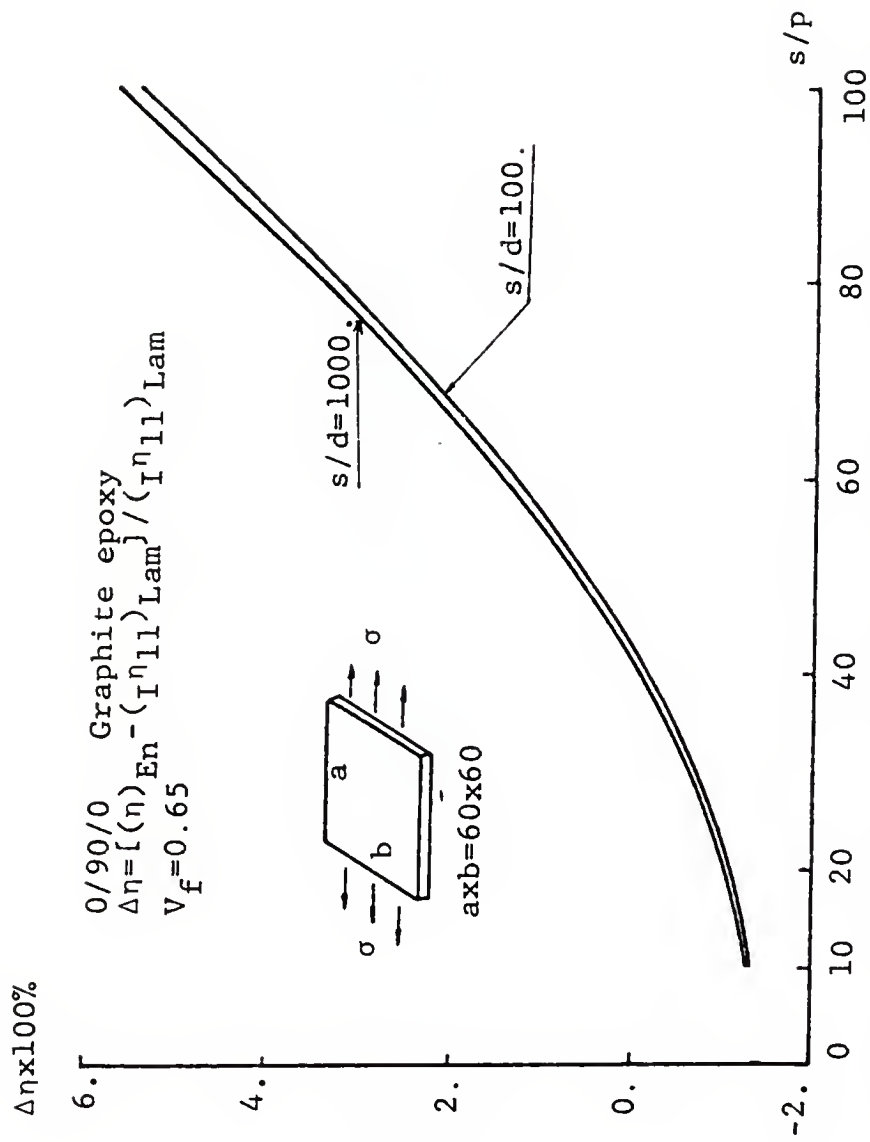


Figure 9.39: Influence of  $s/p$  on the In-Plane Longitudinal Damping Through Energy Approach

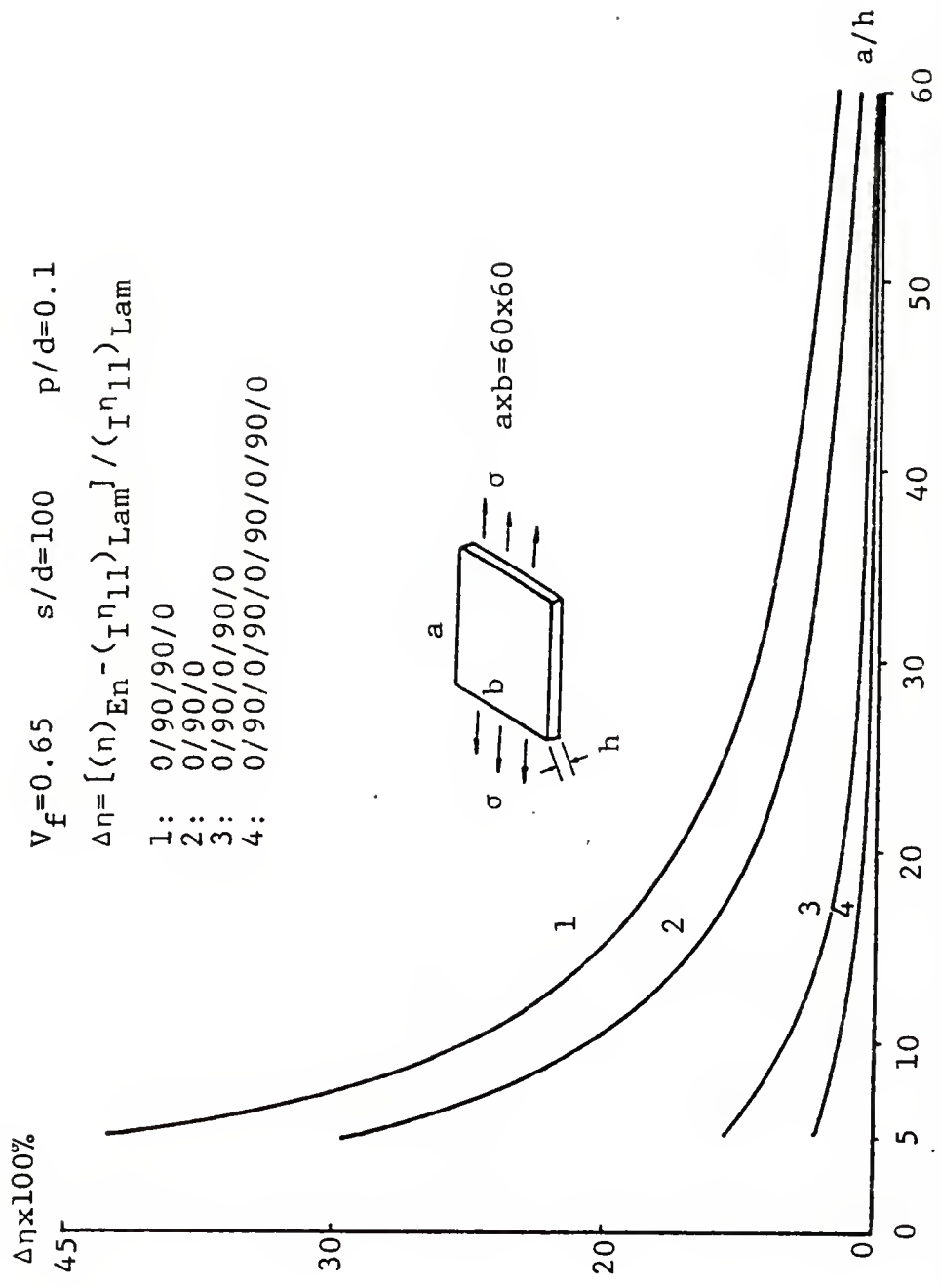


Figure 9.40: Influence of  $a/h$  on the In-Plane Longitudinal Damping of Laminated Graphite Epoxy Composites Through Energy Approach

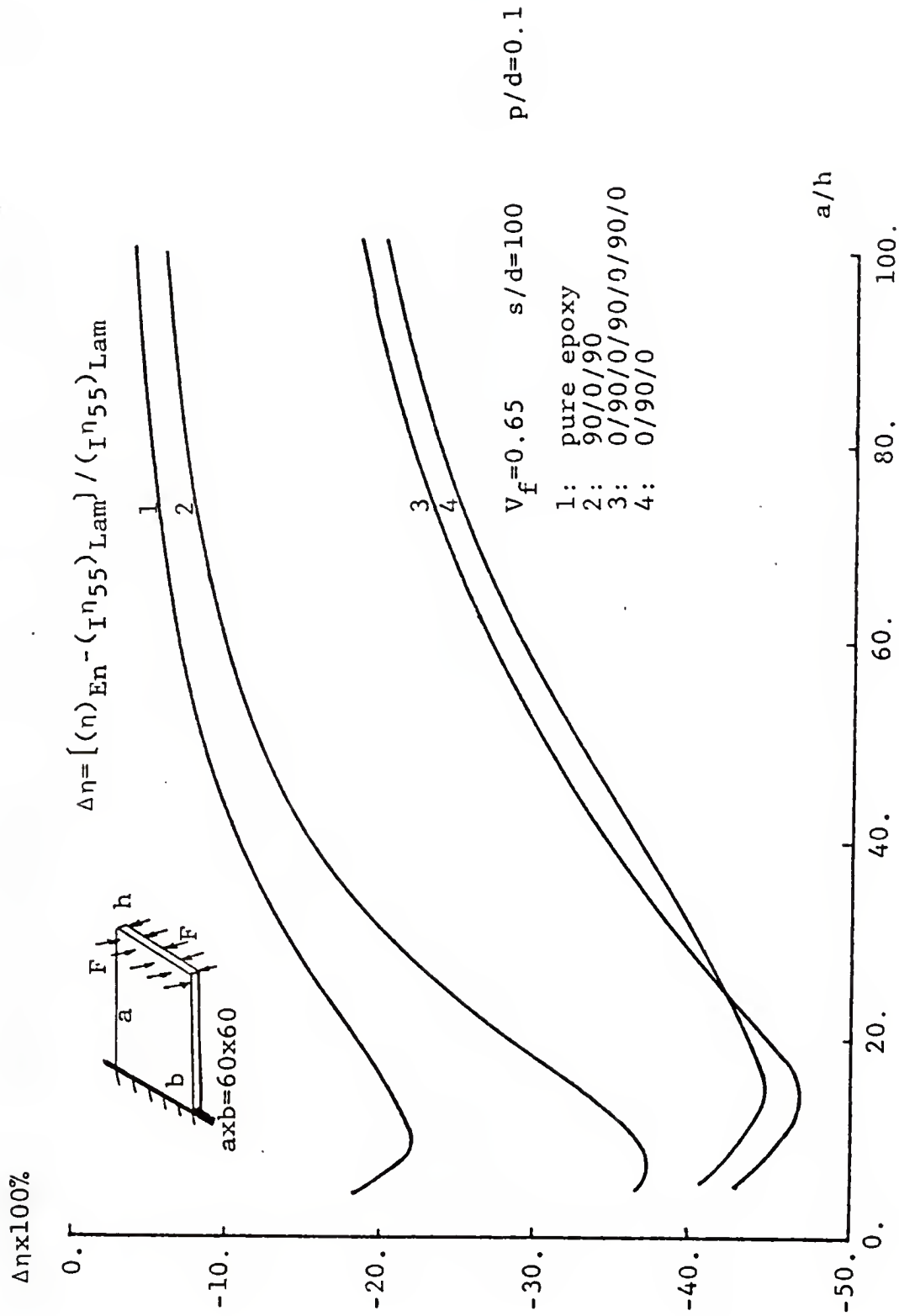


Figure 9.41: Influence of  $a/h$  on the Flexural Normal Damping of Laminated Graphite Epoxy Composites Through Energy Approach

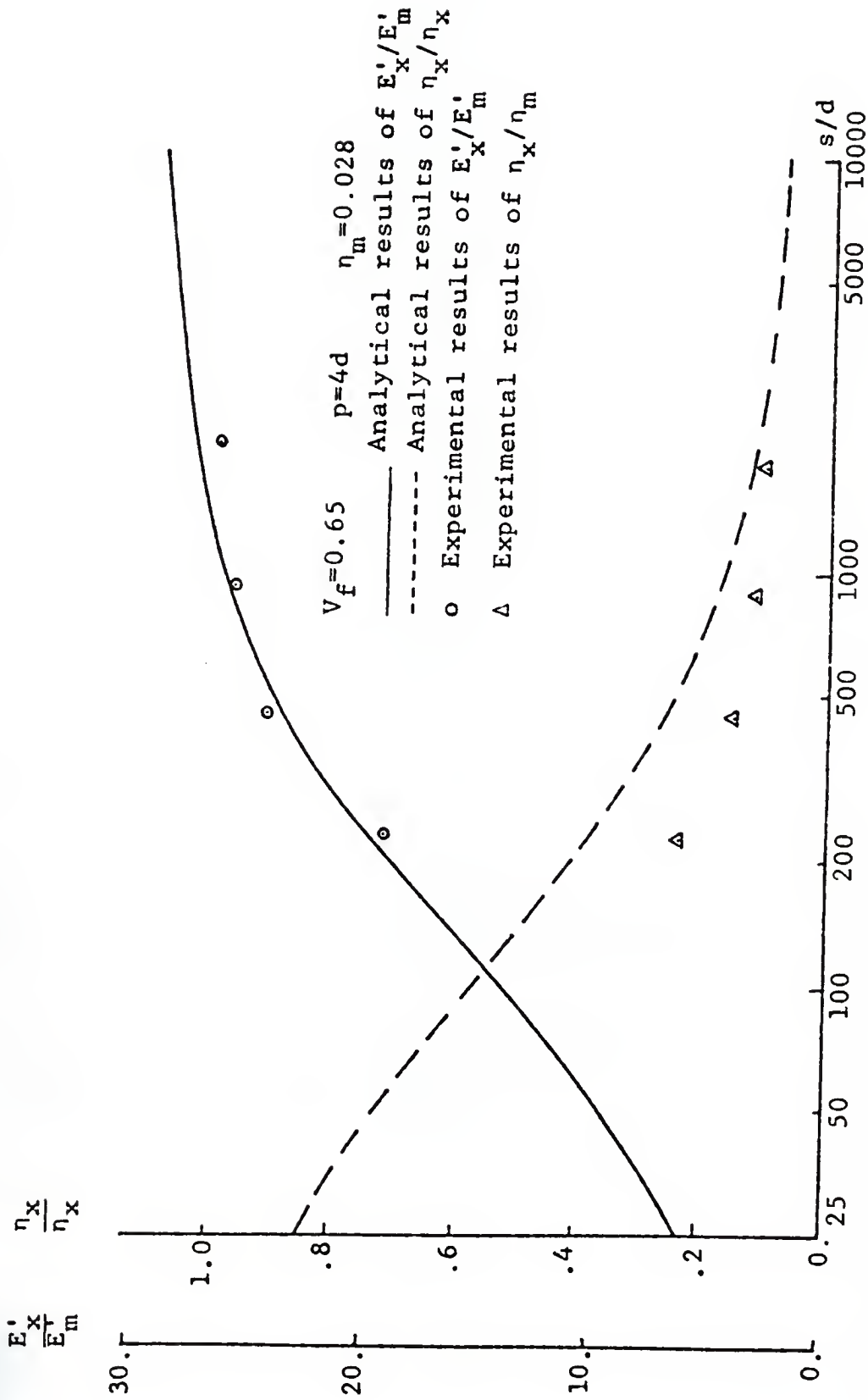


Figure 9.42: Comparison Between Analytical Results and Experimental Results for Unidirectional Discontinuous Graphite Reinforced Epoxy Composite Beams

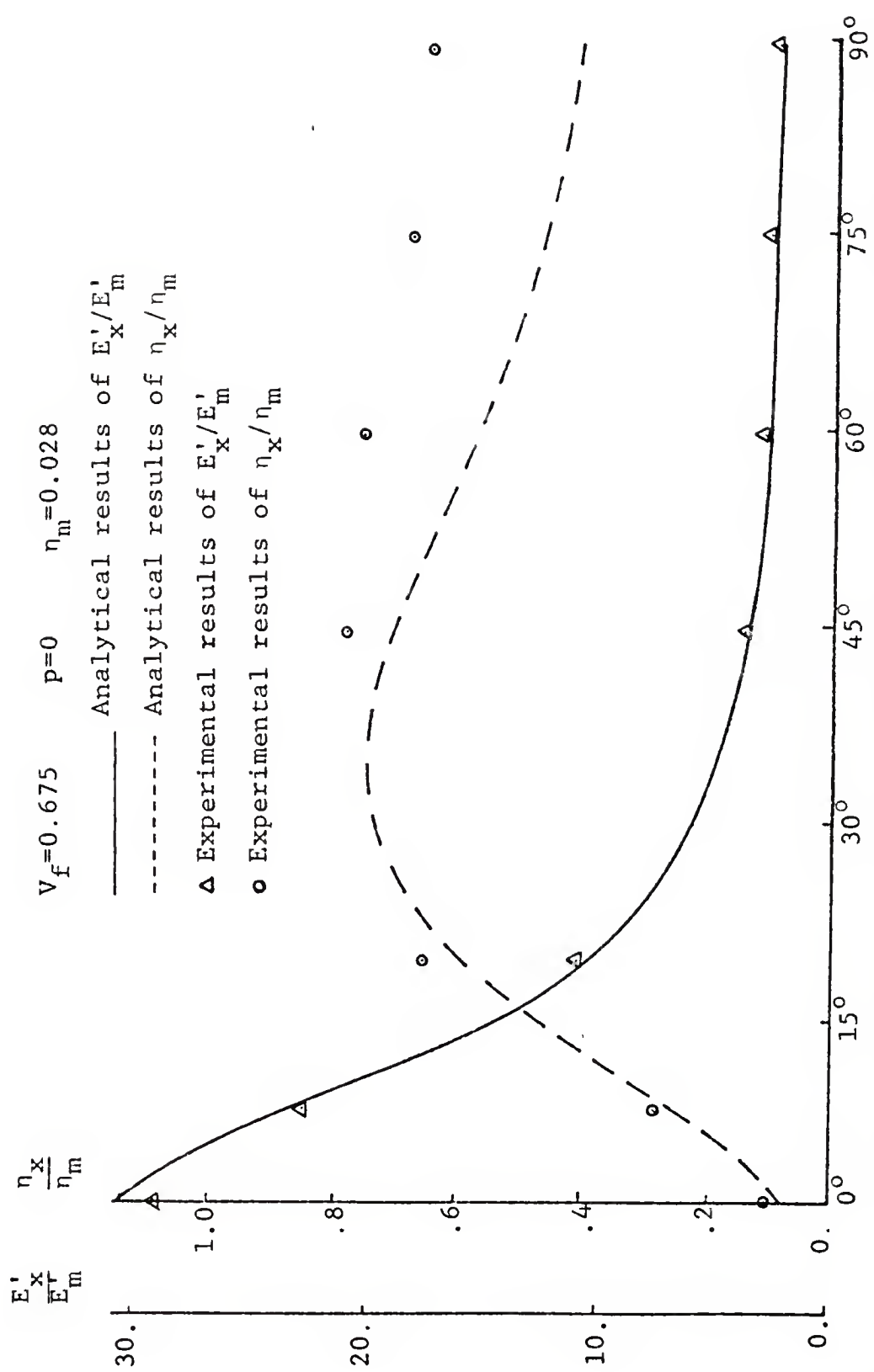


Figure 9.43: Comparison Between Analytical Results and Experimental Results for Off-Axis Unidirectional Continuous Graphite Reinforced Epoxy Composite Beams

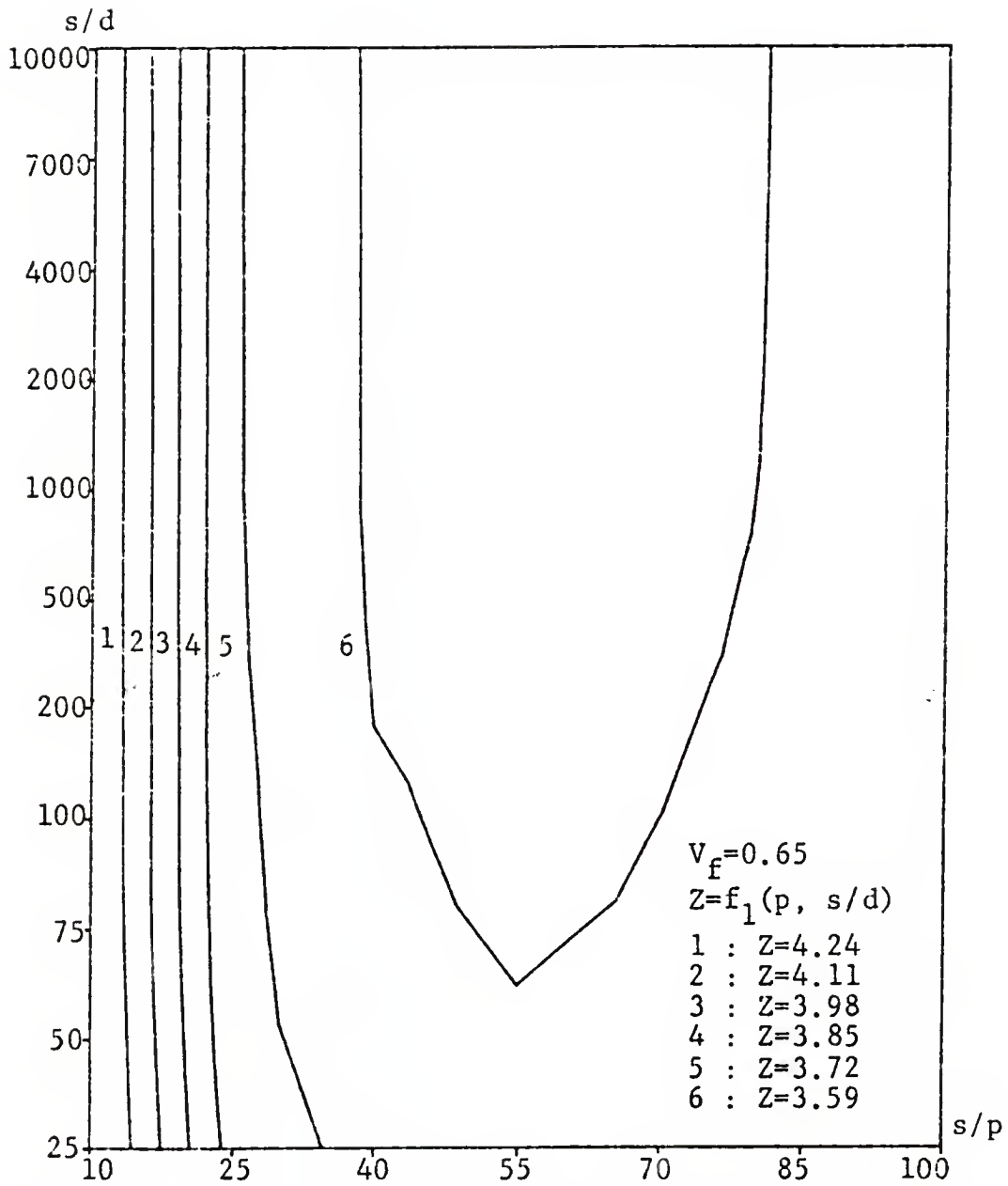


Figure 9.44: Contour Curves of Objective Function for Case One vs  $s/d$  and  $s/p$  for Graphite Epoxy Composite Plate

Table 9.1: Experimental Results of 0<sub>5</sub>/90<sub>5</sub>/0<sub>5</sub> Glass Epoxy Composite Plates

s (mm)	p (mm)	d (mm)	V <sub>f</sub>	f <sub>r</sub> (Hz)	η
19.	1.59	.009	.558	92.8	.0042
25.4	1.59	.009	.565	95.3	.0041
38.1	1.59	.009	.575	97.1	.0040
25.4	0.05	.009	.579	109.8	.0036

Table 9.2: Influence of Weighting Constants on Optimum Design for Case One

Lamination	T <sub>1</sub>	T <sub>2</sub>	s/d	p/d	(s/p) <sub>ave</sub>	$\frac{\tilde{D}'_{\rho_0}}{\rho \tilde{D}_0}$	$\frac{\eta}{\eta_m}$
0/90/0	1	3	9022.	121.	74.4	1.27	.47
0/90/	1	5	9022.	170.	53.1	1.19	.52
0/90/0	1	10	9008.	214.	42.1	1.12	.56
0/90/0	0	5	9020.	267.	33.8	1.06	.60



Table 9.3: Optimum Designs of Cross Ply Composite Plates for Case One

Lamination	$T_1$	$T_2$	$s/d$	$p/d$	$(s/p)_{ave}$	$\frac{\tilde{D}'\rho_0}{\rho\tilde{D}!}$	$\frac{\eta}{\eta_m}$
$(0/90/0)^G$	1	5	9022.	170.	53.1	1.19	.52
$(0/90/0/90/0)^G$	1	5	8994.	169.	53.1	1.19	.52
$0^G/90^G/0^K/90^K/s$	1	5	9007.	152.	59.4	1.29	.53
$0^K/90^K/0^G/90^G/s$	1	5	9993.	3.2	2593.1	1.11	.69

Table 9.4: Optimum Designs of Cross Ply Composite Plates for Case Two

Lamination	$T_1$	$T_2$	$s/d$	$p/d$	$(s/p)_{ave}$	$\frac{\tilde{D}'\rho_0}{\rho\tilde{D}!}$	$\frac{\eta}{\eta_m}$
$(0/90/0)^G$	1	5	9010.	170.	53.0	5.10	.46
$(0/90/0/90/0)^G$	1	5	9020.	170.	53.0	5.10	.46
$0^G/90^G/0^K/90^K/s$	1	5	9010.	152.	59.3	5.53	.48
$0^K/90^K/0^G/90^G/s$	1	5	9993.	3.2	2747.8	4.80	.65

APPENDIX A  
HYSTERESIS LOOP OF VISCOELASTIC MATERIALS

This appendix shows that hysteresis loop could also be observed in a viscoelastic material.

For a viscoelastic body under a cyclic load  $\sigma$  at circular frequency  $\omega$ ,

$$\sigma = \sigma_0 \sin \omega t \quad \text{A.1}$$

strain  $\epsilon$  of this body lags a phase angle  $\phi$  behind stress, i.e.,

$$\epsilon = \epsilon_0 \sin(\omega t - \phi) \quad \text{A.2}$$

where  $\epsilon_0$  and  $\sigma_0$  are the magnitudes of strain and stress respectively, and  $\epsilon_0$ , in general, is proportional to  $\sigma_0$ .

$$\sigma_0 = E \epsilon_0 \quad \text{A.3}$$

where  $E$  is the elastic Young's modulus. Equation A.1 can be rewritten as

$$\sigma = E \epsilon_0 \sin(\omega t - \phi + \phi) \quad \text{A.4}$$

that is

$$\sigma = E \epsilon_0 \cos\phi \sin(\omega t - \phi) + E \epsilon_0 \sin\phi \cos(\omega t - \phi) \quad \text{A.5}$$

By the definitions of storage and loss moduli, Equation A.5 induces to

$$\sigma = E' \epsilon_0 \sin(\omega t - \phi) + E'' \epsilon_0 \cos(\omega t - \phi) \quad \text{A.6}$$

From Equations A.6 and A.2

$$\sin(\omega t - \phi) = \frac{\epsilon}{\epsilon_0} \quad \text{A.7}$$

$$\cos(\omega t - \phi) = \frac{\sigma - E' \epsilon}{E'' \epsilon_0} \quad \text{A.8}$$

Using Equations A.7 and A.8, one will have

$$\left( \frac{\sigma - E' \epsilon}{E'' \epsilon_0} \right)^2 + \left( \frac{\epsilon}{\epsilon_0} \right)^2 = 1 \quad \text{A.9}$$

Figure A.1 is the sketch of Equation A.9.

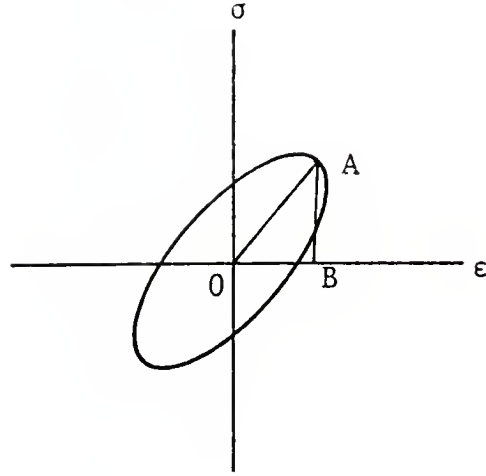


Figure A.1: Hysteresis Loop of a Viscoelastic Material

Equation A.9 shows that hysteresis loop is also presented in viscoelastic material.

The dissipated energy  $U_D$  during a cycle is the area within the ellipse.

$$(U_D)_{\text{cyc}} = \pi \epsilon_0 E'' \epsilon_0 \quad \text{A.10}$$

The maximum energy stored in the body  $U_s$  is the area of the triangle OAB

$$U_s = \frac{1}{2} \epsilon_0 E' \epsilon_0 \quad \text{A.11}$$

Therefore,

$$\frac{E''}{E'} = \frac{(U_D)_{cyc}}{2\pi U_s} \quad \text{A.12}$$

## APPENDIX B EXPRESSIONS OF $\beta$ 's

This appendix presents the expressions of  $\beta$ ,  $\beta_s/2$ , and  $\beta^*s/2$ . The  $\beta$  used in Section 3.1 is originally defined in [20] as

$$\beta = \left[ \frac{G_m}{E_f} \frac{2}{\gamma_o^2 \ln(R/\gamma_o)} \right]^{\frac{1}{2}} \quad \text{B.1}$$

where  $G_m$  is the shear modulus of the matrix,  $E_f$  is the Young's modulus of the fiber,  $\gamma_o$  is the radius of fiber, and  $R$  is the outside radius of the matrix, which surrounds the fiber in a cylindrical shape, as in Figure 3.2 when  $\theta=0^\circ$ . The ratio  $R/\gamma_o$  may be expressed in terms of the fiber volume fraction  $V_f$  [31]. For example, for a hexagonal array

$$\frac{R}{\gamma_o} = \frac{\pi}{2 \sqrt{3} V_f} \quad \text{B.2}$$

and for a square array,

$$\frac{R}{\gamma_O} = \frac{\pi}{4 V_f} \quad \text{B.3}$$

Consequently, for a square array,

$$\frac{\beta s}{2} = \frac{s}{d} \frac{G_m}{E_f} \left[ \frac{4}{\text{Ln}(\frac{\pi}{4V_f})} \right]^{\frac{1}{2}} \quad \text{B.4}$$

where  $s$  and  $d$  are the length and diameter of the fiber, correspondingly.

When a viscoelastic material is considered,

$$\frac{\beta^* s}{2} = \frac{s}{d} \left[ \frac{4}{\text{Ln}(\frac{\pi}{4V_f})} \right]^{\frac{1}{2}} \left[ \frac{G'_m (1 + i \eta_{Gm})}{E'_f (1 + i \eta_f)} \right]^{\frac{1}{2}} \quad \text{B.5}$$

$$\text{where } \eta_{Gm} = G''_m / G'_m \quad \text{B.6}$$

$G''_m$ ,  $G'_m$  and  $\eta_f$  are defined in Equations 3.26 and 3.29.

Since the loss factors are very small, high order terms such as  $\eta_f^2$  and  $\eta_f \eta_{Gm}$  could be neglected. Using a binomial expansion reduces Equation B.5 to

$$\frac{\beta^* s}{2} = \frac{\beta s}{2} \left[ 1 + i \frac{1}{2} (\eta_{Gm} - \eta_f) \right] \quad \text{B.7}$$

Similarly, by Taylor's series expansion and neglect of higher order terms, one gets

$$\tanh \frac{\beta^* s}{2} = \tanh \frac{\beta s}{2} + i \frac{\beta s}{2} \frac{\eta_{Gm} - \eta_f}{2} \frac{1}{\cosh \frac{\beta s}{2}} \quad \text{B.8}$$



APPENDIX C  
AN ALTERNATIVE WAY OF DETERMINING  $\tilde{E}_r$  AND  $\tilde{G}_r$

Another derivation of  $\tilde{E}_r$  and  $\tilde{G}_r$  for in-plane randomly oriented short-fiber composite is presented in this appendix.

Considering an in-plane randomly oriented short-fiber composite plate. Assuming that  $\sigma_x$  is the only nonzero applied stress, one has

$$\begin{aligned}\tilde{Q}_{11} \epsilon_x + \tilde{Q}_{12} \epsilon_y + \tilde{Q}_{16} \gamma_{xy} &= \sigma_x \\ \tilde{Q}_{12} \epsilon_x + \tilde{Q}_{22} \epsilon_y + \tilde{Q}_{26} \gamma_{xy} &= 0 \\ \tilde{Q}_{16} \epsilon_x + \tilde{Q}_{26} \epsilon_y + \tilde{Q}_{66} \gamma_{xy} &= 0\end{aligned}\tag{C.1}$$

where  $\tilde{Q}_{ij}$  ( $i, j=1, 2, 6$ ) are defined in Equations 4.1-4.5. By Cramer's rule

$$\epsilon_x = \frac{\begin{vmatrix} \sigma_x & \tilde{Q}_{12} & \tilde{Q}_{16} \\ 0 & \tilde{Q}_{22} & \tilde{Q}_{26} \\ 0 & \tilde{Q}_{26} & \tilde{Q}_{66} \end{vmatrix}}{\Delta} = \frac{\begin{vmatrix} \tilde{Q}_{22} & \tilde{Q}_{26} \\ \tilde{Q}_{26} & \tilde{Q}_{66} \end{vmatrix}}{\Delta} \sigma_x\tag{C.2}$$

where

$$\Delta = \begin{vmatrix} \tilde{Q}_{11} & \tilde{Q}_{12} & \tilde{Q}_{16} \\ \tilde{Q}_{12} & \tilde{Q}_{22} & \tilde{Q}_{26} \\ \tilde{Q}_{16} & \tilde{Q}_{26} & \tilde{Q}_{66} \end{vmatrix} \quad \text{C.3}$$

According to the definition of Young's modulus,

$$E_R = \frac{\sigma_x}{\epsilon_x} \quad \text{C.4}$$

Therefore,

$$E_R = \frac{\Delta}{\begin{vmatrix} \tilde{Q}_{22} & \tilde{Q}_{26} \\ \tilde{Q}_{26} & \tilde{Q}_{66} \end{vmatrix}} \quad \text{C.5}$$

After simplifying,

$$E_R = \frac{\tilde{Q}_{11}^2 - \tilde{Q}_{12}^2}{\tilde{Q}_{11}} \quad \text{C.6}$$

By Equation 4.6, Equation C.6 can be rewritten as

$$E_R = 4 \tilde{Q}_{66} \left( 1 - \frac{\tilde{Q}_{66}}{\tilde{Q}_{11}} \right) \quad \text{C.7}$$

which is same as Equation 4.11

A similar procedure by letting  $\tau_{xy}$  be the only non-zero applied stress can lead to the same expression of Equation 4.8 for  $\tilde{G}_r$ .

It should be noted that the expression of the denominator in Equation 6.5 is a way to determine the  $\tilde{S}_{11}$ . Where  $\tilde{S}_{11}$  is an element of  $[\tilde{S}]$ , and  $[\tilde{S}]$  is the inverse matrix of  $[\tilde{Q}]$ .

APPENDIX D  
INVERSION OF A SYMMETRIC COMPLEX MATRIX

This appendix presents a way to get the inverse matrix of a symmetric complex matrix.

Considering a 3x3 complex matrix,

$$[A^*] = \begin{bmatrix} A_1' + i A_1'' & A_3' + i A_3'' & A_5' + i A_5'' \\ A_3' + i A_3'' & A_2' + i A_2'' & A_6' + i A_6'' \\ A_5' + i A_5'' & A_6' + i A_6'' & A_4' + i A_4'' \end{bmatrix} \quad D.1$$

where

$$[A_1^* \ A_2^* \ A_3^* \ A_4^* \ A_5^* \ A_6^*] = [A_{11}^* \ A_{22}^* \ A_{12}^* \ A_{66}^* \ A_{16}^* \ A_{26}^*] \quad D.2$$

Let  $[a^*]$  be the inverse matrix of  $[A^*]$ .

$$[a^*] = \begin{bmatrix} a_1' + i a_1'' & a_3' + i a_3'' & a_5' + i a_5'' \\ a_3' + i a_3'' & a_2' + i a_2'' & a_6' + i a_6'' \\ a_5' + i a_5'' & a_6' + i a_6'' & a_4' + i a_4'' \end{bmatrix} \quad D.3$$

where

$$[a_1^* \ a_2^* \ a_3^* \ a_4^* \ a_5^* \ a_6^*] = [a_{11}^* \ a_{22}^* \ a_{12}^* \ a_{66}^* \ a_{16}^* \ a_{26}^*] \quad D.4$$

Therefore,

$$[A^*] [a^*] = [I] \quad D.5$$

where  $[I]$  is a unit matrix:

$$I_{ij} = \begin{cases} 1 & i = j \\ 0 & i \neq j \end{cases} \quad D.6$$

According to matrix operations,

$$I_{11} = 1 + i \cdot 0 = (A_1' + i A_1'') (a_1' + i a_1'') + (A_3' + A_3'') (a_3' + i a_3'') + (A_5' + i A_5'') (a_5' + a_5'') \quad D.7$$

Separating the real and the imaginary parts reduces Equation D.7 to the following two equations:

$$1 = A_1' a_1' - A_1'' a_1'' + A_3' a_3' - A_3'' a_3'' + A_5' a_5' - A_5'' a_5'' \quad D.8$$

$$0 = A_1' a_1'' + A_1'' a_1' + A_3' a_3'' + A_3'' a_3' + A_5' a_5'' + A_5'' a_5' \quad D.9$$

By applying similar procedures to  $I_{12}$ ,  $I_{13}$ ,  $I_{22}$ ,  $I_{23}$ , and  $I_{33}$ , a system of twelve equations containing twelve unknowns  $(a'_1, a''_1 \dots a'_6, a''_6)$  is obtained. The solution to this system of equations determines  $[a^*]$ .

APPENDIX E  
ENERGY EXPRESSION OF DAMPING FOR LAMINATED COMPOSITES

Equation 2.22 indicates that the material damping,  $\eta$ , equals to the ratio of the energy dissipated in a cycle,  $(U_D)_{cyc}$ , the product of  $2f$ , and the maximum strain energy stored in the body,  $U_s$ , under a periodic vibration. Since the maximum strain energy of a beam under static load and under first mode vibration are equal, if the maximum deflection are the same. If the material damping of this beam is known, the energy dissipated in the beam within a cycle of the first mode vibration can be determined by

$$(U_D)_{cyc} = 2\pi \eta U_s \quad \text{E.1}$$

where  $U_s$  can be determined by calculating the strain energy of the statically-deformed beam having the same amplitude of the deflection as that of the first mode vibration. As it is well known that the dominant stress in a beam under flexure vibration is normal stress, say  $\sigma_x$ . Therefore,  $U_s$  and  $(U_D)_{cyc}$  can be obtained approximately as

$$U_s = \int \frac{1}{2} \sigma_x \epsilon_x dV \quad \text{E.2}$$

and

$$(U_D)_{cyc} = 2\sigma \eta_x \int \frac{1}{2} \sigma_x \epsilon_x dV \quad E.3$$

Where  $\epsilon_x$  is the normal strain, and  $\eta_x$  is determined by  $E''_x/E'_x$ . To be more accurate, all stresses and strains in the beam should be included when calculating the maximum strain energy and the dissipated energy.

Ungar and Kerwin [56] derived the expressions for the loss factor of any series-parallel array of  $m$  viscoelastic springs

$$\eta = \frac{\sum_{j=1}^m (U_{Dj})_{cyc}}{\sum_{j=1}^m 2\pi U_{sj}} \quad E.4$$

$$U_{sj} = \frac{1}{2} k_j x_j^2 \quad E.5$$

where  $U_{sj}$  denotes the maximum strain energy stored in a deflection  $x_j$  in the  $j$ th lossless spring of stiffness  $k_j$ , and  $(U_{Dj})_{cyc}$  denotes the energy dissipated in the  $j$ th viscoelastic spring during a cycle. Since there are six different components in the stiffness matrix for an orthotropic material, one can treat an orthotropic material as a structure composed of six springs.



Consequently, the material damping of a laminated  $n$  plies composite,  $\eta$ , in the first mode vibration can be determined by

$$\eta = \frac{\sum_{q=1}^n (q^{U_D})_{cyc}}{\sum_{q=1}^n q^{U_S}} \quad E.6$$

where

$$q^{U_S} = \int_{V_q} \frac{1}{2} \sigma_j \epsilon_j dV = \int_{V_q} \frac{1}{2} \epsilon_k C'_{kj} \epsilon_j dV \quad E.7$$

$$(q^{U_D})_{cyc} = \pi \int_{V_q} \epsilon_k C'_{kj} \eta_{kj} \epsilon_j dV = \pi \int_{V_q} \epsilon_k C''_{kj} \epsilon_j dV \quad E.8$$

$$C'_{kj} + i C''_{kj} \eta_{kj} = C'_{kj} + i C''_{kj} = C^*_{kj} \quad E.9$$

In which  $V_q$  is the volume of the  $q$ th layer in the laminated composite,  $C'_{kj}$ ,  $C''_{kj}$  and  $C^*_{kj}$  are the storage moduli, the loss moduli, and the complex moduli for a viscoelastic material, respectively.

APPENDIX F  
FORMULATION OF FINITE ELEMENT METHOD

This appendix briefly prescribes the formulation of the finite element method utilized in energy approach to determine the displacement and the strain fields for an elastic body. The material constants are also presented here.

F.1 Stiffness Matrix

The nonzero elements of stiffness matrix [C] for an orthotropic material when its coordinates coincide with principal coordinates are given in Reference [57] as:

$$C_{11} = (1 - \nu_{23} \nu_{32}) E_1 \Delta \quad \text{F.1}$$

$$C_{12} = (\nu_{12} + \nu_{32} \nu_{13}) E_2 \Delta \quad \text{F.2}$$

$$C_{13} = (\nu_{13} + \nu_{12} \nu_{23}) E_3 \Delta \quad \text{F.3}$$

$$C_{22} = (1 - \nu_{13} \nu_{31}) E_2 \Delta \quad \text{F.4}$$

$$C_{23} = (\nu_{23} + \nu_{21} \nu_{13}) E_3 \Delta \quad \text{F.5}$$

$$C_{33} = (1 - \nu_{12} \nu_{21}) E_3 \Delta \quad \text{F.6}$$

$$C_{44} = G_{23} \quad \text{F.7}$$

$$C_{55} = G_{31} \quad \text{F.8}$$

$$C_{66} = G_{12} \quad \text{F.9}$$

where

$$\Delta = \frac{1}{1 - \nu_{12}\nu_{21} - \nu_{23}\nu_{32} - \nu_{31}\nu_{13} - 2\nu_{21}\nu_{32}\nu_{13}} \quad \text{F.10}$$

Since the material properties of a laminar fiber composite with the coordinates parallel to and transverse to the fiber, as Figure E.1, can be treated as transversely (in 2, 3 directions) isotropic,

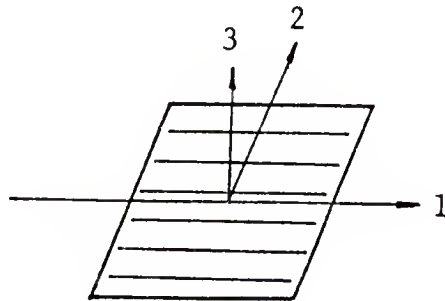


Figure F.1: Principal coordinates of fiber composite material

one has

$$E_1 = E_L$$

$$E_2 = E_T$$

$$E_3 = E_T$$

F.11

$$G_{12} = G_{LT}$$

$$G_{13} = G_{LT}$$

$$G_{23} = \frac{E_T}{2(1 + \nu_{TT'})}$$

and

$$\nu_{12} = \nu_{LT}$$

$$\nu_{21} = \frac{\nu_{LT} E_T}{E_L}$$

$$\nu_{23} = \nu_{TT'}$$

F.12

$$\nu_{32} = \nu_{TT'}$$

$$\nu_{13} = \nu_{LT}$$

$$\nu_{31} = \nu_{TL}$$

where  $E_L$ ,  $E_T$ ,  $G_{LT}$ ,  $\nu_{LT}$  are defined by Equations 3.13, 3.15-3.17, and  $\nu_{TT}$  is assumed to be the Poisson's ratio of the matrix. By substituting Equations F.11 and F.12 into Equations F.1-F.9, the  $[C]$  matrix of transversely isotropic material is then obtained. Equations F.11 and F.12 show that there are only five independent material constants, namely,  $E_L$ ,  $E_T$ ,  $G_{LT}$ ,  $\nu_{LT}$ , and  $\nu_{TT}$ .

## F.2 Formulations of Finite Element Method

A three-dimensional elastic body bounded by surface  $S$  is loaded by concentrated forces  $p$  on nodes and surface traction  $t$  on surface  $S_1$ . Assume that the body force is negligible and that the whole system is adiabatic and conservative. According to the principle of stationary potential energy [58], the equilibrium is ensured if the total potential energy is stationary for variation of admissible displacement, i.e.

$$\delta (U - W_e) = 0 \quad \text{F.13}$$

where  $U$  is the strain energy, and  $w_e$  is the work done by external loads. In fact, in the elastic case, potential energy is not only stationary but is a minimum [59].

If there is not any initial stress or strain, the strain energy  $U$  and the work done by the external load are

$$U = \frac{1}{2} \int_V \{\epsilon\}^T \{\sigma\} dV \quad \text{F.14}$$

and

$$W_e = \sum_{i=1}^m \{p\}_i^T \{u\}_i + \int_{s_1} \{t\}^T \{u\} dA \quad F.15$$

where

$$\{\epsilon\}^T = [\epsilon_x \ \epsilon_y \ \epsilon_z \ \gamma_{yz} \ \gamma_{xz} \ \gamma_{xy}] \quad F.16$$

$$\{\sigma\}^T = [\sigma_x \ \sigma_y \ \sigma_z \ \tau_{yz} \ \tau_{xz} \ \tau_{xy}] \quad F.17$$

$$\{p\}_i^T = [p_{xi} \ p_{yi} \ p_{zi}] \quad F.18$$

$$\{u_i\}_i^T = [u_{xi} \ u_{yi} \ u_{zi}] \quad F.19$$

$$\{u\}^T = [u_x \ u_y \ u_z] \quad F.20$$

$$\{t\}^T = [t_x \ t_y \ t_z] \quad F.21$$

in which  $u_{xi}$  is the nodal displacement in x direction at the  $i$ th node, and  $p_{xi}$  is the concentrated force at the  $i$ th node in x direction,  $m$  is the total number of nodes where concentrated load is applied.

By introducing stiffness matrix  $[C]$  and the shape function matrix  $[N]$ , i.e.

$$\{\sigma\} = [C] \{\epsilon\} \quad \text{F.22}$$

$$\{u\} = [N] \{q\} \quad \text{F.23}$$

strain  $\{\epsilon\}$  can be expressed as function of nodal displacement  $\{q\}$  by using strain-displacement relation

$$\{\epsilon\} = [L] \{q\} \quad \text{F.24}$$

Therefore, Equations F.14 and F.15 can be rewritten as

$$U = \frac{1}{2} \int_V \{q\}^T [L]^T [C] [L] \{q\} dV \quad \text{F.25}$$

$$W_e = \sum_{i=j}^m \{P\}_i^T [N] \{q\}_i + \int_{s_1} \{t\}^T [N] \{q\} dA \quad \text{F.26}$$

By using Equations F.25 and F.26, a system of  $3 \times n$  equations is obtained from Equation F.13, if the total number of nodes is  $n$ .

$$[\bar{k}] \{\bar{q}\} = \{\bar{f}\} \quad \text{F.27}$$

where

$$[\bar{k}]_{3n \times 3n} = [L]^T [C] [L] dV \quad F.28$$

$$\{\bar{q}\}_{3n \times 1} = [q_{x1} \ q_{y1} \ q_{z1} \ \cdot \ \cdot \ \cdot \ q_{xn} \ q_{yn} \ q_{zn}] \quad F.29$$

$$\{\bar{f}\}_{3n \times 1} = \sum_{i=1}^m \{P\}_i^T [N] + \{t\}^T [N] dA \quad F.30$$

In this study, the interpolation functions of linear and parabolic isoparametric elements (eight nodes and twenty nodes, respectively) [55] are chosen for shape functions. Each element has the same thickness as the ply thickness of fiber composite. Once the nodal displacement  $\{q\}$  is determined by solving the system equations (Equation F.27), the displacement and the strain fields can be obtained by Equations F.23 and F.24, respectively.



## REFERENCES

1. Ungar, E.E., The Status of Engineering Knowledge Concerning the Damping of Built-Up Structures, Journal of Sound and Vibration, Volume 26, No. 1, 141-154 (1973).
2. Pian, T.H., Structural Damping, Edited by Crandall, S. Technology Press, New York (1959).
3. WADC-University of Minnesota Conference on Acoustical Fatigue, WADC Technical Report, Edited by Trapp, W.J., and Forney, D.M., Jr., 659-676 (March 1961).
4. Lazan, B.J., Damping Properties of Materials and Material Composites, Applied Mechanics Review, Volume 15, No. 2, 81-88 (1962).
5. Kimball, A.L., and Lovell, D.E., Internal Friction in Solids, Physical Review, Volume 30, 948-959, (December 1927).
6. Crandall, S.H., The Role of Damping in Vibration . Theory, Journal of Sound and Vibration, Volume 11, No. 1, 3-18 (1970).
7. Kume, Y., Hashimoto, F., and Maeda, S., Material Damping of Cantilever Beams, Journal of Sound and Vibration, Volume 80, No. 1, 1-10 (1982).
8. Lazan, B.J., Effect of Damping Constants and Stress Distribution on the Resonance of Members, Journal of Applied Mechanics, 201-209 (1953).
9. Schultz, A.B., and Tsai, S.W., Dynamic Moduli and Damping Ratios in Fiber-Reinforced Composites, Journal of Composite Materials, Volume 2, 368-379 (1968).
10. Ni, R.G., and Adams, R.D., The Damping and Dynamic Moduli of Symmetric Laminated Composite Beams; Theoretical and Experimental Results, Journal of Composite Materials, Volume 8, 104-121 (1984).

11. Lin, D.X., Ni, R.G., and Adams, R.D., Prediction and Measurement of the Vibrational Damping Parameters of Carbon and Glass Fiber Reinforced Plastic Plates, Journal of Composite Materials, Volume 8, 132-152 (1984).
12. Adams, R.D., and Bacon, D.G., Measurement of the Flexural Damping Capacity and Dynamic Young's Modulus of Materials and Reinforced Plastics, Applied Physics, Volume 6, 27-41 (1973).
13. Siu, C.C., and Bert, C.W., Sinusoidal Response of Composite-Material Plate with Material Damping, Journal of Engineering for Industry, 603-610, (May 1974):
14. Suarez, S.A., Gibson, R.F., and Deobald, L.R., Development of Experimental Technique for Measurement of Damping in Composite Materials, 1983 Fall Meeting Proceedings, Society for Experimental Stress Analysis, Salt Lake City, Utah, 55-60 (November 1983).
15. Gibson, R.F., and Plunkett, R., Dynamic Mechanical Behavior of Fiber-Reinforced Composites; Measurement and Analysis, Journal of Composite Materials, Volume 10, 325-341 (1976).
16. Tauchert, T.R., and Hsu, N.N., Influence of Stress Upon Internal Damping in a Fiber Reinforced Composite Material, Journal of Composite Materials, Volume 7, 516-520 (1973).
17. Bert, C.W., Material Damping: An Introductory Review of Mathematical Models; Measures and Experimental Techniques, Journal of Sound and Vibration, Volume 29, No. 2, 129-153 (1973).
18. Bert, C.W., and Clary, R.R., Evaluation of Experimental Methods for Determining Dynamic Stiffness and Damping of Composite Material, American Society for Testing and Materials, Special Technical Publication 546, 250-265 (1974).
19. Plunkett, R., and Lee, C.T., Length Optimization for Constrained Viscoelastic Layer Damping, Journal of Acoustic Society of American Volume 48, 155-161 (1970).
20. Cox, H.L., The Elasticity and Strength of Paper and Other Fibrous Materials, British Journal of Applied Physics, Volume 3, 72-79 (1952).

21. Chon, C.T., and Sun, C.T., Stress Distribution Along a Short Fiber in Reinforced Plastics, Journal of Material Sciences, Volume 15, 931-938 (1980).
22. Fukuda, H., and Chou, T.W., An Advanced Shear-Lag Model Application to Discontinuous Fiber Composites, Journal of Composite Materials, Volume 15, 79-91 (1981).
23. Maclauchlin, T. F., A Photoelastic Analysis of Fiber Discontinuities in Composite Materials, Journal of Composite Materials, Volume 2, 44-55 (1968).
24. Pih, H., and Sutliff, D. R., Effect of Fiber End Fiber Orientation and Spacing in Composite Materials Developments in Theoretical and Applied Mechanics, North Carolina, Vol 5, 883-913 (1970).
25. Sun, C. T., and Wu, J. K., Stress Distribution of Aligned Short-Fiber Composites Under Axial Load, Journal of Reinforced Plastics and Composites, Volume 3, 130-144 (1984).
26. Carrara, A. S., and McGarry, F.J., Matrix Interface Stresses in a Discontinuous Fiber Composite Model, Journal of Composite Materials, Volume 2, 222-243 (1968).
27. Chen, P.E., Strength Properties of Discontinuous Fiber Composites, Polymer Engineering and Science, Volume 11, 51-66 (1971).
28. Lavengood, R. E., Strength of Short-Fiber Reinforced Composites, Polymer Engineering and Science, Volume 12, 48-52 (1972).
29. McLean, D., and Read, B.E., Storage and Loss Moduli in Discontinuous Composites, Journal of Material Science, Volume 10, 481-492 (1975).
30. Wang, G.J., and Sun, C.T., Effects of Fiber Length on Elastic Moduli of Randomly Oriented Chopped-Fiber Composites, ASTM Special Technical Publication 674 149-162 (1979).
31. Gibson, R.F., Chaturvedi, S.K., and Sun, C.T., Complex Moduli of Aligned Discontinuous Fiber-Reinforced Polymer Composites, Journal of Material Science, Volume 17, 3499-3509 (1982).
32. Gibson, R.F., and Yau, A., Complex Moduli of Chopped Fiber and Continuous Fiber Composites; Comparison of Measurements with Estimated Bounds, Journal of Composite Materials, Volume 14, 155-167 (1980).

33. Sun, C.T., Wu, J.K., and Gibson, R.F., Prediction of Material Damping in Randomly Oriented Short-Fiber Polymer Matrix Composites, Journal of Reinforced Plastics and Composites, Volume 4, 262-272 (1985).
34. Sun, C.T., Gibson, R.F., and Chaturvedi, S.K., Internal Material Damping of Polymer Matrix Composites Under Off-Axis Loading, Journal of Material Science, Volume 20, 2575-2585 (1985).
35. Suarez, S.A., Optimization of Internal Damping in Fiber Reinforced Composite Materials, Ph.D. Dissertation, University of Idaho, Moscow, Idaho (October 1984).
36. Suarez, S.A., Gibson, R.F., Sun, C.T., and Chaturvedi, S.K., The Influence of Fiber Length and Fiber Orientation on Damping and Stiffness of Polymer Composite Materials, Experimental Mechanics (in press).
37. Schwatz, M., Composite Materials Handbook, McGraw-Hill (1984).
38. Agarwal, B.D., and Broutman, L.J., Analysis and Performance of Fiber Composites, John Wiley and Sons, Inc., New York (1980).
39. Steidel, R.F., Jr., An Introduction to Mechanical Vibrations, Second Ed., John Wiley and Sons, Inc., New York (1979).
40. Bert, C.W., Composite Materials: A Survey of the Damping Capacity of Fiber-Reinforced Composites. University of Oklahoma, School of Aerospace Mechanical Engineering, Technical Report, No. 18 (August 1980)
41. Leonard, M., Analytical Methods in Vibration, Macmillan Co., London (1967).
42. Thomson, W.T., Theory of Vibration with Applications. Prentice-Hall, Inc., Englewood Cliffs, New Jersey (1981).
43. Volterra, E., and Zachmanoglou, E.C., Dynamics of Vibration, Merrill Books Co., Columbus, Ohio (1965).
44. Malvern, L.E., Introduction to the Mechanics of a Continuous Medium, Prentice-Hall, Inc., Englewood Cliffs, New Jersey (1969).
45. Bland, D.R., Linear Viscoelasticity, Pergamon Press, Inc., New York (1960).



46. Lazan, B.J., Damping Studies in Materials Science and Cyclic Plastic, ASTM, STP 378 (1965).
47. Nelson, D.J., and Hancock, J.W., Interfacial Slip and Damping in Fiber Reinforced Composites, Journal of Material Science, Volume 13, 2429-2440 (1978).
48. Kaelble, D.H., Micromechanisms and Phenomenology of Damping in Polymers. Internal Friction Damping and Cyclic Plasticity, ASTM, STP 378 (1965).
49. Larid, G.W., and Kingsbury, H.B., A Method of Determining Complex Moduli of Viscoelastic Materials, Experimental Mechanics, Volume 13, 126-130 (1973).
50. Tsai, S.W., Introduction to Composite Materials, Technomic Publishing Co., Stamford, Connecticut (1980).
51. Soroka, W.W., Note on the Relations Between Viscous and Structural Damping Coefficient, Journal of the Aeronautical Science, 409-410 (1949).
52. Hashin, Z., Complex Moduli of Viscoelastic Composites --II Fiber Reinforced Materials, International Journal of Solids and Structures, Volume 6, 797-807 (1970).
53. Halpin, J.C., and Tsai, S.W., Effects of Environmental Factors on Composite Material, Air Force Material Laboratory Technical Report 67-423 (June 1969).
54. Pipes, B.R., Interlaminar Stresses in Composite Laminates Under Uniform Axial Extension, Journal of Composite Materials Volume 4, 538-548 (1982).
55. Bathe, K.J., Finite Element Procedures in Engineering Analysis, Prentice-Hall, Inc., New York (1982).
56. Zienkiewicz, O.C., The Finite Element Method, Third Edition, McGraw-Hill Book Co., New York (1977).
57. Ungar, E.E., and Kerwin, E.M., Loss Factors of Viscoelastic System in Terms of Energy Concepts, The Journal of the Acoustical Society of American Volume 34, No. 7, 954-957 (1962).
58. Jones, R.M., Mechanics of Composite Materials, Scripta Book Co., Washington (1975).
59. Langhaar, H.L., Energy Methods in Applied Mechanics John Wiley and Sons, Inc., New York (1962).

60. Granick, N., and Stern, J.E., Material Damping of Aluminum by Resonant Dwell Technique, National Aeronautics and Space Administration TND 2893 (1965).
61. Gibson, R.F., Yau, A., and Riegner, D.A., An Improved Forced-Vibration Technique for Measurement of Material Damping, Experimental Techniques, Volume 6, No. 2, 10-14 (1982).
62. Stahle, C.W., and Forlifer, W.R., Ground Vibration Testing of Complex Structures, Proceeding of the 1958 Flight Flutter Testing Symposium, Reprinted in NASA SP-385, 83-90 (1975).
63. Lang, G.F., Understanding Vibration Measurement, Journal of Sound and Vibration 26-37 (March 1976).
64. Lee, B.T., Measurements of Damping for Nondestructively Assessing the Integrity of Fiber Reinforced Composites, Ph.D. Dissertation, University of Florida, Gainesville, Florida (January 1985).
65. Baker, W.E., Woolam, W.E., and Young D., Air and Internal Damping of Thin Cantilever Beams, International Journal of Mechanical Sciences, Volume 9, 743-766 (1967).
66. Gibson, R.F., and Plunkett, R., A Forced-Vibration Technique for Measurement of Material Damping, Experimental Mechanics, Volume 11, No. 8, 297-302 (1977).
67. Mitchell, L.D., Signal Processing With the Fast Fourier Transform Analyzer, SESA, Fall Meeting Proceeding, Salt Lake City, Utah, 22-32 (1983).
68. Spendley, W., Hext, G.R., and Himsworth, F.R., Sequential Application of Simplex Designs in Optimization and Evolutionary Operation, Technometrics, Volume 4, No. 4, 441-461, (1962).
69. Beveridge, G.S., and Schechter, R.S., Optimization Theory and Practice, McGraw-Hill Book Co., New York (1970).
70. Ashton, J.E., and Whitney, J.M., Theory of Laminated Plates, Technomic Publication Co., Stamford, Connecticut (1970).


## BIOGRAPHICAL SKETCH

Jiing-Kae Wu was born in Taiwan, Republic of China, on April 1, 1954. He received a Bachelor of Science degree in Naval Architecture Engineering from National Taiwan College of Marine Science and Oceanic Technology, Taiwan, R.O.C., in June 1977.


After working as a Third Marine Engineer at the Energy Shipping Co. from December 1977 to December 1979, he worked as a junior engineer at the United Ship Design and Development Center from February 1980 to July 1981. During this period, he married Mong-Shya Rau Wu in December 1980.

In August 1981, he enrolled in the Department of Engineering Sciences, University of Florida, for graduate study. After he received a Master of Science degree in Engineering Mechanics in December 1982, he enrolled in the same department to study for the Doctor of Philosophy.

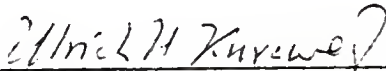
I certify that I have read this study and that in my opinion it conforms to acceptable standards of scholarly presentation and is fully adequate, in scope and quality, as a dissertation for the degree of Doctor of Philosophy.

  
Chang-Tsan Sun, Chairman  
Professor of Engineering  
Sciences

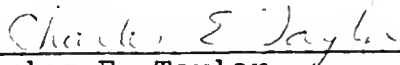
I certify that I have read this study and that in my opinion it conforms to acceptable standards of scholarly presentation and is fully adequate, in scope and quality, as a dissertation for the degree of Doctor of Philosophy.

  
Lawrence E. Malvern  
Professor of Engineering  
Sciences

I certify that I have read this study and that in my opinion it conforms to acceptable standards of scholarly presentation and is fully adequate, in scope and quality, as a dissertation for the degree of Doctor of Philosophy.

  
Ulrich H. Kurzweg  
Professor of Engineering  
Sciences

I certify that I have read this study and that in my opinion it conforms to acceptable standards of scholarly presentation and is fully adequate, in scope and quality, as a dissertation for the degree of Doctor of Philosophy.

  
Charles E. Taylor  
Professor of Engineering  
Sciences



I certify that I have read this study and that in my opinion it conforms to acceptable standards of scholarly presentation and is fully adequate, in scope and quality, as a dissertation for the degree of Doctor of Philosophy.

Arun K. Varma

Arun K. Varma  
Professor of Mathematics

This dissertation was submitted to the Graduate Faculty of the College of Engineering and to the Graduate School and was accepted as partial fulfillment of the requirements for the degree of Doctor of Philosophy.

December 1985

Wayne H. Chen

Dean, College of Engineering

Dean, Graduate School

UNIVERSITY OF FLORIDA



3 1262 07332 050 8